

Development of novel hybrid catalysis for carbon-carbon couplings by titanium oxide photocatalyst and metal cocatalyst

Akanksha Tyagi

**Development of novel hybrid
catalysis for carbon-carbon couplings
by titanium oxide photocatalyst and
metal cocatalyst**

Akanksha Tyagi

Department of Interdisciplinary Environment
Graduate School of Human and Environmental Studies
Kyoto University

Preface

The world is witnessing an extensive industrial growth to improve the quality of life but, at the cost of the environment. Deforestation and an unregulated release of toxic wastes into the environment has resulted in global warming and scarcity of pure air and water. And hence, environmental pollution is a main challenge of the current century. The chemical industry is one of the largest sources of the environmental pollution. Most of the current processes are energy intensive, involving multiple steps, and generating lots of waste. With the environmental regulations getting stringent with each passing day, the chemical industry faces a challenging task to design new and sustainable methods for organic synthesis.

Heterogeneous photocatalysis is a promising solution to this issue. It is often employed for the degradation of pollutants to purify air and water, production of renewable energy like hydrogen by water splitting, and many more. However, its application to the organic synthesis is still an emerging field. The present work is devoted to the development of new C–C coupling reactions by using heterogeneous photocatalysis and understand the mechanisms to design efficient catalysts. The work was carried out in the Graduate School of Human and Environmental Studies, Kyoto University, Japan under the supervision of Prof. Hisao Yoshida.

The author expresses her sincere gratitude to Prof. Hisao Yoshida for his constant support and encouragement throughout this work. The author is also grateful to Dr. Akira Yamamoto, assistant professor, Hisao Yoshida laboratory, Kyoto University, for his valuable discussions and suggestions. Heartfelt thanks to Prof. Tatsuhiisa Kato, Kyoto University for helping with the ESR measurements, Dr. Tomoko Yoshida, Osaka City University for the XAFS measurements, Dr. Tsutomu Kiyomura, Kyoto University for technical assistance with the TEM measurements, and Prof. Kenichi Fujita and his laboratory members at Kyoto University for providing the facilities and help to synthesize specific compounds.

Special thanks to Prof. Setsuhisa Tanabe and Prof. Yoshiharu Uchimoto at Graduate School of Human and Environmental Studies, Kyoto University for their valuable comments on this thesis which helped in its improvement.

Many thanks to all students, previous and current alike, of Hisao Yoshida laboratory and Ms. Yuri Bonnitcha for providing a healthy and friendly environment all these years. Special thanks to Mr. Tomoya Matsumoto, Mr. Tomoaki Takeuchi, Dr. Emiko Wada, and Mr. Shinpei Naniwa for their help and discussions.

The author is proud of being an IITH-JAPAN FRIENDSHIP Scholar and is indebted to Japan International Cooperation Agency (JICA) for providing the financial assistance during all these years.

This whole journey would be impossible without the eternal love, encouragement, and patience of my parents and sister. Special thanks to my husband and new family for the continuous love and support. And above all, the author is grateful to the Almighty for its blessings.

Akanksha Tyagi

16th January, 2018

Kyoto, Japan

Contents

Chapter I General Introduction	1
I-1. Synthetic organic chemistry	1
I-2. Catalytic organic synthesis	2
I-3. Photocatalytic organic synthesis.....	5
I-4. Conclusion	14
I-5. Objective.....	15
I-6. References	15
Chapter II Metal loaded titanium oxide photocatalysts for carbon- carbon cross-coupling between hydrocarbons and ethers	21
II-1. Introduction	21
II-2. Photocatalytic cross-coupling between arenes and ethers.....	24
II-3. Photocatalytic cross-coupling between alkanes and tetrahydrofuran	43
II-4. Photocatalytic cross-coupling between alkenes and tetrahydrofuran	57
II-5. Summary	73

Chapter III Blended catalysts consisting of titanium oxide photocatalyst and supported metal catalyst for the carbon-carbon coupling reactions	74
III-1. Introduction	74
III-2. Photocatalytic cross-coupling between arenes and tetrahydrofuran	76
III-3. Photocatalytic cross-coupling between cyclohexane and tetrahydrofuran	95
III-4. Photocatalytic Ullmann coupling of aryl halides	101
III-5. Summary	118
Chapter IV General Conclusion.....	119
List of publications	121
Achievements.....	123

Chapter I General Introduction

I-1. Synthetic organic chemistry

Synthetic organic chemistry refers to the science of the formation of organic compounds by using simple and readily available raw materials. Organic compounds are vital for sustaining life on earth and have a profound presence in our daily life. They include fine chemicals like DNA, proteins, and medicines, and bulk chemicals like fertilizers, polymers, plastics (Figure 1). All organic molecules have the carbon skeleton. Thus, C–C bond formation is the basic reaction of synthetic organic chemistry. A direct construction of new C–C bonds from the C–H bonds is one of the long-desired goals of the organic chemists. However, this reaction is quite challenging as the C–H bonds have low reactivity due to their high stability. Hence, extensive research is going on to develop methodologies to perform this important reaction in mild conditions.

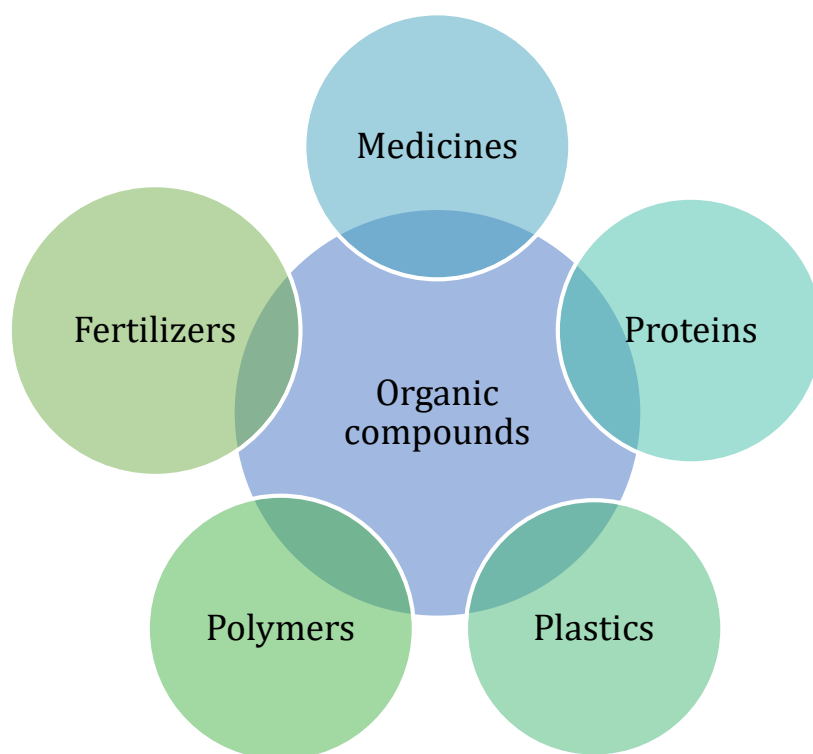
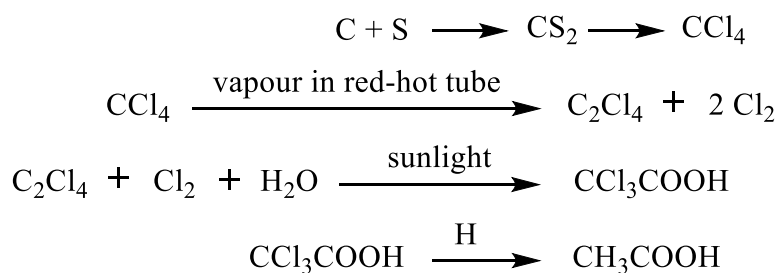


Figure 1 Several commonly used organic compounds in daily life

Historically, the synthesis of Urea from an inorganic compound (ammonium cyanate) by Wohler in 1828 was the first report of the synthesis of an organic compound in the laboratory.¹ Although a simple molecule, its synthesis was a milestone as it questioned the existing notion about the organic synthesis. In those times, it was believed that synthesis of organic compounds requires

some vital forces and thus they couldn't be synthesized in the laboratory. Later, the synthesis of acetic acid by Kolbe (1845)² (Scheme 1)³ and methane by Berthelot (1856)⁴ further cemented the proposal that organic compounds could be synthesized in the laboratory and opened a new field for chemists which led to an exponential growth in the field of organic chemistry. As a result, now, almost all the everyday use compounds can be prepared industrially.



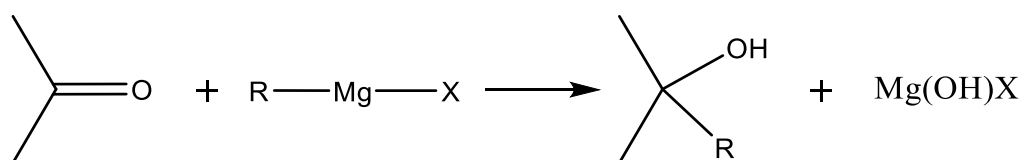
Scheme 1 Acetic acid synthesis by H. Kolbe reproduced from reference 3

I-2. Catalytic organic synthesis

Over the years, not only the range of compounds but also the chemical processes have evolved with time. In earlier days, the reactions were carried out in harsh conditions like large quantities of bases, high temperatures, etc. which made the industrial production of the compounds un-economical. However, significant developments have been made in the past decades to design milder processes in which the use of various catalysts for the reaction is the most commonly employed technique. Broadly, there are two types of catalysts: Homogeneous and heterogeneous. Homogeneous catalysts refer to compounds which are in the same phase as the reactants so that the reaction mixture has a uniform composition throughout. On the other hand, heterogeneous catalysts are those compounds which are in the different phase from the reactants and hence the reaction mixture has a non-uniform composition. Both catalysts have some limitations. Due to the same phase, the homogeneous catalysts are in close contact with the reactants which makes them more efficient than the heterogeneous catalysts. However, the same reason makes their separation and recovery from the reaction mixture more difficult than heterogeneous catalysts. As most of these catalysts contain expensive and rare metals, their recovery and reuse are of utmost importance, but with homogeneous catalysts, it is not possible. In spite of the limitations, both catalysts are often used in organic synthesis.

I-2.1. Homogeneous catalysis

Organometallic compounds of transition metals are one of the major class of homogeneous catalysts. They generally refer to chemical compounds that contain a chemical bond between the metal ion and carbon atom like in hydrocarbons. However, sometimes, it also refers to metal hydrides or metal-phosphine complexes. The discovery of Grignard reagents (organomagnesium compounds) by Victor Grignard in 1900 pioneered the usage of organometallic compounds in the synthetic organic chemistry.⁵ The reaction between a Grignard reagent and carbonyl compound is one of the most widely used C–C bond formation reaction (Scheme 2). After it, several other organometallic compounds were developed like organolithium, organoborane, Gilman reagent (organometallic compound of lithium and copper) to name a few. The usage of these reagents has greatly simplified the C–C bond formation reactions and enhanced the efficiency when compared to the traditional methods. However, such reactions have some limitations. The main problem is the employment of stoichiometric amounts of the organometallic reagents for the reactions. Due to the high cost of these reagents and the special preparation and storage requirements, the industrial application of these reactions is difficult and impractical. Thus, it is essential to develop processes requiring a catalytic amount of these organometallic compounds.

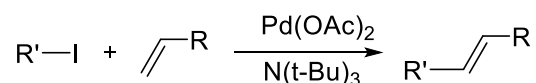


Scheme 2 Reaction between carbonyl compound and Grignard reagent

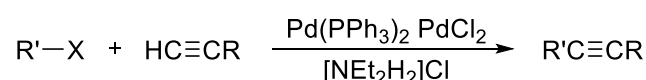
Last decades have seen significant advancement in the field of metal catalyzed coupling reactions. Organometallic compounds of metals like Pd, Ni, and Cu are often used to catalyze the organic reactions. Some famous examples are Heck reaction,⁶ Sonogashira coupling,⁷ Negishi coupling,⁸ and Suzuki reaction⁹ (Scheme 3). In these reactions, the metal undergoes an oxidative addition to an organic molecule like an aryl halide followed by reaction with the coupling partner, which places both molecules on the same metal. Finally, the coupling product is released by reductive elimination and, the catalyst is regenerated. These methods have several advantages over the

previously employed methods especially for the product yield and selectivity. Thus, most of the current processes employ these catalysts.

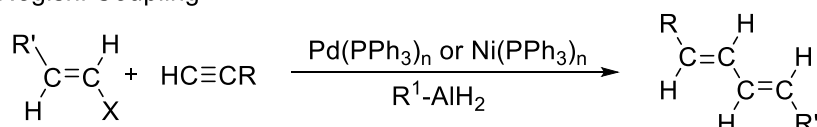
Heck Reaction



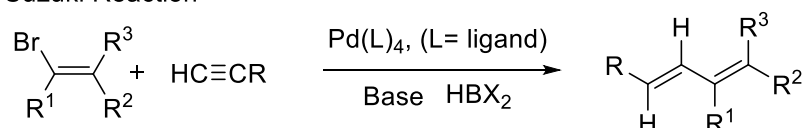
Sonogashira Coupling



Negishi Coupling



Suzuki Reaction



Scheme 3 Some reactions catalyzed by organometallic compounds

In spite of the advantages mentioned above, the usage of the organometallic catalysts has some limitations as discussed below. The main problem is related to their preparation and storage. Some of these compounds are sensitive to air and moisture and thus need to be prepared and stored under inert gas and moisture free conditions. These requirements add to the infrastructural facilities required for the usage of these catalysts for the reactions and thus increase the cost of the process. Also, since most of these catalysts are homogeneous, they cannot be recovered after the reaction and can't be reused. The reuse of these catalysts is of utmost importance as they contain the precious noble metals. Finally, such reactions are energy intensive requiring high temperatures and a lot of co-catalysts to get appreciable product yields. The usage of the additional reagents that generate a lot of waste doesn't adhere to the principles of green chemistry. As the environmental regulations for the chemical synthesis are getting stringent with each passing year, there is an urgent need to design sustainable reactions procedures and catalysts.

I-2.2. Heterogeneous catalysis

Heterogeneous catalysts are solid materials like clays, supported metals, or metal compounds like oxides and sulfides. Heterogeneous catalysts are widely used in the industrial synthesis of fine chemicals.¹⁰ Some famous examples are Fischer-Tropsch process for the synthesis of liquid hydrocarbons from synthesis gas (CO and H₂) by using alkalized Fe turnings as catalyst, styrene production by dehydrogenation of ethylbenzene by using Fe oxide based catalysts, Friedel-Crafts alkylation using zeolites, and polyene polymerization by Ziegler-Natta catalyst consisting of supported titanium catalyst and triethylaluminium (Al(C₂H₅)₃). Although these processes are industrialized and serve as the main production source for the mentioned compounds, they have some limitations like high temperatures and pressures. Hence, there is room for the development of new methodologies for organic synthesis, among which photocatalysis seems promising.

I-3. Photocatalytic organic synthesis

Solar radiation is a clean and abundant natural resource. Several natural phenomena are driven by solar light like photosynthesis by plants to convert CO₂ and H₂O to glucose and oxygen and Vitamin D synthesis in human skin. But, the efficient utilization of the incident solar energy for human use remains a great challenge for the scientific community. A photocatalyst can convert the solar energy into chemical energy at room temperature and thus it can catalyze reactions under much milder conditions when compared to a thermal catalyst. Also, by modifying its physical and electronic properties, selective excitation of the photocatalyst which can minimize side reactions to enhance product selectivity. Hence photocatalysis offers a sustainable methodology for various processes. Since the discovery of the Honda-Fujishima effect,¹¹ the application of photocatalysis for various purposes has drawn keen interest. Numerous reports are published every year discussing the employment of photocatalysts for various reactions like alternative energy sources,¹²⁻¹⁴ CO₂ reduction,¹⁵⁻¹⁷ methane reforming,¹⁸⁻²⁰ and air and water purification.²¹⁻²³ However, the field of photocatalyzed organic transformations is still an emerging area.²⁴⁻²⁷ The various photocatalysts tested for organic synthesis reactions fall under two main categories: homogeneous and heterogeneous photocatalysts.

I-3.1. Homogeneous photocatalysis

Most of the homogeneous photocatalysts refer to the organic complexes of some precious metals like Rh and Ir, or conjugated organics like dye. The metal complexes show a characteristic absorption band in their UV-Vis spectra corresponding to the metal to ligand charge transfer transitions (MLCT). When they absorb solar radiation corresponding to this wavelength, they get excited and generate a redox-active photoexcited state (Figure 2, a). This state can then undergo an oxidative quenching cycle (Figure 2, b) or a reductive quenching cycle (Figure 2, c) to return to the ground state and bring out the reaction.

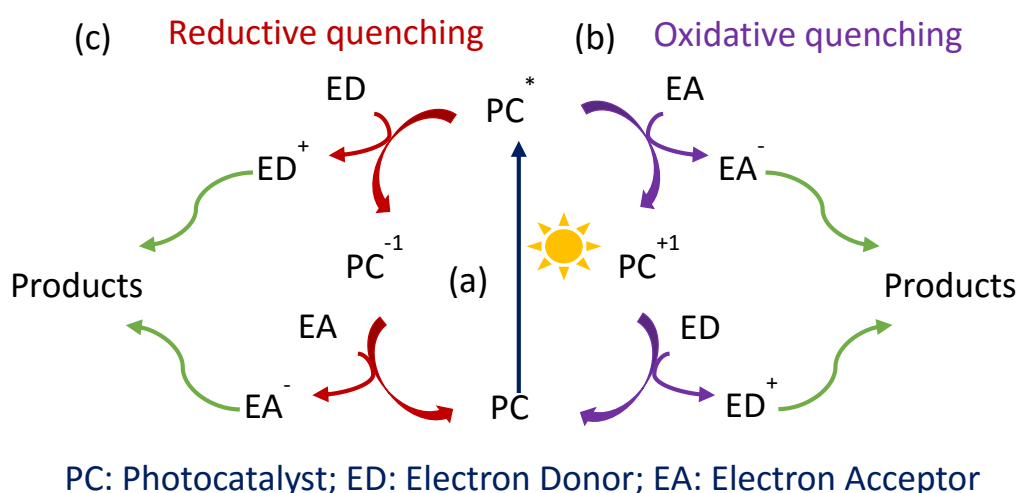
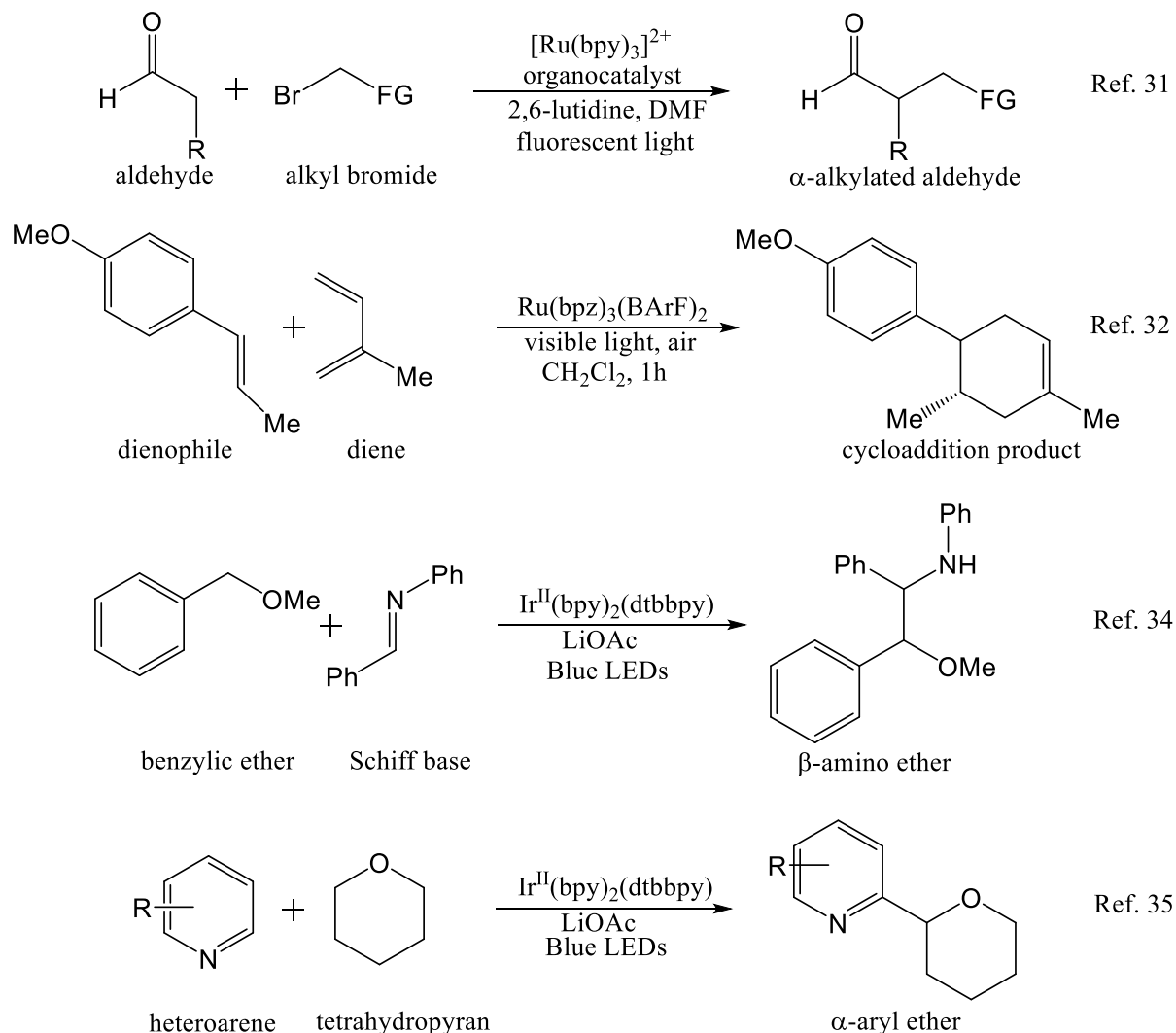


Figure 2 Schematic representation of photocatalysis by a metal complex

Several research groups have investigated the usage of these catalysts for various organic reactions (Scheme 4).^{28,29} Ru complexes are one of the most commonly studied homogeneous photocatalysts. MacMillan *et al.* have used its complex for different reactions like asymmetric alkylation³⁰ and enolation³¹ of aldehydes. Yoon *et al.* have also reported a radical cation Diels-Alder reaction catalyzed by this complex.³² Ir complexes have also been investigated for various organic reactions. MacMillan *et al.* have employed these catalysts for the heterocoupling of aminoalkyl radicals and arene radical anions,³³ benzylic ethers and Schiff bases,³⁴ and the selective arylation of ethers.³⁵ Conjugated organic molecules can also absorb solar radiation and generate an excited state which can also undergo single electron transfer reactions like metal complexes. König *et al.* have used conjugated organics like perylene diimides (PDI) to carry out the photocatalytic reduction of organic halides.³⁶ Thus, these metal complexes have proven to

be successful catalysts for various organic reactions. Although the reaction discovery is increasing at a faster rate, the mechanistic studies are lagging behind. Most of the researchers propose only a tentative mechanism without having substantial evidence.



Scheme 4 Some examples of organic synthesis by homogeneous catalysts

Although extremely popular, these catalysts have some limitations, main being their homogeneity, which makes their reuse difficult. From the industrial point of view, it is an important topic, considering the cost of the process. The toxicity of these metal ions is another issue in using these catalysts. As the catalysts remain in the solution after the reaction, they are passed on to the environment and cause harm. Hence, there is still scope for improvement for the catalyst part. Heterogeneous photocatalysis is a promising solution to this problem.

I-3.2. Heterogeneous photocatalysis

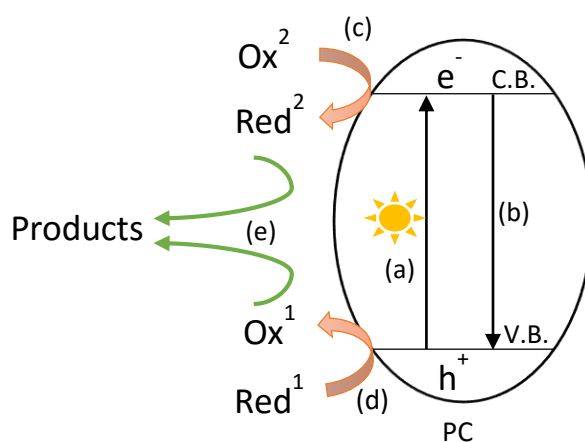
Heterogeneous photocatalysts often refer to the semiconductors, plasmonic metals or other photoactive materials like polymers and inorganic composites. These photocatalysts involve the photoexcitation of the electrons in these materials.

Photocatalysis by semiconductors

Various inorganic semiconductors like TiO_2 , CdS , and BiVO_4 have been tested for photocatalytic organic synthesis, however TiO_2 remains the most investigated photocatalyst due to its high abundance, low toxicity, and high stability and photocatalytic activity for most of the reactions. Figure 3 shows a simplified working mechanism of a semiconductor photocatalyst.³⁷ These materials work by absorbing the solar radiation of energy more than or equal to their band gap, which is the energy difference between the top of the valence band (V.B.) and the bottom of the conduction band (C.B.). Depending on the band gap, the radiation used for the photocatalyst's activation can fall in the UV, visible or IR region of the solar light. Upon light absorption, hole and electron are generated in the valence and conduction bands of the photocatalyst, respectively (Figure 3, a). There is high possibility of a quick recombination of these photogenerated species, either in the bulk or on the surface (Figure 3, b). Further, depending on the energy level of the conduction band and the valence band of the photocatalyst and the redox potential of the organic substrates, the photogenerated electrons and holes can bring out reduction and/or oxidation reactions (Figure 3, c and d). In some cases, the reduced and oxidized products are the final products, while these compounds can also react further and give other products (Figure 3, e). Since the activation of the photocatalyst requires only light irradiation, the photocatalytic organic reactions are often carried out at room temperature, which makes them green and sustainable.

Several organic transformations have been successfully carried out with semiconductor photocatalysts.^{38, 39} Different organic compounds like hydrocarbons, aromatics, and alcohols can be oxidized photocatalytically.⁴⁰⁻⁴³ These reactions can either be catalyzed by the photogenerated holes in the valence band of the photocatalyst or by the OH radicals generated by the photo-oxidation of water adsorbed on the photocatalyst's surface, which react with the organic molecules. Similarly, the photogenerated electrons in

the conduction band of semiconductor can bring out the reduction of different molecules.⁴⁴⁻⁴⁶

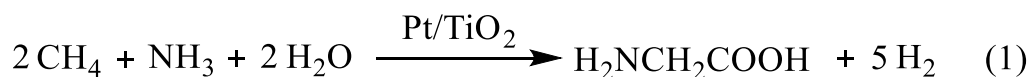


PC: Photocatalyst; Ox: oxidant; Red: Reductant

Figure 3 Schematic representation of photocatalysis by a semiconductor photocatalyst

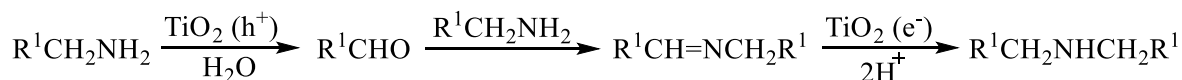
The use of photogenerated electrons and holes eliminates the use of toxic oxidizing and reducing agents, which makes this methodology safe when compared to the traditional methods.

As mentioned before, the excitation of a semiconductor photocatalyst generates both reducing and oxidizing centers in the vicinity. A combined utilization of these two centers allows a multistep organic synthesis in one-pot. Based on this strategy, various coupling reactions have been successfully done by semiconductor photocatalysis which allows synthesis of some complex organic compounds. Dunn *et al.* reported the synthesis of various amino acids like glycine, serine etc. from a mixture of methane, ammonia, and water with Pt/TiO₂ under UV and visible irradiation (equation 1).⁴⁷ The authors propose that similar reactions might be prevalent in the initial stages of chemical evolution and might have been the source of nutrition for early living organisms.



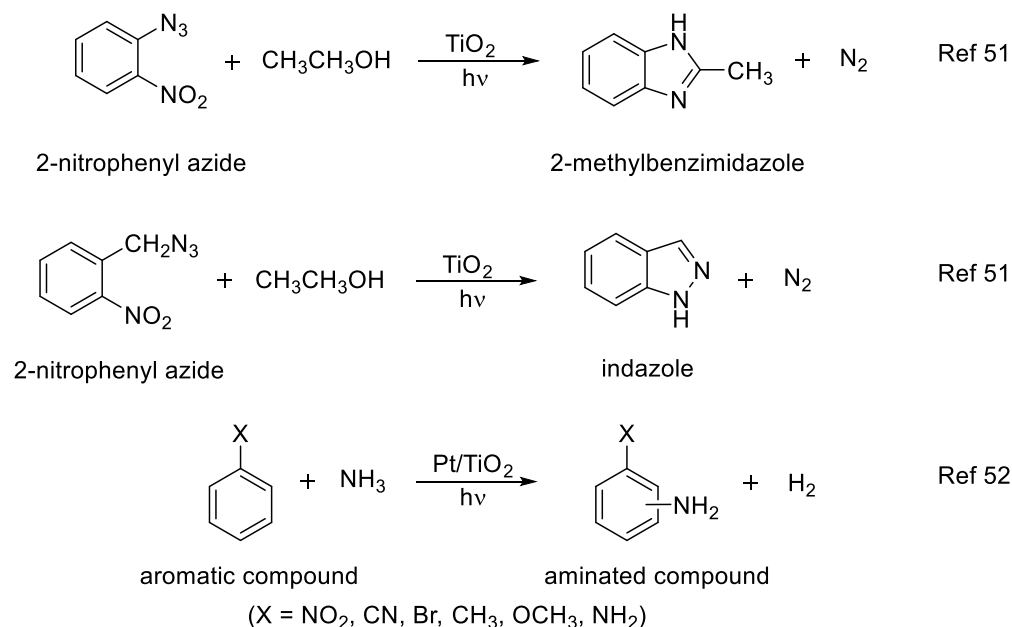
Ohtani *et al.* reported the photocatalytic synthesis of secondary amines from the aqueous solution of primary amines and a Pt/TiO₂ photocatalyst.⁴⁸ The reaction involved the photooxidation of the amine molecule to generate an

imine on TiO₂ and its subsequent reaction with second amine molecule to generate another imine which finally gets hydrogenated to yield the secondary amine (Scheme 5). They extended this methodology to the one-pot synthesis of cyclic imino acids like L-pipecolic acid from amino acids like L-lysine.⁴⁹



Scheme 5 Conversion of primary amines to secondary amines by heterogeneous Pt/TiO₂ photocatalyst

Wang *et al.* reported the synthesis of substituted benzimidazoles from dinitrobenzene and alcohol in the presence of TiO₂ photocatalyst.⁵⁰ The reaction involved the photo-oxidation of alcohols and photo-reduction of nitrobenzene followed by C–N coupling making it an efficient one-pot reaction. Apart from these intermolecular cross-couplings, some intramolecular photocatalytic C–N coupling reactions have also been reported (Scheme 6).

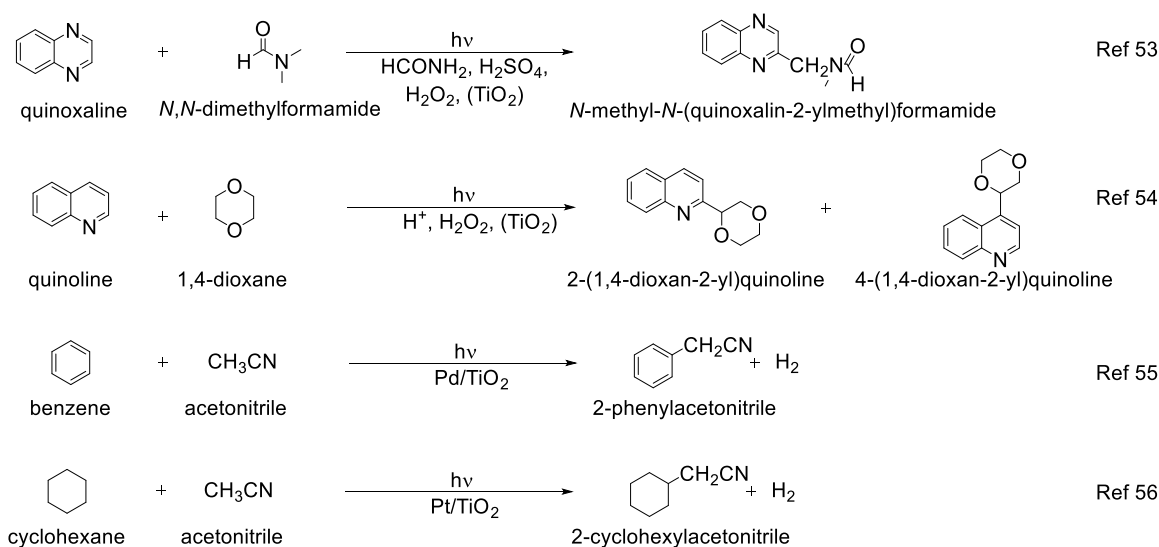


Scheme 6 C–N coupling by heterogeneous TiO₂ photocatalysis

Selvam *et al.* reported a one-pot synthesis of alkylbenzimidazoles and indazole from aromatic azides by using a TiO₂ photocatalyst under irradiation.⁵¹ This reaction involved photo-reduction of the azide whereas alcohol was used as hole scavenger. Yuzawa *et al.* reported the photocatalytic amination of various aromatics by NH₃ over a Pt loaded TiO₂

photocatalyst.⁵² The reaction proceeded by the photooxidation of NH₃ which attacked the aromatic molecule to give the aminated products.

C–C coupling has also been investigated over different heterogeneous photocatalysts (Scheme 7). Corona et al. reported the functionalization of heterocyclic bases like quinoline by amides⁵³ and ethers⁵⁴ in water/acetonitrile mixture with a TiO₂ photocatalyst. Yoshida et al. reported the cyanomethylation of benzene by acetonitrile by using a Pd loaded TiO₂ photocatalyst.⁵⁵ Later, the reaction was extended to other aliphatic hydrocarbons like cyclohexane and cyclohexene.⁵⁶ These reactions follow the same mechanism as C–N couplings and involve the photooxidation of the substrates on the surface of the photocatalyst. The protons released during the oxidation reaction were reduced to hydrogen by the photogenerated electrons.^{55, 56}



Scheme 7 C–C coupling by heterogeneous TiO₂ photocatalysis

Photocatalysis by plasmonic metals

Organic synthesis by plasmonic photocatalysis is a relatively new field when compared to semiconductor photocatalysis but has been gaining interest from the researchers in photocatalysis field.⁵⁷ The working mechanism of plasmonic photocatalysis differs slightly from the semiconductor photocatalysis. These materials utilize the Localized Surface Plasmon Resonance (LSPR) of the metals to absorb the solar radiation which can be used either directly^{58, 59} or indirectly⁶⁰⁻⁶², for example in a plasmonic metal-semiconductor composite, to bring out a photocatalytic reaction. LSPR of

plasmonic metals includes several plasmon modes.⁶³ However, in photocatalytic applications, it mainly refers to the oscillation of the electrons in the metals upon light irradiation.⁶⁴ When the noble metal nanoparticles are irradiated with light of wavelength much larger than them, the oscillating electric field of the incident light displaces their electron cloud relative to the nuclei to induce an electric dipole (Figure 4, left). These displaced electrons which are not in thermal equilibrium with the atoms in the metal are called 'hot electrons'. The induced dipole then oscillates at the same frequency as the incident field and a collective oscillation of such dipoles is called LSPR. The wavelength and absorption efficiency of the LSPR varies with the electronic (composition and dielectric constant) and physical (shape and size) properties of the metal nanoparticles. The LSPR can generate an electric field in the vicinity of the metals which is several times more intense than the incident field. This is called near-field enhancement and is responsible for plasmonic photocatalysis by these metals either by direct transfer of hot electrons to an adsorbed molecule or an indirect injection to the nearby semiconductor (Figure 4, right). The hole left on the metal is generally consumed by a hole scavenger (X).

The plasmonic photocatalysis has been used to carry out different organic transformations. For example, supported gold plasmonic photocatalysts have been used for reactions like oxidation of alcohols to carbonyl compounds,^{65,66} reduction of different hydrocarbons like nitrobenzene to azobenzene, ketones to alcohols, deoxygenation of epoxides to alkenes, and one-pot synthesis of propargylamine.⁶⁷⁻⁶⁹ Christopher *et al.* used supported Ag nanocubes to carry out some important reactions like ethylene epoxidation, with low intensity solar radiation.⁷⁰ Sometimes the plasmonic metals are used in combination with other metals either as co-catalysts or in as an alloy to achieve higher photocatalytic activity in an organic reaction. Many researchers have explored the photocatalytic activity of supported Au-Pd alloy nanoparticles for organic reactions. Sarina *et al.* found that the alloyed nanoparticles exhibited much higher activity for several reactions like selective oxidation of alcohols, different cross-coupling reactions like Suzuki-Miyaura coupling than the supported monometallic Au and Pd photocatalysts.⁷¹⁻⁷³

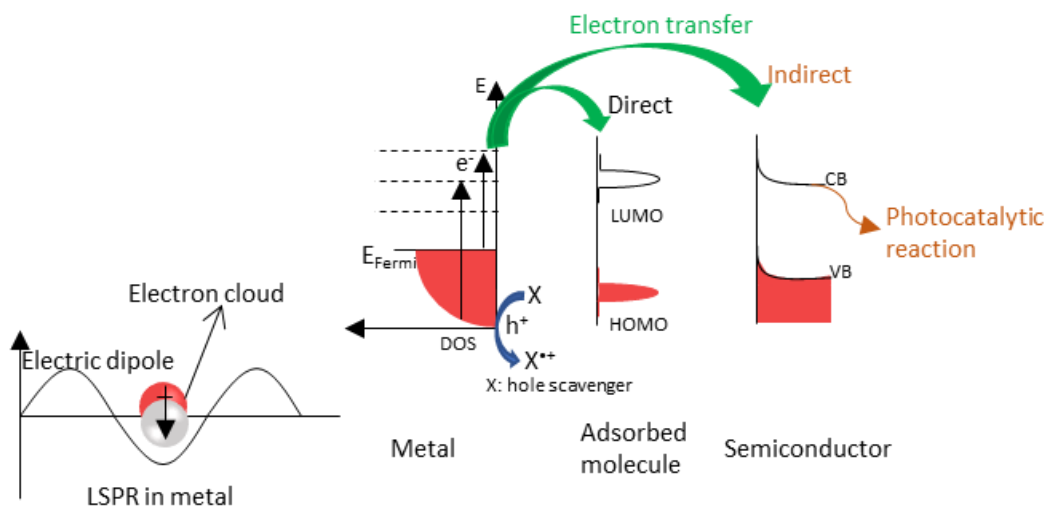


Figure 4 Schematic representation of LSPR and plasmonic photocatalysis

Photocatalysis by composite materials

Composite photocatalysts commonly refer to the materials formed by the combination of a) two or more semiconductors like TiO_2 and BiVO_4 or b) semiconductor and an inorganic or organic material, for example metals or carbonaceous materials like graphene. The aim of these composites is to overcome the limitations of a single photocatalyst like low visible light photocatalytic activity, charge recombination, and so on. The working mechanism of these composite materials varies with its composition. For example, in the composite of two semiconductors, heterojunctions are created between the semiconductors. Depending on the wavelength of the irradiated light, one of the semiconductor photocatalyst can be excited and the photogenerated electrons or holes are transferred to the other semiconductors via the heterojunctions (Figure 5 left). This type of system can allow enhanced visible light activity as well as efficient charge separation.^{74, 75} On the other hand in the composites of semiconductor with carbonaceous materials like graphene or carbon nitride, apart from the above process, new levels could also be generated (e.g. CB') which narrows the band gap of the new photocatalytic material (Figure 5, right). This works well for semiconductors like TiO_2 and ZnO which have a wide band-gap and can only work in UV light.^{76, 77} Further, in some other graphene-semiconductor composites, the role of graphene could just be an electron receiver and migrator so as to improve the separation of photogenerated electrons and holes on the photocatalyst (Figure 5 right).^{78, 79}

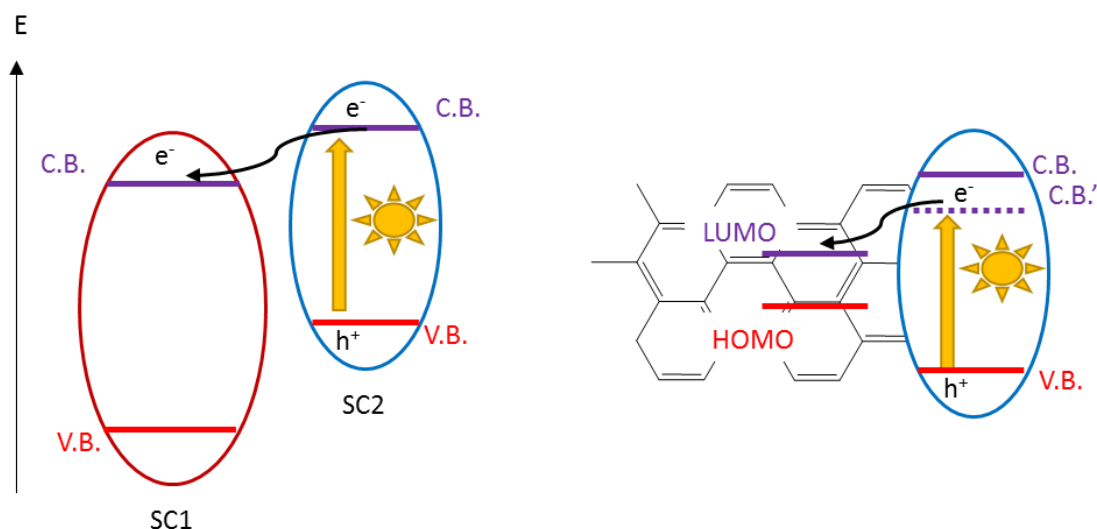


Figure 5 Graphical representation of the working mechanism of composite photocatalysts

These composite materials have been extensively utilized for photocatalytic water splitting, CO₂ reduction, and decomposition of organic pollutants but, their application for organic synthesis is relatively less known. Chen *et al.* carried out the selective photocatalytic reduction of nitro-organics in water by using a nanocomposite of CdS nanospheres and graphene.⁸⁰ The intimate contact between the graphene sheet and CdS nanospheres enhanced the conductivity and mobility of photogenerated electrons on CdS under visible light irradiation. In another report, Qin *et al.* reported a TiO₂-CdS heterojunction in the form of nanofiber to carry out the selective oxidation of various alcohols to aldehydes.⁸¹ CdS was excited by visible light irradiation and the photogenerated electrons were transferred to TiO₂, while the holes remained on CdS allowing efficient charge separation. Wang *et al.* employed a polyaniline-g-C₃N₄-TiO₂ composite to perform the photocatalytic synthesis of chloro aryl ketone.⁸² The presence of the three materials allowed the reaction to proceed under visible light and with efficient separation of the photogenerated electrons and holes by hindering their recombination.

I-4. Conclusion

The field of synthetic organic chemistry is constantly evolving. Several technologies have been developed to allow an efficient synthesis of different compounds. However, as discussed, none of them is perfect. With the environmental regulations getting stricter every year and the depletion of natural resources, there is an urgent need for improvement in the existing

practices and also for the innovation of new technologies. Photocatalysis has emerged to be a promising solution for some major environmental problems like the production of renewable energy and degradation of pollutants for clean air and water. On the other hand, photocatalytic organic synthesis is still an emerging field but, has shown encouraging results on synthesis routes and obtained products. However, these processes are poorly understood. Thus, more detailed studies are needed to understand the underlying principles and develop new reactions, which would allow the industrial application of this methodology.

I-5. Objective

This thesis is devoted to the development of new and selective C–C coupling reactions by using TiO₂ photocatalyst and metal cocatalyst.

In the second chapter (Chapter II), I mentioned the C–C cross-coupling of various aromatic and non-aromatic hydrocarbons with ethers by using metal loaded TiO₂ photocatalysts. A detailed study was conducted to elucidate the reaction mechanism which was a hybrid of TiO₂ photocatalysis and metal catalysis. Based on those findings, we developed a new type of catalytic system having blended TiO₂ photocatalyst and metal catalyst and examined it for C–C cross-coupling of hydrocarbons with ethers and the Ullmann coupling of aryl halides, as discussed in the third chapter (Chapter III).

In the present work, we succeeded to develop selective C–C coupling reactions under mild conditions by using an abundant, safe and inexpensive metal loaded TiO₂ photocatalyst. Further, we clarified the role of both metal and the TiO₂ photocatalyst in such reactions, which strengthened our understanding of the mechanism of photocatalytic reactions and helped me to develop a new and efficient blended catalytic system.

I-6. References

- [1] F. Wohler, *Ann. Phys. Chem.*, vol. 12, p. 253, **1828**.
- [2] H. Kolbe, *Mem. Proc. Chem. Soc*, vol. 3, pp. 285, **1845**.
- [3] D. McKie, *Nature*, vol. 153, p. 608, **1944**.
- [4] M. Berthelot, *Ann. Chim. Phys.*, vol. 67, p. 52, **1863**.

- [5] V. Grignard, *Compt. rend. Hebd. Séances Acad. Sci.*, vol. 130, p. 1322, **1900**.
- [6] R. F. Heck and J. P. Nolley, *J. Org. Chem.*, vol. 37, pp. 2320, **1972**.
- [7] K. Sonogashira, Y. Tohda and N. Hagihara, *Tetrahedron Lett.*, vol. 16, pp. 4467, **1975**.
- [8] S. Baba and E.I. Negishi, *J. Am. Chem. Soc.*, vol. 98, pp. 6729, **1976**.
- [9] N. Miyaoura, K. Yamada and A. Suzuki, *Tetrahedron Lett.*, vol. 36, pp. 3437, **1979**.
- [10] G. Ertl, H. Knozinger, F. Schuth, J. Weitkamp, *Handbook of Heterogeneous Catalysis*, Wiley-VCH, **2007**.
- [11] A. Fujishima and K. Honda, *Nature*, vol. 238, pp. 37, **1972**.
- [12] A. Kudo and Y. Miseki, *Chem. Soc. Rev.*, vol. 38, p. 253, **2009**.
- [13] K. Maeda and K. Domen, *J. Phys. Chem. Lett.*, vol. 1, p. 2655, **2010**.
- [14] M. Murdoch, G. I. N. Waterhouse, M. A. Nadeem, J. B. Metson, M. A. Keane, R. F. Howe, J. Llorca and H. Idriss, *Nature Chemistry*, vol. 3, p. 489, **2011**.
- [15] K. Iizuka, T. Wato, Y. Miseki, K. Saito and A. Kudo, *J. Am. Chem. Soc.*, vol. 133, p. 20863, **2011**.
- [16] J. Yu, J. Low, W. Xiao, P. Zhou and M. Jaroniec, *J. Am. Chem. Soc.*, vol. 136, p. 8839, **2014**.
- [17] B. Gholamkhash, H. Mametsuka, K. Koike, T. Tanabe, M. Furue and O. Ishitani, *Inorg. Chem.*, vol. 44, p. 2326, **2005**.
- [18] K. Shimura and H. Yoshida, *Energy Environ. Sci.*, vol. 3, p. 615, **2010**.
- [19] K. Shimura, H. Kawai, T. Yoshida and H. Yoshida, *ACS Catal.*, vol. 2, p. 2126, **2012**.
- [20] B. Han, C. Wei, H. Peifu and H. Yun, *ACS Catal.*, vol. 6, p. 494, **2016**.
- [21] R. J. Davis, J. L. Gainer, G. O'Neal and I. W. Wu, *Water Environ Res*, vol. 66, p. 50, **1994**.
- [22] A. Fujishima, X. Zhang and D. A. Tryk, *Int. J. Hydrogen Energy*, vol. 32, p. 2664, **2007**.

- [23] A. Di Paola, E. G. Lopez, G. Marci and L. Palmisano, *J. Hazard Mater*, vol. 211, p. 3, **2012**.
- [24] Y. Shiraishi and T. Hirai, *J. Photochem. Photobiol. C.*, vol. 9, p. 157, **2008**.
- [25] H. Kisch, *Angew. Chem. Int. Ed.*, vol. 52, p. 812, **2013**.
- [26] H. Kominami, S. Yamamoto, K. Imamura, A. Tanaka and K. Hashimoto, *Chem. Commun.*, vol. 50, p. 4558, **2014**.
- [27] J. Chen, J. Cen, X. Xu and X. Li, *Catal. Sci. Technol.*, vol. 6, p. 349, **2016**.
- [28] C. R. J. Stephenson and J. M. R. Narayanam, *Chem. Soc. Rev.*, vol. 40, pp. 102, **2011**.
- [29] C. K. Prier, D. A. Rankic and D. W. C. MacMillan, *Chem. Reviews*, vol. 113, pp. 5322, **2013**.
- [30] H. Y. Jang, J. B. Hong and D. W. C. MacMillan, *J. Am. Chem. Soc.*, vol. 129, pp. 7004, **2007**.
- [31] D. A. Nicewicz and D. W. C. MacMillan, *Science*, vol. 322, pp. 77, **2008**.
- [32] S. Lin, M. A. Ischay, C. G. Fry and T. P. Yoon, *J. Am. Chem. Soc.*, vol. 133, pp. 19350, **2011**.
- [33] A. McNally, C. K. Prier and D. W. C. MacMillan, *Science*, vol. 334, pp. 1114, **2011**.
- [34] D. Hager and D. W. C. MacMillan, *J. Am. Chem. Soc.*, vol. 136, pp. 16986, **2014**.
- [35] J. Jin and D. W. C. MacMillan, *Angew. Chem. Int. Ed.*, vol. 53, pp. 1, **2014**.
- [36] I. Ghosh, T. Ghosh, B. Javier and B. König, *Science*, vol. 346, pp. 725, **2014**.
- [37] A. Mills and S. L. Hunte, *J. Photochem. Photobiol. A*, vol. 108, p. 1, **1997**.
- [38] D. Friedmann, A. Hakki, H. Kim, W. Choi and D. Bahnemann, *Green Chem.*, vol. 18, p. 5391, **2016**.
- [39] J. Chen, J. Cen, X. Xu and X. Li, *Catal. Sci. Technol.*, vol. 6, p. 349, **2016**.
- [40] T. Kawai and T. Sakata, *Nature*, vol. 286, p. 474, **1980**.
- [41] M. Fujihira, Y. Satoh and T. Osa, *Nature*, vol. 293, p. 259, **1981**.

- [42] H. Yoshida, H. Yuzawa, M. Aoki, K. Otake, H. Itoh and T. Hattori, *Chem. Commun.*, p. 4634, **2008**.
- [43] S. Furukawa, T. Shishido, K. Teramura and T. Tanaka, *ACS Catal.*, vol. 2, p. 175, **2012**.
- [44] V. Brezova, A. Blazkova, I. Surina and B. Havlinova, *J. Photochem. Photobiol. A*, vol. 107, p. 233, **1997**.
- [45] H. Tada, A. Takao, T. Akita and K. Tanaka, *ChemPhysChem*, vol. 7, p. 1687, **2006**.
- [46] K. Imamura, K. Hashimoto and H. Kominami, *Chem. Commun.*, vol. 48, p. 4356, **2012**.
- [47] H. Reiche and A. Bard, *J. Am. Chem. Soc.*, vol. 101, p. 3127, **1979**.
- [48] S. Nishimoto, B. Ohtani, T. Yoshikawa and T. Kagiya, *J. Am. Chem. Soc.*, vol. 105, p. 7180, **1983**.
- [49] B. Ohtani, S. Tsuru, S. Nishimoto, T. Kagiya and K. Izawa, *J. Org. Chem.*, vol. 55, p. 5551, **1990**.
- [50] H. Wang, R. E. Partch and Y. Li, *J. Org. Chem.*, vol. 62, p. 5222, **1997**.
- [51] K. Selvam, B. Krishnakumar, R. Velmurugan and M. Swaminathan, *Catal. Commun.*, vol. 11, p. 280, **2009**.
- [52] H. Yuzawa, J. Kumagai and H. Yoshida, *J. Phys. Chem. C*, vol. 117, p. 11047, **2013**.
- [53] T. Coronna, C. Gambarotti, C. Punta and F. Recupero, *Chem. Commun.*, p. 2350, **2003**.
- [54] T. Coronna, C. Gambarotti, L. Palmisano, C. Punta and F. Recupero, *J. Photochem. Photobiol. A: Chem.*, vol. 171, p. 237, **2005**.
- [55] H. Yoshida, Y. Fujimura, H. Yuzawa, J. Kumagai and T. Yoshida, *Chem. Commun.*, vol. 49, p. 3793, **2013**.
- [56] E. Wada, T. Takeuchi, Y. Fujimura, A. Tyagi and H. Yoshida, *Catal. Sci. Technol.*, vol. 7, p. 2457, **2017**.
- [57] C. Wang and D. Astruc, *Chem. Soc. Rev.*, vol. 43, p. 7188, **2014**.
- [58] S. Linic, P. Christopher, H. Xin and A. Marimuthu, *Acc. Chem. Res.*, vol. 46, p. 1890, **2013**.

- [59] M. J. Kale, T. Avanesian and P. Christopher, *ACS Catal.*, vol. 4, p. 116, **2014**.
- [60] K. Awazu, M. Fujimaki, C. Rockstuhl, J. Tominaga, H. Murakami, Y. Ohki, N. Yoshida and T. Watanabe, *J. Am. Chem. Soc.*, vol. 130, p. 1676, **2008**.
- [61] P. Wang, B. Huang, X. Qin, X. Zhang, Y. Dai, J. Wei and H. Whangbo, *Angew. Chem. Int. Ed.*, vol. 47, p. 7931, **2008**.
- [62] X. Zhou, G. Liu, J. Yu and W. Fan, *J. Mater. Chem.*, vol. 22, p. 21337, **2012**.
- [63] D. D. Evanoff Jr. and G. Chumanov, *Chem. Phys. Chem.*, vol. 6, p. 1221, **2005**.
- [64] X. C. Ma, Y. Dai, L. Yu and B. B. Huang, *Light Sci. Appl.*, vol. 5, p. 16017, **2016**.
- [65] X. Chen, H. Y. Zhu, J. C. Zhao, Z. F. Zheng and X. P. Gao, *Angew. Chem. Int. Ed.*, vol. 47, p. 5353, **2008**.
- [66] G. L. Hallett-Tapley, M. J. Silvero, C. J. Bueno-Alejo, M. Gonzalez-Bejar, C. D. McTiernan, M. Grenier, J. C. Netto-Ferreira and J. C. Scaiano, *J. Phys. Chem. C*, vol. 117, p. 12279, **2013**.
- [67] H. Zhu, X. Ke, X. Yang, S. Sarina and H. Liu, *Angew. Chem. Int. Ed.*, vol. 49, p. 9657, **2010**.
- [68] X. B. Ke, X. G. Zhang, J. Zhao, S. Sarina, J. Barry and H. Y. Zhu, *Green Chem.*, vol. 15, p. 236, **2013**.
- [69] M. Gonzalez-Bejar, K. Peters, G. L. Hallett-Tapley, M. Grenier and J. C. Scaiano, *Chem. Commun.*, vol. 49, p. 1732, **2013**.
- [70] P. Christopher, H. Xin and S. Linic, *Nat. Chem.*, vol. 3, p. 467, **2011**.
- [71] S. Sarina, H. Zhu, E. Jaatinen, Q. Xiao, H. Liu, J. Jia, C. Chen and J. Zhao, *J. Am. Chem. Soc.*, vol. 135, p. 5793, **2013**.
- [72] Q. Xiao, S. Sarina, A. Bo, J. Jia, H. Liu, D. P. Arnold, Y. Huang, H. Wu and H. Zhu, *ACS Catal.*, vol. 4, p. 1725, **2014**.
- [73] Q. Xiao, S. Sarina, E. Jaatinen, J. Jianfeng, D. P. Arnold, H. Liu and H. Zhu, *Green Chem.*, vol. 16, p. 4272, **2014**.
- [74] J. Sun, X. Li, Q. Zhao, J. Ke and D. Zhang, *J. Phys. Chem. C*, vol. 118, p. 10113, **2014**.

- [75] K. Pingmuang, J. Chen, W. Kangwansupamonkon, G. G. Wallace, S. Phanichphant and A. Nattestad, *Sci. Rep.*, vol. 7, **2017**.
- [76] H. Zhang, X. Lv, Y. Li, Y. Wang and J. Li, *ACS Nano*, vol. 4, p. 380, **2010**.
- [77] J. Chen, H. Zhang, P. Liu, Y. Liu, X. Liu, G. Li, P. K. Wong, T. An and H. Zhao, *Appl. Catal. B*, vol. 168, p. 266, **2015**.
- [78] I. V. Lightcap, T. H. Kosel and P. V. Kamat, *Nano Lett.*, vol. 10, p. 577, **2010**.
- [79] Q. Li, B. Guo, J. Yu, J. Ran, B. Zhang, H. Yan and J. R. Gong, *J. Am. Chem. Soc.*, vol. 133, p. 10878, **2011**.
- [80] Z. Chen, S. Liu, M. Q. Yang and Y. J. Xu, *ACS Appl. Mater. Interfaces*, vol. 5, p. 4309, **2013**.
- [81] N. Qin, Y. Liu, W. Wu, L. Shen, X. Chen, Z. Li and L. Wu, *Langmuir*, vol. 31, p. 1203, **2015**.
- [82] W. Liu, C. Wang and L. Wang, *Ind. Eng. Chem. Res.*, vol. 56, p. 6114, **2017**.

Chapter II Metal loaded titanium oxide photocatalysts for carbon-carbon cross-coupling between hydrocarbons and ethers

II-1. Introduction

Ethers are an important chemical feedstock and commonly used as solvents in organic chemistry. They are also found in various organic compounds used in medicines and as chemical intermediates.¹⁻⁴ However, the direct construction of ether moiety in an organic compound is a challenging task and often involves multiple steps. So, construction of new C–C bonds from the C–H bond in ether molecules is a promising strategy to incorporate them into organic compounds.

Numerous methods have been developed to perform this important reaction but they have some drawbacks like excess use of base, organometallic catalyst, high reaction temperature, and so on.⁵⁻⁹ Hence, it is important to develop a sustainable reaction methodology. Recently, the use of heterogeneous photocatalysis is receiving a lot of attention as a promising technique for organic synthesis.¹⁰⁻¹² The photogenerated electrons and holes can activate various organic molecules at room temperature which provides a green route for organic synthesis. Among the different photocatalysts, TiO₂ stands out because of its high photocatalytic activity, stability, and less-toxicity. Several organic reactions like photocatalytic aromatic hydroxylation,^{13,14} amination,^{15,16} cyanomethylation^{17,18} and much more have been successfully carried out by using TiO₂ photocatalysis.

In the present study, we have focused on the cross-coupling between ethers and different hydrocarbons like arenes,¹⁹ alkanes,²⁰ and alkenes,²¹ by the direct activation of their C–H bonds with metal loaded TiO₂ photocatalysts. All reactions were carried out at room temperatures without any additional chemicals like base, solvent or oxidizing agent. Appreciable product yields were obtained in some reactions indicating that the TiO₂ photocatalysis is a useful technology for organic synthesis. A systematic study was carried out for each system to elucidate the mechanism and the role of metal nanoparticles and TiO₂ photocatalyst in these reactions. The results suggested that the metal nanoparticles have two roles: an electron receiver

and a catalyst, and these roles vary with the substrates employed for the reaction.

References

- [1] P. G. Wuts and T. W. Greene, "Protective Groups in Organic Synthesis," New York, Wiley & Sons, **2007**, pp. 102-120.
- [2] P. P. Pradhan, J. M. Bobbitt and W. F. Bailey, *J. Org. Chem.*, vol. 74, pp. 9524, **2009**.
- [3] C. E. Rye and D. Barker, *Synlett*, p. 3315, **2009**.
- [4] V. Mammoli, A. Bonifazi, F. Del Bello, E. Diamanti, M. Giannella, A. L. Hudson, L. Mattioli, M. Perfumi, A. Piergentili, W. Quaglia, F. Titomanlio and M. Pigini, *Bioorg. Med. Chem.*, vol. 20, p. 2259, **2012**.
- [5] H. M. L. Davies, T. Hansen and M. R. Churchill, *J. Am. Chem. Soc.*, vol. 122, p. 3063, **2000**.
- [6] P. P. Singh, S. Gudup, H. Aruri, U. Singh, S. Ambala, M. Yadav, S. D. Sawant and R. A. Vishwakarma, *Org. Biomol. Chem.*, vol. 10, p. 1587, **2012**.
- [7] D. Liu, C. Liu, H. Li and A. Lei, *Angew. Chem. Int. Ed.*, vol. 52, p. 4453, **2013**.
- [8] R. P. Pandit and Y. R. Lee, *Adv. Synth. Catal.*, vol. 356, p. 3171, **2014**.
- [9] R. Parella and S. A. Babu, *J. Org. Chem.*, vol. 80, p. 2339, **2015**.
- [10] M. Fagnoni, D. Dondi, D. Ravelli and A. Albini, *Chem. Rev.*, vol. 107, p. 2725, **2007**.
- [11] H. Yoshida, P. V. Kamat and M. Anpo, *Environmentally benign photocatalysts: Applications of titanium oxide-based material*, Springer, **2010**.
- [12] G. Palmisano, V. Augugliaro, M. Pagliaro and L. Palmisano, *Chem. Commun.*, p. 3425, **2007**.
- [13] H. Yoshida, H. Yuzawa, M. Aoki, K. Otake, H. Itoh and T. Hattori, *Chem. Commun.*, p. 4634, **2008**.
- [14] H. Yuzawa, M. Aoki, K. Otake, T. Hattori, H. Itoh and H. Yoshida, *J. Phys. Chem. C*, vol. 116, p. 25376, **2012**.

- [15] H. Yuzawa and H. Yoshida, *Chem. Commun.*, vol. 46, p. 8854, **2010**.
- [16] H. Yuzawa, J. Kumagai and H. Yoshida, *J. Phys. Chem. C*, vol. 117, p. 11047, **2013**.
- [17] H. Yoshida, Y. Fujimura, H. Yuzawa, J. Kumagai and T. Yoshida, *Chem. Commun.*, vol. 49, p. 3793, **2013**.
- [18] A. Tyagi, T. Matsumoto, T. Kato and H. Yoshida, *Catal. Sci. Technol.*, vol. 6, p. 4577, **2016**.
- [19] E. Wada, T. Takeuchi, Y. Fujimura, A. Tyagi, T. Kato and H. Yoshida, *Catal. Sci. Technol.*, vol. 7, p. 2457, **2017**.
- [20] A. Tyagi, A. Yamamoto, T. Kato and H. Yoshida, *Catal. Sci. Technol.*, vol. 7, p. 2616, **2017**.
- [21] A. Tyagi, A. Yamamoto, M. Yamamoto, T. Yoshida and H. Yoshida, *submitted*.

II-2. Photocatalytic cross-coupling between arenes and ethers

Abstract

A Pd loaded TiO₂ photocatalyst successfully catalyzed the sp²C–sp³C cross-coupling between different arene molecules and ethers to give alpha arylated ethers. For un-substituted benzene, the selectivity for the cross-coupling product was more than 99%. The reaction between benzene and diethyl ether (DEE) was studied in detail by using various techniques like ESR spectroscopy, kinetic experiments, and temperature control reactions. Based on those results, a radical addition-elimination pathway was proposed for the cross-coupling reaction: The TiO₂ photocatalyst oxidizes DEE molecule to make radicals which attacks the benzene molecule with the assistance of Pd nanoparticles as metal catalyst. Thus, the reaction was a hybrid of TiO₂ photocatalysis and Pd metal catalysis.

1. Introduction

Straightforward C–C bond formation from the abundant sp³C–H bonds under mild conditions is one of the most desirable reactions in synthetic organic chemistry. However, these sp³C–H bonds have low reactivity due to high stability. Hence, this reaction is one of the biggest challenges in current synthetic chemistry. In the present work, we have employed a heterogeneous TiO₂ photocatalyst to carry out the cross-coupling between various arenes and ethers. Although there are various C–H bonds in ethers, only those at alpha position were selectively activated, which resulted in selective formation of alpha arylated ethers. These products are an important class of compounds and are also found in natural products and pharmaceuticals drugs. Thus, an extensive research is going on to develop safe and mild synthesis processes for the preparation of arylated ethers. There are some reports about the photocatalytic synthesis of arylated ethers.^{1,2} Qvortrup *et. al.* used an Ir based homogeneous photocatalyst to carry out the arylation of benzylic ethers.¹ Although the reaction exhibited a broad substrate scope, it had some limitations like catalyst recovery and use of additional solvents to name a few. Caronna *et. al.* used a heterogeneous TiO₂ photocatalyst to carry out the alpha arylation of ethers.² However, appreciable product yields could be obtained only after the usage of hydrogen peroxide. As these reported methods have some limitations, there

is still room for improvement in the reaction techniques. In the present work, we have found that a safe and abundant heterogeneous TiO₂ photocatalyst, loaded with metal nanoparticles, could successfully catalyze this reaction at room temperature. Also, we succeeded in obtaining substantial product yields without using any excess solvent or additives. The reaction between benzene and DEE was systematically studied and temperature controlled reactions and a tentative mechanism was proposed.

2. Experimental section

2.1. Preparation of catalysts

The metal loaded TiO₂ samples (M(*x*)/TiO₂, *x*: loading amount of metal, M, in weight %) were prepared by a photodeposition method by using the desired TiO₂ sample and the metal precursor solution. The various TiO₂ samples were obtained from the Catalysis Society of Japan as JRC-TIO-8 (anatase phase, 338 m²g⁻¹), JRC-TIO-6 (rutile phase, 100 m²g⁻¹) and JRC-TIO-4 (a mixture of rutile and anatase phase, 50 m²g⁻¹). The various metal precursor solution used were PdCl₂ (Kishida 99%) for Pd, H₂PtCl₆.6H₂O (Wako Pure Chemicals, 99.9%) for Pt, RhCl₃.3H₂O (Kishida 99%) for Rh, and HAuCl₄.4H₂O (Kishida 99.9%), for Au. To prepare the samples, 4 g of the TiO₂ powder was dispersed in ion-exchanged water (300 ml) and irradiated for 30 min from a ceramic xenon lamp (PE300 BUV). Then, 100 ml methanol and desired amount of the aqueous solution of the metal precursor were added to the suspension and the contents were stirred for 15 min without irradiation, followed by 1 h stirring under the light. It was then filtered off with suction, washed with ion-exchanged water, and dried at 323 K for 12 h to get the metal loaded TiO₂ samples, M(*x*)/TiO₂, where M indicates the loaded metal, and *x* indicates its loading amount in weight %.

2.2. Characterization of catalysts

The prepared M(*x*)/TiO₂ samples were characterized by different techniques. Powder X-ray diffraction (XRD), CO pulse adsorption, and X-ray absorption fine structure (XAFS) were used to determine the size, dispersion, and electronic state of Pd on TiO₂ in the Pd(*x*)/TiO₂ sample. XRD measurements were carried out on Shimadzu XRD-6000. CO pulse adsorption tests were carried out on a self-constructed experimental set-up. The procedure involved reduction of the M(*x*)/TiO₂ (M: Pd and Pt) samples, as pre-treatment, under hydrogen (11%) and argon mixture at 473 K for 15 min followed by cooling to room temperature in argon (100%). The CO

analysis was done by a GC coupled with a TCD (Shimadzu, GC-8A). Pd K-edge XAFS spectra were recorded at NW10A of Photon Factory at the Institute of Materials Structure Science, High Energy Accelerator Research Organization (KEK-PF, Tsukuba Japan) with a Si(311) double-crystal monochromator at room temperature. The spectra of the reference samples (Pd metal and PdO) were measured in a transmission mode while the Pd(x)/TiO₂ sample was measured in fluorescence mode by using a Lytle detector filled a Kr(100%) flow and having a Ru filter ($\mu t = 6$) for fluorescence and an ion chamber filled with an Ar(100%) flow for the incident X-ray. The obtained spectra were analyzed with a REX 2000 software (Rigaku).³

2.3. Photocatalytic activity tests

2.3.1. Materials

All chemicals were of analytical grade and were used without further purification; benzene (Nacalai Tesque, >99%), diethyl ether (DEE) (Wako Pure Chemicals, >99%), butyl methyl ether (TCI Research Chemicals, >99%), tetrahydrofuran (Wako Pure Chemicals, 99%), tetrahydropyran (Wako Pure Chemicals, >99%), aniline (Kishida Chemical, >99%), toluene (Nacalai Tesque, 99%), benzonitrile (Kishida Chemical, >99%), diethyl ether-*d*₁₀ (Cambridge Isotope Laboratories, Inc. Stable Isotopes, 99.5%), benzene-*d*₆ (Cambridge Isotope Laboratories, Inc. Stable Isotopes, 99%), 1-ethoxyethylbenzene (**1a**) (Princeton Building Blocks, 99%). An authentic sample of 4-(tetrahydrofuran-2yl)benzonitrile was prepared by a method reported in the literature.⁴

2.3.2. Procedure for the photocatalytic activity tests

The prepared M(x)/TiO₂ samples were tested for the cross-coupling between arenes and ethers. The reactions were carried out in a Pyrex test tube using the xenon lamp as the light source. The wavelength of the irradiated light was limited by using a long pass optical filter. In a typical reaction, 100 mg of the M(x)/TiO₂ sample was taken in the Pyrex test tube and pre-treated for 60 min under the xenon lamp light. Then, the test tube was sealed with a silicon septum and purged with argon gas for 10 min. followed by the addition of the reactants (arene and ether). Then, the suspension was stirred with irradiation for desired time. After the completion of the reaction time, a part of the gaseous phase was collected in an air-tight syringe and analyzed by GC (Shimadzu, GC-8A) coupled with TCD.

The liquid phase was diluted by ethanol, filtered by a syringe having PTFE filter, and analyzed by GC-MS (Shimadzu, GCMS-QP5050A). To test the stability and longtime activity of $M(x)/TiO_2$ samples, some reactions were carried out in a fixed-bed flow reactor. Figure 1 shows the experimental set-up. The $Pd(0.2)/TiO_2$ sample (0.1 g) was mixed with quartz sand and transferred to a quartz cell ($60 \times 20 \times 1 \text{ mm}^3$). It was pretreated with light irradiation from a UV LED ($\lambda = 365 \text{ nm}$) for 1 h and argon purging for 20 min. Then, the reaction mixture, comprising of 1.4 ml (15.7 mmol) benzene and 6.5 ml (62.5 mmol) DEE was introduced to the catalyst bed at a constant flow rate of 6 ml h^{-1} with continuous light irradiation. After the reaction mixture had completely wet the catalyst bed, time recording was started. At the end of each hour, the mixture at the outlet was collected, diluted with ethanol, and analyzed by GC-MS. To test the reusability of the $Pd(0.2)/TiO_2$ sample, the reactor was removed from the flow system, left as it was overnight for drying in air and used for experiments on the next day.

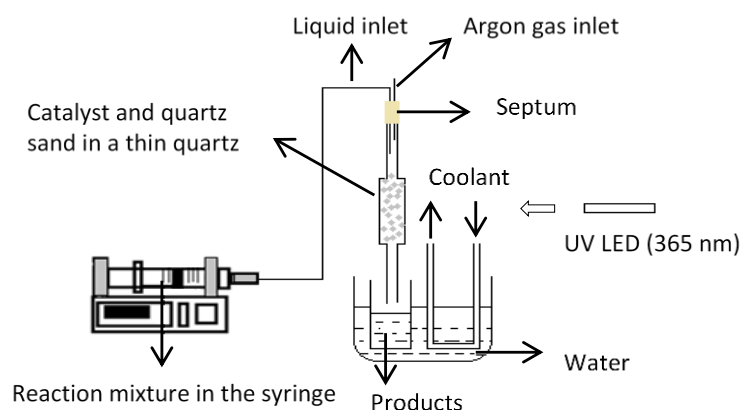


Figure 1 Pictorial representation of the fixed-bed flow reactor

2.4. Mechanistic studies

Different experimental techniques were used to elucidate the mechanism of the photocatalytic cross-coupling reaction between arenes and ethers. ESR spectroscopy confirmed the formation of the ether radicals during the photocatalytic reaction. These measurements were carried out at room temperature with an X-band spectrometer (JEOL-RE2X) by using JEOL's TE011 cavity for the samples. N-tert-butyl- α -phenylnitron (PBN) was used as a spin trapping agent. A suspension of PBN (0.09 g), DEE (1 ml), and the $Pd(0.1)/TiO_2$ sample (0.02 g) was prepared and introduced into the ESR cavity. The contents were irradiated from a xenon lamp (Asahi Spectra MAX-

150) emitting light of wavelength more than 400 nm through a long-pass filter for 20 min with simultaneous ESR measurement. Kinetic experiments carried out with deuterated reagents clarified the rate determining step of the reaction. Temperature control reactions revealed the role of the Pd nanoparticles loaded on the TiO₂ photocatalyst. The photocatalytic reactions were carried out at different temperatures, maintained by a water bath, while the products were analyzed at room temperature.

3. Results and discussion

3.1. Catalyst characterization

Powder XRD: Figure 2 shows the powder XRD pattern of the Pd(0.1)/TiO₂ (JRC TI08-ST01) sample prepared by a photodeposition method. The patterns were assigned to anatase phase of TiO₂ (ICSD Coll. Code 9161). No diffraction lines assignable for Pd were visible in the pattern, which suggested that the Pd nanoparticles might be very small and well dispersed on the TiO₂ surface.

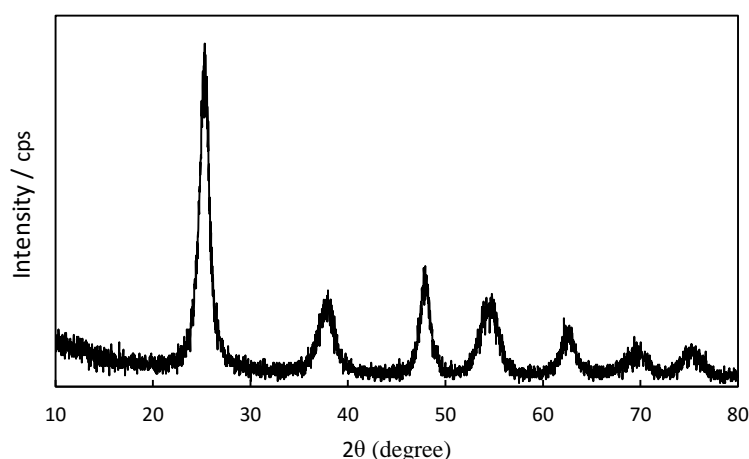


Figure 2 Powder XRD pattern of the Pd(0.1)/TiO₂ sample

CO pulse adsorption: Table 1 shows the results of the CO pulse adsorption experiments performed with Pd and Pt loaded M(x)/TiO₂ samples. It was suggested that well dispersed small nanoparticles were obtained for Pt in the sample (Table 1, entry 1). When compared to Pt, Pd had a poorer dispersion and larger particle size (Table 1, entry 2).

Table 1 Results of CO pulse adsorption experiments with the Pd and Pt loaded M(x)/TiO₂ samples

Entry	Sample	Metal dispersion	Particle size (nm)
1	Pt(0.1)/TiO ₂	42.6	2.7
2	Pd(0.1)/TiO ₂	19.8	5.6

X-ray Absorption Fine Structure (XAFS): Pd K-edge XAFS measurements were carried out to determine the electronic state of Pd nanoparticles on the surface of the Pd(0.2)/TiO₂ sample after the photocatalytic tests. Figure 3 shows the normalized XANES spectra. The XANES feature of the Pd nanoparticles in the Pd(0.2)/TiO₂ sample obtained after the photocatalytic reaction were similar to that of Pd foil and much different from that of PdO (Figure 3A). The value of the absorption edge in this sample (24.337 keV) was lower than those for Pd metal (24.346 keV) and PdO (24.349 keV), suggesting that the Pd species in this sample might be metallic and electron rich (Figure 3B). This could be explained by the capability of the noble metal nanoparticles like Pd to act as electron receiver on the TiO₂ surface.⁵ When these nanoparticles are loaded on the TiO₂ surface, a heterojunction is created to align the Fermi level of the TiO₂ and the metal, which can be achieved by the transfer of the electrons from TiO₂ to the metal. This results an increase of the electron density of the metal nanoparticles. The XANES results imply that the Pd nanoparticles can efficiently function as electron receiver on the TiO₂ surface.

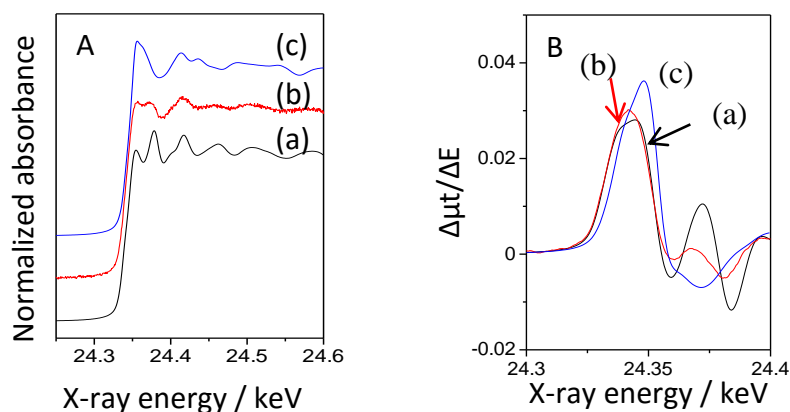


Figure 3 (A) Normalized Pd K-edge XANES spectra and (B) differential curves for the XANES spectra of (a) Pd foil, (b) the Pd(0.2)/TiO₂ sample obtained after the photocatalytic reaction, and (c) PdO.

Fourier transform of the EXAFS region was carried out to understand the local structure of Pd in the Pd(0.2)/TiO₂ sample (Figure 4 and Table 2). The theoretical curves of Teo and Lee were used for the fitting of Pd foil EXAFS, which gave a coordination number of 12. However, it wasn't the case for other samples like Pd(0.2)/TiO₂ and so, the coordination number was 3.7. This result shows the deviation from the theory. The peaks around 2.5 Å in Pd foil and the Pd(0.2)/TiO₂ sample were assigned to Pd-Pd shell (Figure 4

spectra (a) and (b)). Further, the peaks at 1.6 Å and 3.0 Å in PdO were assigned to Pd–O shell and Pd–Pd shell, respectively (Figure 4, spectra (c)).

Table 2 Results of the curve fitting analysis of the Fourier transformed EXAFS ^a

Sample	Shell	Coordination number	Interatomic distance (Å)	Debye-Waller factor
Pd	Pd–Pd	12	2.74	0.079
Pd(0.2)/TiO ₂ ^b	Pd–O	1.5	2.02	0.062
	Pd–Pd	3.9	2.76	0.075
PdO	Pd–O	3.7	2.02	0.073
	Pd–Pd	4.9	3.06	0.074
	Pd–Pd	4.9	3.43	0.065

^a The region of EXAFS used for Fourier transform was (a) 4.05–12.15 Å⁻¹ (b) 3.3–11.5 Å⁻¹ and (c) 3.85–12.05 Å⁻¹, respectively, and the region for the inverse Fourier transform was (a) 1.69–3.04 Å⁻¹, (b) 1.32–3.04 Å⁻¹ and (c) 1.11–3.74 Å⁻¹, respectively. ^b The sample was recovered after the photocatalytic reaction test.

The appearance of the Pd–Pd shell in the Pd(0.2)/TiO₂ sample supports the proposal that the Pd nanoparticles in this samples were metallic. The peak at 1.5 Å visible in the Pd(0.2)/TiO₂ sample was assigned to the Pd–O shell. Table 2 shows the fitting analysis. These results suggested that the metallic Pd species was connected to the TiO₂ surface via the oxygen atoms. So, it was concluded that the Pd nanoparticles in the Pd/TiO₂ samples were metallic and electron rich.

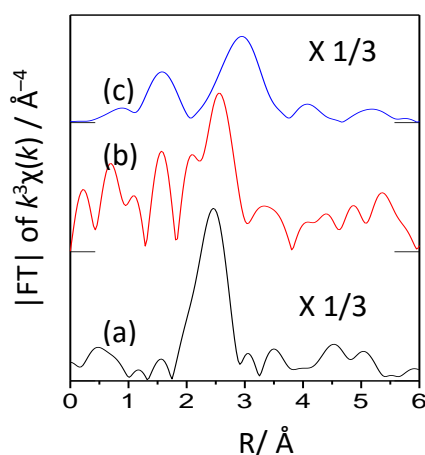


Figure 4 Fourier transforms (FT) of k^3 -weighted EXAFS of (a) Pd foil, (b) the Pd(0.2)/TiO₂ sample obtained after the photocatalytic reaction, and (c) PdO. The intensity of the FT of the reference samples (Pd foil and PdO) was reduced to one third.

Pd loaded sample gave the largest yield of the cross-coupling product (Table 4, entry 1). The loading amount of Pd on TiO₂ was varied, which revealed that 0.2 wt.% was the optimum value (Table 4, entries 1 and 5–7). The reactions done in dark or without the M(x)/TiO₂ sample did not yield any product, confirming that the reaction was photocatalytic (Table 4, entries 8 and 9). Further, the reaction done with pristine TiO₂ (JRC-TIO-8) sample gave a very low yield of **1a** and **1b** indicating the importance of metal loading (Table 4, entry 10). After optimizing the reaction conditions, we achieved 23% yield of **1a** within 3 hours with 99% selectivity (Table 4, entry 11). Increasing the reaction time to 5 hours was not helpful to achieve higher product yield. One possible reason could be the adsorption of the products on the M(x)/TiO₂ photocatalyst's surface which might block the active sites and inhibit the reaction. This is a limitation of the closed reactors, like the one used in the present study. To overcome this problem and test the photocatalyst's stability, reactions were carried out in a fixed-bed flow reactor. Figure 5 shows the results of those experiments. The reaction rate for the formation of the product did not decrease for at least 7 hours and the reaction proceeded for several hours (Figure 5a), which shows the stability of the Pd(0.2)/TiO₂ photocatalyst for a long time. After the day's experiment, the photocatalyst was removed and left overnight in the air for natural drying. Next day, the same sample was used for the reactions in the same set-up without any pretreatment. Figure 5b shows the result of the experiments. Although the reaction rate was slower than the previous experiments done with the fresh photocatalyst, the reaction constantly proceeded for at least ten hours indicating the reusability of the photocatalyst. One explanation for the slower reaction rate observed in the reusability tests can be the strong adsorption of the chemicals on the photocatalyst's surface which could not be removed in the present conditions and might require pretreatment.

3.2.2. Reaction between benzene and different ethers

Under the optimized reaction conditions, we explored the scope of the ether substrates suitable for this photocatalytic cross-coupling reaction with benzene (Table 5). Both acyclic and cyclic ethers successfully underwent this cross-coupling reaction (Table 5, entries 1–3). Reaction with butyl methyl ether gave two products (**2a** and **2b**), while the cyclic ethers gave only one product (**3a** and **4a**). Interestingly, irrespective of their structure, all ethers gave the alpha substituted compound as the main product of the cross-

coupling reaction indicating that the photocatalyst selectively activated the α C-H bond in all ethers.

Table 4 Cross-coupling reaction between benzene and DEE with different M(x)/TiO₂ samples ^a

Entry	M(x)/TiO ₂ Sample	Products (μmol)		Selectivity	Yield ^b
		1a	1b		
1	Pd(0.1) /TiO ₂	18.8	0.3	98	0.057
2	Pt(0.1) /TiO ₂	1.8	0.2	90	0.005
3	Rh(0.1) /TiO ₂	1.6	0.2	88	0.005
4	Au(0.1) /TiO ₂	0.0	0.0	0	0.000
5	Pd(0.05) /TiO ₂	10.8	0.2	98	0.034
6	Pd(0.2) /TiO ₂	19.2	0.4	98	0.060
7	Pd(0.5) /TiO ₂	12.8	0.1	99	0.040
8 ^c	Pd(0.1) /TiO ₂	0.0	0.0	0	0.000
9 ^d	–	0.0	0.0	0	0.000
10 ^e	TiO ₂	0.6	0.1	86	0.001
11 ^f	Pd(0.2)/TiO ₂	12.9	Trace	99	23.035

^a Light intensity = 40 mW cm⁻² (at 365 \pm 20 nm), reaction temperature was 304 K, other conditions were same as Table 3. ^b Yield of **1a** calculated as 100 \times (amount of **1a**)/(initial amount of benzene). ^c Reaction was done in dark. ^d Reaction was done without the M(x)/TiO₂ sample. ^e 0.1 g of the pristine TiO₂ (JRC-TIO-8) sample was used for the reaction. ^f 5 μl (56 μmol) of benzene, 2 ml (19.2 mmol) of DEE and 0.4 μl of water, reaction time was 3 h.

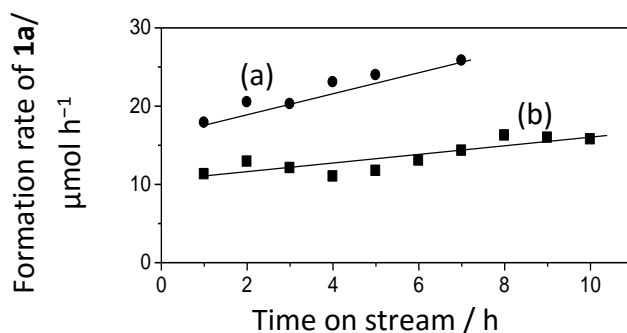


Figure 5 Results of the reaction tests in a fixed-bed flow reactor

This selectivity can be explained by the C–H bond dissociation energies in the ethers (Figure 6).⁶ Due to a lower bond dissociation energy of the α C–H bond than β , its oxidation is fast. Further, due to proximity to oxygen, the alpha-alkoxy radical produced by the photocatalyzed oxidation is more stable than the beta radical, thus the reaction selectively gives the alpha substituted product.

Table 5 Scope of ethers for the cross-coupling with benzene by using the Pd(0.2)/TiO₂ photocatalyst ^a

Ether Alpha substituted product

Entry	Ether	Product (μmol) ^b	Selectivity	Yield
1 ^c	Butyl methyl ether	 2a (4.1 μmol) 2b (7.9 μmol)	99	1.1
2 ^d	Tetrahydrofuran	 3a (4.1 μmol)	99	18
3 ^e	Tetrahydropyran	 4a (16.8 μmol)	99	30

^a All reaction conditions were same as Table 3. ^b The amount of all products was approximately determined from the calibration curve of **1a**. ^c 100 μl (1.12 mmol) of benzene, 0.35 ml (1.19 mmol) of butyl methyl ether and 0.4 μl of water were used for 1 h reaction; %S= [100 X (sum of the amount of **2a** and **2b** (μmol))/(total amount of benzene containing products)]. ^d 5 μl (56 μmol) of benzene, 2 ml (20 mmol) of tetrahydrofuran and 0.4 μl of water were used for 3 h reaction. ^e 2 μl (22 μmol) of benzene, 1 ml (12 mmol) of tetrahydropyran and 0.4 μl of water were used for 3 h reaction.

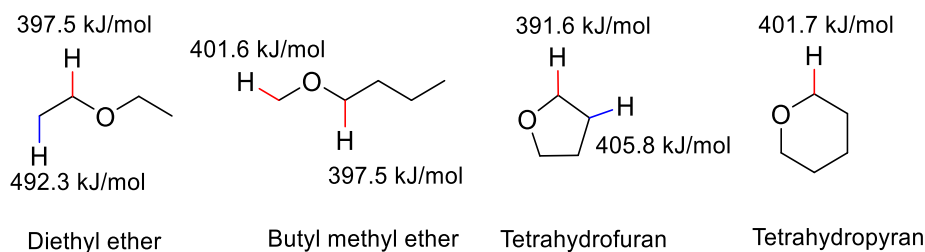


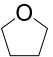
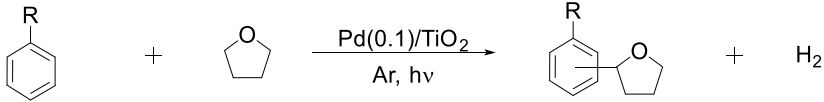
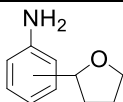
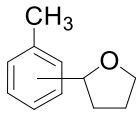
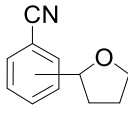
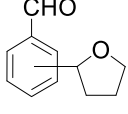
Figure 6 C–H bond dissociation energies in the ethers screened for the photocatalytic cross-coupling with benzene

3.2.3. Reaction between substituted benzenes and tetrahydrofuran

After screening the ether, we examined different arenes for the photocatalytic cross-coupling between arenes and ethers. Table 6 shows the results of the reaction between different substituted benzene and tetrahydrofuran done with the Pd(0.1)/TiO₂ photocatalysts. The reaction gave a mixture of ortho, meta, and para-substituted cross-coupling products and the amount indicated in Table 6 shows the total amount of all cross-coupling products. The reaction between aniline and THF gave a mixture of 2-(tetrahydrofuran-2-yl)aniline and 4-(tetrahydrofuran-2-yl)aniline

(collectively shown as **5a**) as cross-coupling products (Table 6, entry 1) along with the homocoupling products of aniline namely, 2-diphenyldiazene, probably formed by the oxidation of aniline by the photogenerated holes on TiO₂.⁷ The reaction between toluene and THF gave a mixture of 2-(o-tolyl)tetrahydrofuran, 2-(m-tolyl)tetrahydrofuran, and 2-(p-tolyl)tetrahydrofuran (shown collectively as **6a**) as the cross-coupling products (Table 6, entry 2), along with the oxidation products of toluene namely, benzaldehyde and benzyl alcohol. These products might have been formed by the surface OH groups of TiO₂ or the water contamination in the starting materials.⁸ The reaction between benzonitrile and THF gave a mixture of 2-(tetrahydrofuran-2-yl)benzonitrile, 3-(tetrahydrofuran-2-yl)benzonitrile, and 4-(tetrahydrofuran-2-yl)benzonitrile (collectively shown as **7a**) as cross-coupling products (Table 6, entry 3).

Table 6 Scope of arenes for the photocatalytic cross-coupling with ether by using the Pd(0.1)/TiO₂ photocatalyst ^a

Entry	Substituted benzene	Tetrahydrofuran	Cross-coupling products
1	Aniline (R: NH ₂) (21.9 mmol)		 Product (μmol) ^b  5a (0.65)
2	Toluene (R: CH ₃) (19.0 mmol)		 6a (0.41)
3	Benzonitrile (R: CN) (19.4 mmol)		 7a (5.31)
4	Benzaldehyde (R: CHO) (19.9 mmol)		 8a (107.4)

^a 2 ml tetrahydrofuran and 50 mg of the Pd(0.1)/TiO₂ photocatalyst was used for 3 h reaction. Other conditions were same as Table 3. ^b The total amount of all cross-coupling products is mentioned which was approximately determined by GC-MS by using the calibration curve of 4-(tetrahydrofuran-2-yl)benzonitrile.

The reaction between benzaldehyde and THF gave a mixture of 2-(tetrahydrofuran2-yl)benzaldehyde, 3-(tetrahydrofuran2-yl)benzaldehyde, and 4-(tetrahydrofuran2-yl)benzaldehyde (collectively shown as **8a**) as cross-coupling products (Table 6, entry 4), along with oxidation and reduction products of benzaldehyde namely benzoic acid and benzyl alcohol. These products might be formed by a direct reaction of benzaldehyde with the photogenerated holes and electrons on TiO₂. Thus, various mono-substituted benzene successfully underwent the photocatalytic cross-coupling with THF by using a Pd/TiO₂ photocatalyst, indicating a good substrate scope.

3.3. Mechanistic studies

After establishing the reaction, we focused on the investigation of the mechanism. The following sections discuss the results of mechanistic studies by using some techniques.

3.3.1. ESR Spectroscopy

The first step to study the reaction mechanism was the elucidation of the oxidation of the ether by the photogenerated holes on TiO₂ photocatalyst. As mentioned before, the reaction between benzene and DEE gave small amount of homocoupling product from DEE suggesting the photooxidation of DEE to a radical species. To support this proposal, we tried to detect the DEE radical species by using ESR spectroscopy. Figure 7 shows the ESR spectrum of the DEE radical trapped by the spin trapping agent PBN under photoirradiation ($\lambda > 400$ nm) and with the Pd(0.1)/TiO₂ photocatalyst. The two signals at the either ends correspond to the signals from Mn marker. Between these two signals are the signals from the trapped DEE radical. The inset of figure 7 shows the probable structure of this radical species. The g-value for these signals was 2.0060. They represent a triple doublet originating from the nitrogen (N) and alpha hydrogen (H) in PBN. The hyperfine coupling constants (A) were 1.39 mT for N and 0.23 mT for H. Some signals were detected in the ESR spectrum when DEE and PBN solution was photoirradiated without any optical filter in the absence of the Pd/TiO₂ photocatalyst. Their origin was believed to be the photolysis of PBN which might have oxidized DEE. Photolysis of PBN is often observed in some solvents.⁹

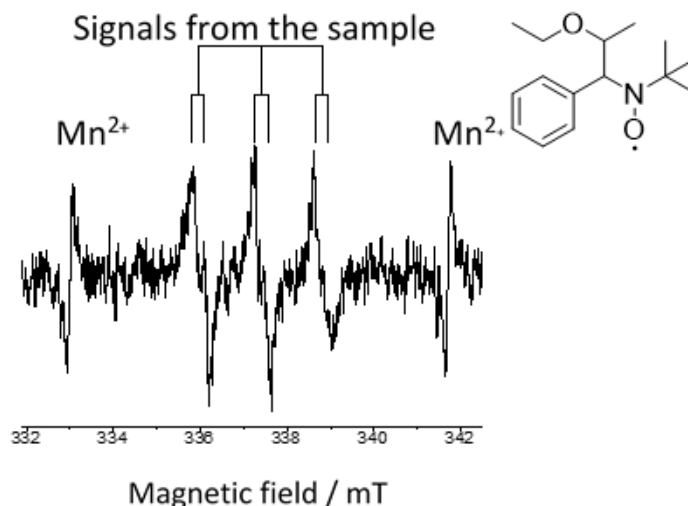
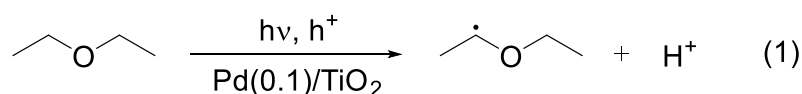


Figure 7 ESR spectrum of DEE radical trapped by PBN

To avoid this unwanted process, measurements were conducted in the light of wavelength more than 400 nm, which suppressed that process and enabled us to record the signals from trapped DEE radical produced by photocatalyzed oxidation. Thus, we confirmed the oxidation of DEE by the photogenerated holes on the Pd/TiO₂ photocatalyst as per equation 1.



3.3.2. Kinetic experiments

After confirming the photocatalyzed oxidation of DEE, we performed kinetic experiments by using deuterated reagents. Table 7 shows the results of the reactions done with deuterated benzene and DEE. The reaction carried out by using deuterated benzene and DEE gave a larger amount of **1a** than the reaction done without any deuterated reagent (Table 7 entries 1 and 2). The value of $k_{\text{H}}/k_{\text{D}}$ calculated from this result was 0.92, indicating an inverse kinetic isotope effect (Table 7 entry 2). The amount of **1a** also increased in the reaction carried out with benzene and deuterated DEE (Table 7 entries 1 and 3) and the value of $k_{\text{H}}/k_{\text{D}}$ was 0.93 (Table 7 entry 3), indicating an inverse kinetic isotope effect. One important conclusion from these results was that the photocatalyzed oxidation of DEE was not the rate determining step (RDS) for the formation of **1a**. Understanding the inverse kinetic isotope effect observed for both reactions was important to elucidate the reaction

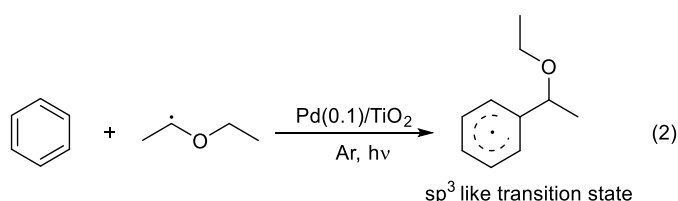
mechanism. In the present reaction conditions, only DEE was oxidized to radicals while benzene was not.

Table 7 Kinetic experiments with benzene and DEE ^a

Entry	Deuterated Reactant	1a (μmol)	$k_{\text{H}}/k_{\text{D}}$ ^b
1	None	7.0	-
2	Benzene- <i>d</i> ₆	7.6	0.92
3	DEE- <i>d</i> ₁₀	7.5	0.93

^a 0.1 ml (1.1 mmol) of benzene, 0.4 ml (3.8 mmol) of DEE and 0.0125 g of the Pd(0.2)/TiO₂ was used, other conditions were same as Table 3. ^b $k_{\text{H}}/k_{\text{D}}$ was determined from the amounts of **1a** produced in entries 1 and 2 for entry 2 and from entries 1 and 3 for entry 3.

Thus, the formation of **1a** must involve the attack of the radical species on the benzene ring (equation 2). In this process, the hybridization of the benzene carbon would change from sp^2 to sp^3 . This change would mainly affect the out-of-plane bending vibration of the C–H bond which is 1350 cm^{-1} for sp^3C atom and 800 cm^{-1} for sp^2C atom.¹⁰ Thus, the change of the zero-point energies of the reactants (sp^2C) to the transition state (sp^3C) was important in the reaction carried out deuterated benzene and DEE. For a C–H bond this difference is about 550 cm^{-1} (800 cm^{-1} for sp^2 and 1350 cm^{-1} for sp^3) whereas for C–D bond it is 403.2 cm^{-1} (586.8 cm^{-1} for sp^2 and 990 cm^{-1} for sp^3). Since the difference in the zero-point energies is smaller for the C–D bonds than the C–H bonds, an inverse kinetic isotope effect should be observed. Thus the observation of inverse kinetic isotope effect for the reaction between deuterated benzene and DEE was justified (Table 7, entry 2). The above reasoning can also explain the results of the reaction carried out with benzene and deuterated DEE (Table 7, entry 3). The proposed sp^3 carbon like transition state of benzene and DEE radical might have some steric requirements. As a C–D bond is slightly shorter than a C–H bond so, the transition state with deuterated DEE would be less crowded than unlabeled DEE, so that the reaction carried out with deuterated DEE might proceed more smoothly and give larger product yield than normal conditions. Thus the kinetic experiments revealed that formation of **1a** would involve the attack of ether radical on benzene molecule, which would also be the RDS (equation 2).



3.3.3. Temperature control reactions

The attack of the photogenerated DEE radical on the benzene molecule would be a thermal process. To confirm this proposal, we studied the effect of temperature on the photocatalytic reaction. The photocatalytic reaction between benzene and DEE was carried out at different temperatures (Table 8). The amount of **1a** increased steadily with temperature. This can be due to various reasons like desorption of products from photocatalyst's surface, acceleration of metal catalysis with temperature, and so on. The results were plotted as a pseudo-Arrhenius graph to calculate the apparent activation energy which was found to be 35.4 kJ/mol (Figure 8, (a)). To confirm that the increase in the amount of **1a** with temperature was not because of its increased desorption from the Pd/TiO₂ photocatalyst's surface, we performed desorption tests for **1a** (Table 9). A fixed amount of **1a**, dissolved in benzene-DEE mixture, was added to the test tube containing a fixed amount of Pd/TiO₂ photocatalyst. The suspension was heated for 10 min at different temperatures without photoirradiation. The amount of **1a** was determined by GC-MS. A pseudo-Arrhenius plot of this data gave an apparent activation energy as 5.5 kJ/mol (Figure 8, (b)). This difference in the activation energies implied that the increase in the amount of **1a** with temperature would be due to an acceleration of the metal catalysis with temperature. Thus, the rate determining step of this photocatalytic cross-coupling reaction would be the Pd metal catalyzed attack of the DEE radical on benzene molecule, which would be accelerated by increasing the reaction temperature, i.e. thermal energy. The EXAFS results indicated that the Pd species on the TiO₂ photocatalysts was metallic. So, the proposed Pd metal catalysis should be acceptable.

Table 8 Temperature control reaction between benzene and THF with different catalysts ^a

Entry	Catalyst	Temperature (K)	1a (μmol)
1	Pd(0.1)/TiO ₂	291	11.5
2		299	20.3
3		306	26.8
4		313	32.4
5 ^b		313	0.0

^a 0.7 ml benzene, 3.3 ml DEE, 0.1 g of Pd(0.2)/TiO₂ photocatalyst, other conditions were same as Table 3. ^b The reaction was done in dark, other conditions were same as before.

Table 9 Adsorption experiments for **1a** over Pd/TiO₂ photocatalyst ^a

Entry	Temperature (K)	1a (μmol)
1	298	8.1
2	306	8.3
3	309	8.5
4	320	9.5

^a 10 μmol of **1a**, 0.6 ml of benzene, 1.6 ml of DEE and 0.02 g of Pd(0.2)/TiO₂ photocatalyst were used and the contents were stirred in the dark for 10 min.

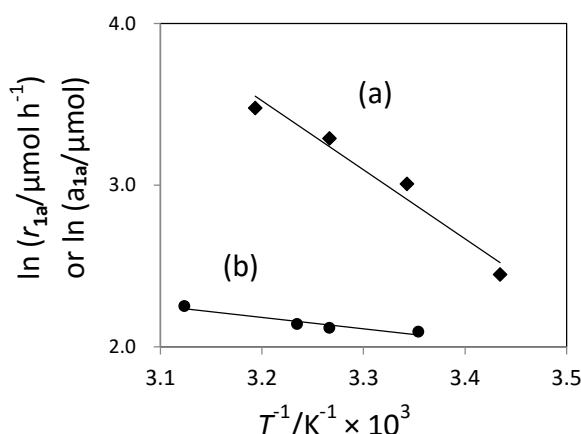


Figure 8 Pseudo-Arrhenius plot of temperature controlled photocatalytic reaction between benzene and DEE (a) and desorption tests of **1a** (b) with the Pd(0.2)/TiO₂ photocatalyst. r_{1a} : Formation rate of **1a**; a_{1a} : Amount of desorbed **1a** in the solution.

3.4. Proposed mechanism

The above observations reveal that the Pd/TiO₂ photocatalyst is a hybrid of TiO₂ photocatalyst and Pd nanoparticles as a metal catalyst that catalyzes the cross-coupling reaction as follows (Figure 9). (i) TiO₂ can be excited by photoirradiation to generate the excited electron (e^-) and hole (h^+) in the conduction and valence band, respectively. Holes will remain on TiO₂ while electrons would move to Pd nanoparticles. (ii) The hole would activate the α C–H bond of ether to generate the α -oxyalkyl radical and a proton. (iii) Then the Pd nanoparticle would thermally catalyze the C–C bond formation between benzene and the ether radical to form the reaction intermediate having a sp^3 -like carbon center in the aromatic ring. This thermally promoted step would be the rate determining step under the present conditions. (iv) The intermediate would release a hydrogen radical to give the desired alpha substituted product. (v) A proton would be reduced to

hydrogen radical by the photoexcited electrons present on the Pd nanoparticle which would couple with the hydrogen radical produced before to yield hydrogen gas.

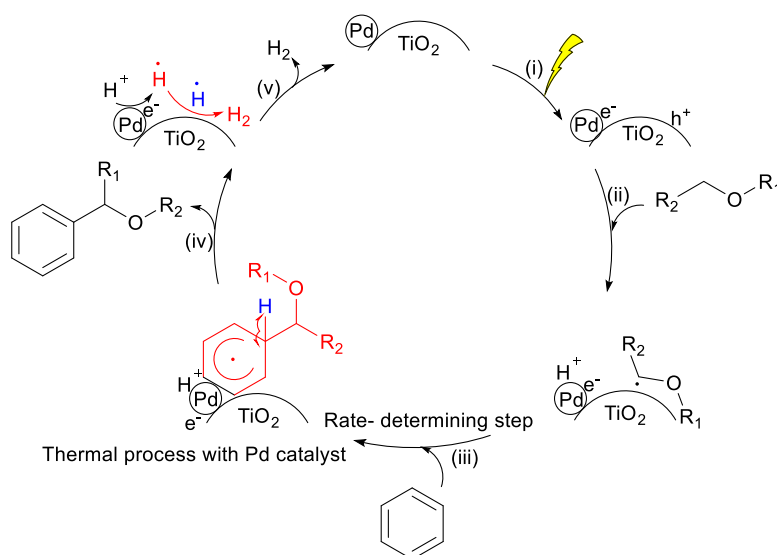


Figure 9 Proposed reaction mechanism for the cross-coupling between arene and ether by the Pd/TiO₂ hybrid catalyst

4. Conclusion

The results of the present study can be summarized as follows. Various arenes and ethers successfully underwent cross-coupling reaction by using a heterogeneous Pd/TiO₂ photocatalyst. The reaction proceeded by the oxidation of the ether molecules by the TiO₂ photocatalyst and their attack on the aromatic ring, assisted by the palladium catalyst. High conversion and product yield were obtained in the present system. The study also clarified the bifunctional role of the Pd nanoparticles, deposited on the TiO₂ photocatalyst in the organic synthesis reactions. These nanoparticles function as a bifunctional co-catalyst, that is, as an electron receiver and a metal catalyst. The realization of the dual role of metal nanoparticles on photocatalyst would widely allow the design of efficient catalysts depending on the reaction.

5. References

- [1] K. Qvortrup, D. A. Rankic and D. W. C. MacMillan, *J. Am. Chem. Soc.*, vol. 136, p. 629, **2014**.

- [2] T. Corona, C. Gambarotti, L. Palmisano, C. Punta and F. Recuperi, *J. Photochem. Photobiol. A: Chem.*, vol. 171, p. 237, **2005**.
- [3] T. Tagauchi, T. Ozawa and H. Yashiro, *Phys. Scr.*, vol. T115, p. 205, **2005**.
- [4] D. R. Heitz, J. C. Tellis and G. A. Molander, *J. Am Chem. Soc.*, vol. 138, p. 12715, **2016**.
- [5] C. M. Wang, A. Heller and H. Gerischer, *J. Am. Chem. Soc.*, vol. 114, p. 5230, **1992**.
- [6] K. R. Przybylak and M. T. Cronin, *J. Mol. Struc-Theochem.*, vol. 955, pp. 165, **2010**.
- [7] C. Karunakaran, S. Senthilvelan and S. Karuthapandian, *J. Photochem. Photobiol. A*, vol 172, p. 207, **2005**.
- [8] J. A. Navio, M. G. Gomez, M. A. P. Adrian and J. F. Mota, *J. Mol. Catal.*, vol. 104, p. 329, **1996**.
- [7] E. G. Janzen, *Acc. Chem. Res.*, vol. 4, p. 31, **1971**.
- [8] E. V. Anslyn and D. A. Dougherty, *Modern Physical Organic Chemistry* (Chapter 8, page 428), Edwards Brothers, **2005**.

II-3. Photocatalytic cross-coupling between alkanes and tetrahydrofuran

Abstract

Cross-coupling of various alkanes and tetrahydrofuran successfully underwent with a Pt/TiO₂ photocatalyst under photoirradiation, without the use of any additional reagents. The reaction between cyclohexane and tetrahydrofuran was studied in detail by using various techniques, to elucidate the mechanism of the cross-coupling reactions. Based on those results, the reaction was proposed to follow two pathways; the primary path is the photocatalytic oxidation of both substrates to radicals by TiO₂ photocatalyst which coupled to give the cross-coupling product. The minor one was the reaction between a surface adsorbed tetrahydrofuran or cyclohexane molecule on Pt and a photogenerated radical of either substrate where the Pt nanoparticles on TiO₂ plays a dual role of an electron receiver and a metal catalyst.

1. Introduction

Alkanes are an abundant chemical feedstock, and thus efficient utilization of alkanes for various purposes like fuels and chemical synthesis is desirable. Photocatalysis is an innovative methodology to carry out organic synthesis reactions. In the previous chapter, we developed a novel photocatalytic sp²C–sp³C cross-coupling reaction between arene and ether molecules under mild conditions by using a heterogeneous Pd/TiO₂ photocatalyst. The presence of arene molecule seemed to facilitate the reaction as they have delocalized electron density which makes them susceptible to undergo various reactions. In the present study, we challenge to activate the C–H bonds in two saturated molecules (alkane and ether) to carry out the sp³C–sp³C cross-coupling reaction. These bonds are quite stable and unreactive so that they don't react under mild conditions. There are several reports on the cross-coupling reactions between cyclic ethers like tetrahydrofuran (THF) and alkanes or aromatics.¹⁻⁶ However, since the C–H bonds of the sp³ carbon are too stable to react under mild conditions, most of those reactions are energy intensive processes^{3,4,6} requiring an organometallic catalyst,^{1,3,4} a large amount of metal co-catalyst^{4,6} and strong base.^{1,2} As a result, these methods are not sustainable and have room for improvement. In the present

work, we found that an inexpensive, safe, and abundant TiO₂ photocatalyst can successfully bring out this transformation at room temperature without any additional chemicals or catalyst.⁷ Several experimental techniques were used to propose the reaction mechanism.

2. Experimental Section

2.1. Preparation of catalysts

The various metal loaded TiO₂ (M(x)/TiO₂) samples were prepared by a photodeposition method as mentioned in the previous chapter (Chapter II-2).

2.2. Characterization of catalysts

Pt dispersion and particle size on TiO₂ was determined by CO pulse adsorption as discussed in previous (Chapter II-2, 3.1). X-ray absorption fine structure (XAFS) was used to elucidate the electronic state of the Pt nanoparticles on TiO₂. The spectra were recorded at BL9C of Photon Factory at the Institute of Materials Structure Science, High Energy Accelerator Research Organization (KEK-PF, Tsukuba Japan). The reference sample, Pt foil was measured in a transmission mode, while the prepared Pt/TiO₂ sample was measured in a fluorescence mode. Athena software was used to analyze the obtained spectra.⁸

2.3. Photocatalytic activity tests

2.3.1. Materials

All of the chemicals were of analytical grade and were used without further purification (cyclohexane, cyclopentane, *n*-hexane and 1,1'-bicyclohexyl (Nacalai Tesque, 99.7%)), tetrahydrofuran (THF) (Wako Pure Chemicals, 99%), cyclohexane-*d*₁₂ (Aldrich, 99.6 atom%) and THF-*d*₈ (Euriso-Top)). An authentic sample of the cross-coupling product from THF and cyclohexane (**1a**) was synthesized by following the procedure reported in the literature.⁹

2.3.2. Procedure for the photocatalytic activity tests

The photocatalytic reaction tests for the cross-coupling between various alkanes and THF was carried out in a Pyrex test tube under the light irradiation from a xenon lamp. The light wavelength was controlled by an optical filter. Before carrying out the activity test, the M(x)/TiO₂ photocatalyst was pre-treated by photoirradiation for 1 h. Then, the reactor

was sealed with a silicon septum and purged with argon gas for 10 min. Then, the reactants (alkane and THF) were introduced by a syringe and stirred with light irradiation for the desired time. Upon the completion of the reaction, a portion of the gas phase was taken in an air-tight syringe and analyzed by GC-TCD (Shimadzu GC-8A) while the liquid phase was diluted by ethanol, filtrated by a syringe equipped with a PTFE filter, and analyzed by GC-MS (Shimadzu, GC-MS-QP5050A).

2.3.3. Mechanistic studies

The reaction between cyclohexane and THF was studied by several techniques to investigate the mechanism of the photocatalytic sp^3C - sp^3C cross-coupling between alkanes and THF. ESR spectroscopy confirmed the formation of radical species during the photocatalytic reactions in the presence of UV light and the Pt/TiO₂ photocatalyst. The measurements were carried out by using an X-band spectrometer (JEOL-RE2X) in JEOL's TE011 cavity and N-tert-butyl- α -phenylnitron (PBN), a spin trapping agent as follows. A suspension of the Pt(0.1)/TiO₂ (0.02 g) in cyclohexane (1 ml)-PBN (0.09 g) solution was introduced into an ESR cell and irradiated with light of a xenon lamp for 20 min with simultaneous measurements at room temperature. The light's wavelength was restricted to more than 400 nm to avoid the photolysis of PBN. Kinetic experiments carried out with deuterated reagents revealed the rate determining step of the cross-coupling reaction. Temperature control reactions revealed the role of the Pt nanoparticles in the photocatalytic reaction.

3. Results and Discussion

3.1. Catalyst characterization

CO adsorption tests: The results of the CO pulse adsorption with various M(x)/TiO₂ samples was discussed in Chapter II-2. The results showed that finely dispersed Pt nanoparticles in the range of 2–3 nm were obtained for the Pt(0.1)/TiO₂ sample.

X-ray Absorption Fine Structure (XAFS): XAFS revealed the electronic state of the Pt nanoparticles in the Pt(0.1)/TiO₂ sample. Figure 1 shows normalized Pt-L_{III} edge XANES region of the reference Pt foil (Figure 1 (a)) and PtO₂ (Figure 1 (c)), and the Pt(0.1)/TiO₂ (Figure 1 (b)) sample recovered after the photocatalytic activity test. The Pt(0.1)/TiO₂ sample exhibited

similar features to that of Pt foil and was clearly different from the PtO₂ sample. These results suggest that the Pt nanoparticles on the TiO₂ surface were almost metallic which meant that they could effectively function as the electron receiver on the TiO₂ photocatalyst under photoirradiation.

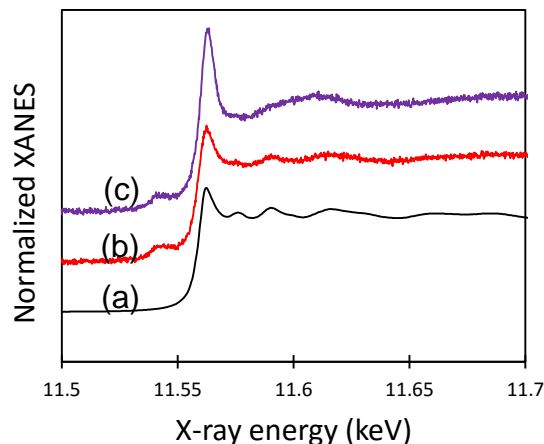


Figure 1 Normalized Pt-L_{III} edge XANES spectra of (a) Pt foil, (b) Pt(0.1)/TiO₂ sample recovered after the activity test, and (c) PtO₂ powder

3.2. Photocatalytic activity tests

3.2.1. Cross-coupling between cyclohexane and tetrahydrofuran

Reaction with Pt/TiO₂ photocatalyst

The photocatalytic sp³C–sp³C cross-coupling with between alkanes and ethers was studied by investigating the reaction between cyclohexane and THF with the Pt(0.1)/TiO₂ sample (Table 1). At first, we optimized the reaction conditions. The reaction tests carried out with an equal volume of both reactants (cyclohexane and THF) gave a small amount of 2-cyclohexyltetrahydrofuran (**1a**), the cross-coupling product (Table 1, entry 1). The homocoupling products of THF namely, octahydro-2,2'-bifuran (**1b**), and octahydro-2,3'-bifuran (**1c**), and 2-butyltetrahydrofuran (**1d**) were the major products in this condition. Hydrogen was the only gaseous product formed in these reactions, however as its amount was very large, it couldn't be quantified accurately. The formation of homocoupling products from THF suggests that the photogenerated holes on the TiO₂ photocatalyst oxidize THF to radical species (equation 1). A decrease in the amount of THF decreased its homocoupling and increased the amount of **1a** (Table 1, entry 2). However, homocoupling of cyclohexane to give 1,1'-bi(cyclohexane) (**1e**) proceeded in this reaction, which indicated that cyclohexane could also be oxidized to radical species by the TiO₂ photocatalyst (equation 2). A further

decrease in the amount of THF completely suppressed its homocoupling and the selectivity to **1a**, based on THF (S_{THF}), reached 100% (Table 1, entry 3).

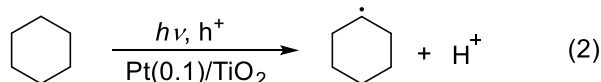
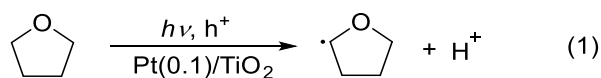
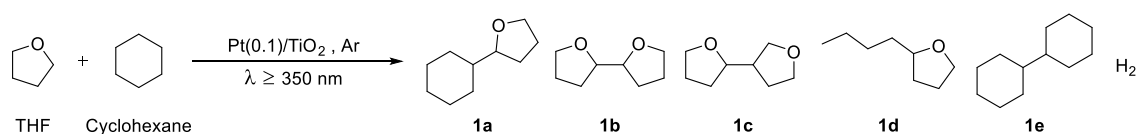


Table 1 Cross-coupling between cyclohexane and THF with the Pt(0.1)/TiO₂ sample ^a



Entry	Reactants (ml)		Products (μmol) ^b				Selectivity ^c	
	THF	Cyclohexane	1a	1b + 1c	1d	1e	S_{THF}	S_{CyH}
1	2.00	2.00	0.4	19.2	0.7	0.0	2	> 99
2	0.10	3.00	1.9	1.5	0.5	0.3	51	80
3	0.01	3.00	1.4	0.0	0.0	3.9	> 99	26
4	3.00	0.01	0.0	6.7	0.0	0.0	-	-
5 ^d	0.01	3.00	0.0	0.0	0.0	0.0	-	-
6 ^e	0.01	3.00	0.0	0.0	0.0	0.0	-	-

^a Reaction conditions: various amount of the reactants with 50 mg of the Pt(0.1)/TiO₂ sample was used, reaction time was 1 h, wavelength of incident light was ≥ 350 nm and the light intensity was 21 mW cm⁻² (at 365 \pm 20 nm), reactor's temperature was *ca.* 298 K.

^b Amount of **1a**, **1b**, **1c** and **1d** was determined from the calibration curve of an authentic sample of **1a** that was synthesized as per a literature.⁹ Amount of **1e** was determined from the calibration curve of its authentic sample purchased from the company.

^c Selectivity to **1a**. S_{THF} : Selectivity to **1a** based on the THF, calculated as: [100 \times amount of **1a** (μmol)] / [(**1a**+**1b**+**1c**+**1d**) (μmol)]; S_{CyH} : Selectivity to **1a** based on the cyclohexane, calculated as: [100 \times amount of **1a** (μmol)] / [(**1a**+**1e**) (μmol)]. ^d Reaction was performed in the dark. ^e Reaction was performed under irradiation without the Pt/TiO₂ sample.

However, the homocoupling of cyclohexane increased in these conditions which decreased the selectivity to **1a**, based on cyclohexane (S_{CyH}). The reaction carried out with a small amount of cyclohexane did not give **1a** (Table 1, entry 4). The reactions carried out without light (Table 1, entry 5) or the Pt(0.1)/TiO₂ sample (Table 1, entry 6) did not yield any product confirming that the formation of **1a** and other homocoupling products was a photocatalytic reaction. As entry 2 gave an appreciable amount of **1a** with the highest selectivity for both reactants, it was chosen as the optimum reaction condition, and further tests were carried out under this condition.

Screening of M(x)/TiO₂ photocatalysts

After optimizing the reaction conditions, we screened the metals on TiO₂. Table 2 shows the results. Apart from Pt, Au showed some activity for the formation of **1a** (Table 2, entries 1 and 2). Metals like Pd and Rh were inactive for the formation of **1a** (Table 2, entries 3 and 4). Reaction carried out with a pristine TiO₂ photocatalyst (JRC-TIO-8, anatase) gave low yield of **1a** (Table 2, entry 5). All M(0.1)/TiO₂ photocatalysts were active for the homocoupling of cyclohexane to give **1e** (Table 2, entries 1–5) however, only Pt(0.1)/TiO₂ photocatalysts gave an appreciable yield of the cross-coupling product **1a** (Table 2, entry 1) thus, further reactions were performed with this photocatalyst.

Table 2 Photocatalytic reaction tests between THF and cyclohexane with the M(x)/TiO₂ samples ^a

Entry	Sample	Products (μmol)			Selectivity		Yield
		1a	1b+1c	1e	S _{THF}	S _{CyH}	
1	Pt(0.1)/TiO ₂	1.41	0.00	3.91	> 99	26	1.14
2	Pd(0.1)/TiO ₂	0.00	0.00	0.09	-	-	-
3	Au(0.1)/TiO ₂	0.09	0.00	0.16	> 99	36	0.07
4	Rh(0.1)/TiO ₂	0.00	0.00	0.27	-	-	-
5 ^c	TiO ₂	0.02	0.00	0.03	> 99	40	0.02

^a 0.01 ml (123 μmol) THF, 3 ml (27.7 mmol) cyclohexane, other conditions were same as Table 1. ^b Yield (%) for **1a** was calculated as 100×(amount of **1a**)/(initial amount of THF). ^c Reaction was done with 50 mg of pristine TiO₂.

Effect of water

In our previous studies, we found that the addition of small amount of water to the reaction mixture increased the product yield (Chapter II-2, Tables 4 and 5). The small amount of water was believed to interact with surface OH groups on the TiO₂ photocatalyst and facilitate the migration of proton.^{10,11} So, we studied the effect of the addition of water to the reaction between cyclohexane and THF. Table 3 shows the result of the reactions carried out with different amount of water. Addition of a small amount of water significantly improved the amount of **1a** (Table 3, entry 2), but a further addition was unproductive (Table 3, entries 3–5). Addition of water also affected the yield of **1e**. It gradually decreased with water which improved the selectivity of **1a**, S_{CyH} based on cyclohexane (Table 3, entries 2–5). For a fixed amount of water, the yield of **1a** initially increased with time (Table 3, entries 2 and 6) but decreased later (Table 3, entry 7). After increasing the reaction time from 1 h to 2 h, we successfully achieved 4% yield, although

with low overall selectivity (Table 3, entry 6), however further increase of reaction time was not helpful to obtain high yield of **1a** (Table 3, entry 7).

Table 3 Effect of water on the cross-coupling reaction between cyclohexane and THF with the Pt(0.1)/TiO₂ photocatalyst ^a

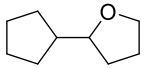
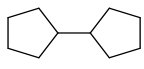
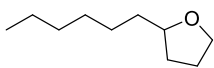
Entry	Water (μl)	Products (μmol)		Selectivity		Yield
		1a	1e	S _{THF}	S _{CyH}	
1	0	1.41	3.91	> 99	27	1.14
2	2	2.06	2.92	> 99	41	1.67
3	10	1.12	1.08	> 99	51	0.91
4	20	0.35	0.12	> 99	74	0.28
5	50	0.0	0.0	-	-	-
6 ^b	2	5.72	7.37	> 99	44	4.65
7 ^c	2	4.74	7.45	> 99	39	3.85

^a Various amount of water was added, reaction temperature was *ca.* 308 K, other conditions were same as Table 1. ^b Reaction time was 2 h. ^c Reaction time was 4 h.

3.2.2. Cross-coupling between various alkanes and THF

After establishing the reaction between cyclohexane and THF, we screened other alkanes for the photocatalytic sp³C–sp³C cross-coupling reaction (Table 4). The reaction proceeded well with other cyclic and acyclic alkanes indicating good substrate scope of these cross-coupling reactions. The reaction between cyclopentane and THF gave 2-cyclopentyltetrahydrofuran (**2a**) as the cross-coupling product along with the homocoupling products from both the reactants (**1b-1d** and **2b**) (Table 4, entry 1).

Table 4 Photocatalytic sp³C–sp³C cross-coupling between different alkanes and THF with Pt(0.1)/TiO₂ ^a

Entry	Alkane	Cross-coupling product (μmol) ^b	Homocoupling products (μmol) ^b	
			Alkane	THF ^c
1 ^d	cyclopentane	 2a 1.7 μmol	 2b 0.2 μmol	3.8
2 ^e	<i>n</i> -hexane	 3a 0.2 μmol	0.0	6.5

^a Reaction conditions: 100 μl (1.2 mmol) THF, reaction temperature was *ca.* 298 K, other conditions were same as Table 1. ^b Amount of all products was approximately determined from the calibration curve of **1a**. ^c Total amount of homocoupling products from THF (**1b-1d**) is mentioned. ^d 3 ml (32.1 mmol) cyclopentane was used. ^e 3 ml (22.7 mmol) *n*-hexane was used.

The reaction between n-hexane and THF gave 2-hexyltetrahydrofuran (**3a**) as the cross-coupling product and homocoupling product from THF (Table 4, entry 2). The homocoupling of n-hexane did not proceed in these conditions. The cyclic alkanes (cyclohexane and cyclopentane) gave larger amount of cross-coupling product than exhibited straight chain alkane (n-hexane) along with their homocoupling products. These results indicate that the cyclic alkanes were more reactive than straight chain alkanes. It could be due to the lower C–H bond dissociation enthalpy in the former than later (e.g. 416 kJ/mol in cyclohexane¹² and 456.89 kJ/mol in n-hexane for primary hexyl radical¹³).

3.3. Mechanistic studies

The reaction between cyclohexane and THF was examined by various techniques to elucidate the mechanism of the photocatalytic sp^3C – sp^3C cross-coupling between alkanes and THF. The results are discussed in the following sections.

3.3.1. ESR Spectroscopy

ESR spectroscopy evidenced the production of the radical species in the photocatalytic reaction. The experiments were carried out with the Pt(0.1)/TiO₂ photocatalyst under photoirradiation from a xenon lamp ($\lambda > 400$ nm) with PBN as a spin trapping agent. Figure 2 shows the ESR spectrum of cyclohexane solution with PBN. It consisted of the signals from the cyclohexane-THF spin adduct (proposed structure shown inset of Figure 2) along with the signals from Mn⁺² marker at either end. The signals represented a triple doublet arising from the nitrogen and the alpha hydrogen of PBN. The g value and coupling constants were found to be 2.0011 and $A_N = 1.43$ mT and $A_H = 0.206$ mT, respectively. The measurements carried out without the Pt/TiO₂ sample or photoirradiation did not give any signal, confirming the photooxidation of cyclohexane to radical species by the Pt/TiO₂ photocatalyst.

In chapter II-2, we evidenced that the TiO₂ photocatalyst could oxidize DEE to radical species under photoirradiation. As, all screened ethers were proposed to follow the same mechanism for the photocatalytic cross-coupling between arenes and ethers, it should be acceptable to propose that all were oxidized to corresponding radical species by the TiO₂ photocatalyst.

Thus, even in the present system, it can be proposed that under photoirradiation, THF was oxidized to radicals by TiO₂. The observation of homocoupling products of THF (**1b-1d**) supports this proposal. Thus, photocatalytic cross-coupling of cyclohexane and THF would involve the generation of radicals from both reactants.

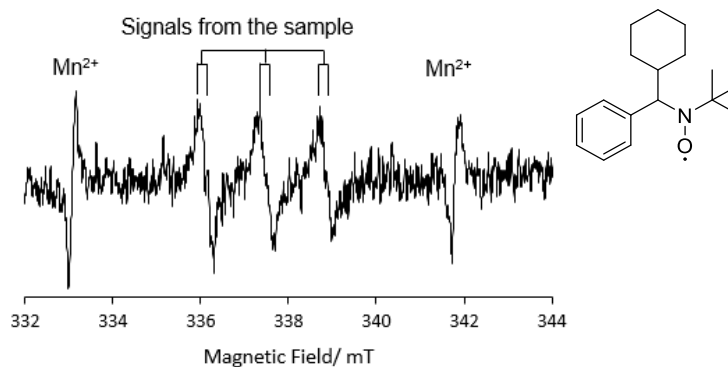


Figure 2 ESR spectrum of cyclohexyl radical with PBN as a spin trap in the presence of the Pt/TiO₂ photocatalyst under photoirradiation

3.3.2. Kinetic experiments

Next, kinetic experiments were carried out by using deuterated reagents (Table 5). When compared to the reaction carried out in the normal condition (Table 5, entry 1), the yield of **1a** decreased in the reaction carried out with deuterated cyclohexane and THF (Table 5, entry 2). The value of k_H/k_D , for this reaction, was more than 1, indicating a primary kinetic isotopic effect (KIE). On the other hand, the amount of **1a** increased in the reaction carried out with cyclohexane and deuterated THF (Table 5, entry 3). The value of k_H/k_D , for this reaction, was less than 1, which indicates an inverse KIE.

The decrease in the amount of **1a** in the reaction carried out with deuterated cyclohexane means that the photooxidation of cyclohexane was the rate determining step for the formation of **1a**. As a C–D bond is stronger than a C–H bond, its cleavage will be more difficult, which would decrease the amount of **1a** (Table 5, entry 2). The increase in the amount of **1a** in the reaction carried out with deuterated THF can also be explained by the C–H bond dissociation energy. The photooxidation of THF and cyclohexane is a competitive process. However, due to a lower C–H bond dissociation energy, photooxidation of THF is easier than cyclohexane (416 kJ/mol in cyclohexane and 385.3 kJ/mol in THF).⁹ Replacement of THF with

deuterated THF would slightly decrease its rate of photooxidation and increase the photooxidation rate of cyclohexane. Thus, the yield of **1a** would increase in the reaction carried out with deuterated THF (Table 5, entry 3). Hence, the kinetic experiments revealed that the oxidation of cyclohexane was the rate determining step for the formation of **1a** and supported that the photooxidation of cyclohexane and THF was a competitive reaction.

Table 5 Kinetic experiments with cyclohexane and THF ^a

Entry	Deuterated reactant	1a (μmol)	$k_{\text{H}}/k_{\text{D}}$ ^b
1	None	1.2	-
2	Cyclohexane - d_{12}	0.6	2.0
3	THF- d_8	2.4	0.5

^a 0.5 ml of THF, 1.5 ml of cyclohexane and 50 mg of the Pt(0.1)/TiO₂ photocatalyst were used for the reaction. For other details see Table 1. ^b $k_{\text{H}}/k_{\text{D}}$ was determined from the amount of **1a** produced in entries 1 and 2 for entry 2, and those in entries 1 and 3 for entry 3, respectively.

3.3.3. Temperature control reactions

The loading of Pt metal to the TiO₂ photocatalyst improved the activity for the photocatalytic cross-coupling of cyclohexane and THF. This could primarily be ascribed to its high efficiency as an electron receiver on the TiO₂ photocatalyst. However, the possibility of the catalysis by Pt metal nanoparticles operating in this reaction cannot be neglected. In the photocatalytic cross-coupling between arenes and ethers (Chapter II-2), we had proved that the Pd nanoparticles on the TiO₂ photocatalyst functioned as a thermal catalyst in the photocatalytic reaction. So, it was necessary to confirm whether a similar catalysis by the Pt nanoparticles in the present reaction system contributed or not. For this, we studied the effect of the reaction temperature on the photocatalytic cross-coupling reaction between cyclohexane and THF (Table 6). The photocatalytic reaction was carried out at different temperatures. In the given experimental conditions, the reaction gave **1a** and the homocoupling products from THF (**1b-1d**). The yield of both products increased with temperature (Table 6, entries 1-3). However, the reaction performed at high temperature without photoirradiation yielded no products (Table 6, entry 4), indicating that the reaction required the TiO₂ photocatalysis. A pseudo-Arrhenius plot of this data gave the apparent activation energy as 65.5 kJ/mol for **1a** and 37.0 kJ/mol for the homocoupling of THF (**1b-1d**). Similar experiments were carried out with pristine TiO₂, and the activation energies calculated from that data were 21.3 kJ/mol for **1a** and 33.8 kJ/mol for homocoupling of THF (**1b-1d**).

Table 6 Temperature control reaction between cyclohexane and THF with different photocatalysts ^a

Entry	Catalyst	Temperature (K)	1a (μmol)	1b+1c+1d (μmol)	E_a (kJ/mol)	
					1a	1b+1c+1d
1	Pt(0.1)/TiO ₂	299	0.42	1.17	65.5	37.0
2		305	0.53	8.98		
3		313	1.03	13.11		
4 ^b		313	0.0	0.0		
5	TiO ₂	308	0.32	0.32	21.3	33.8
6		313	0.39	0.39		

^a 1 ml THF, 3 ml cyclohexane, other conditions were same as Table 1. ^b The reaction was performed in dark.

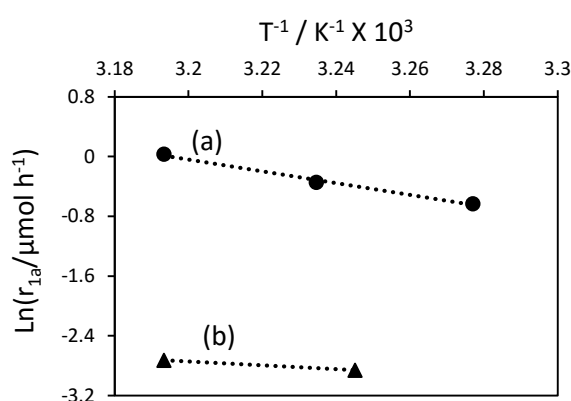


Figure 3 Pseudo-Arrhenius plot of temperature controlled photocatalytic reaction between THF and cyclohexane with (a) Pt(0.1)/TiO₂ and (b) TiO₂ photocatalyst. r_{1a} the rate of formation of **1a**.

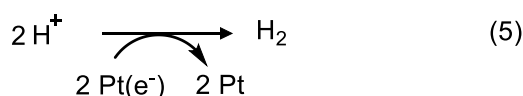
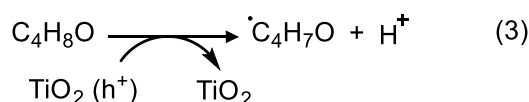
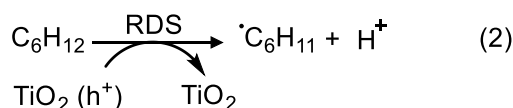
Figure 3 shows the comparison of the activation energies for **1a** on the Pt/TiO₂ photocatalyst (a) and pristine the TiO₂ photocatalyst (b). The different values of activation energies for **1a** on the two photocatalysts indicate that the Pt nanoparticles might have some catalytic role in its formation. On the other hand, the similar activation energies for the homocoupling of THF (**1b-1d**) on the two photocatalysts indicate that the thermal energy might not correspond any catalysis but could be utilized for some other processes like desorption of products or surface reactions, and so on. Thus, the temperature controlled reactions indicated that only the formation of **1a** might involve Pt catalysis. The nature of this catalysis is believed to be the thermal activation of the C–H bonds in cyclohexane and THF on the metal surfaces. There are several reports which confirm that the noble metals like Pt and Pd can activate the C–H bonds in different alkanes.¹⁴⁻¹⁶ So, this might also be possible in the present system to activate cyclohexane and THF on the metal surface. Further, as no products were

obtained in the reaction carried out in dark at high temperature, it meant that the proposed catalysis cannot function independently. Instead, it might be possible that these activated molecules react with a photogenerated radical, which would provide an alternate path for the product formation.

3.3.4. Proposed reaction mechanism

The above observations are used to propose a tentative mechanism for the photocatalytic sp^3C - sp^3C cross-coupling between cyclohexane and THF. Figure 4 shows the details of the proposed mechanism.

Pt/TiO₂ photocatalytic process



Hybrid process: Pt/TiO₂ photocatalysis + Pt thermal catalysis

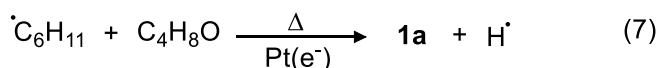
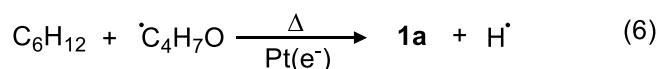


Figure 4 Proposed hybrid reaction mechanism for the cross-coupling reaction between cyclohexane (C₆H₁₂) and THF (C₄H₈O) to give **1a** with Pt/TiO₂ photocatalyst.

(1) The photo-excitation of TiO₂ would generate electrons and holes in the conduction and valence band respectively. The electrons would move to Pt nanoparticles while the holes would remain on TiO₂. (2) The holes would oxidize the adsorbed cyclohexane (C₆H₁₂) and (3) THF (C₄H₈O) molecules to generate their corresponding radicals ($\cdot\text{C}_6\text{H}_{11}$ and $\cdot\text{C}_4\text{H}_7\text{O}$) and protons. Due to a larger C–H bond dissociation enthalpy, oxidation of cyclohexane would be the rate determining step for the formation of **1a**. (4) The radicals would combine to give **1a**, while (5) the two protons would be reduced by the electron on Pt, to form hydrogen. Thus, the photocatalytic formation of **1a**

would be a two-photon process. Simultaneously, the photogenerated radicals of cyclohexane and THF could move to Pt nanoparticles where they can react with the adsorbed THF and cyclohexane molecules to give **1a** (Figure 4, equations 6 and 7). It will be an alternate route for the formation of **1a** involving the TiO₂ photocatalysis and the Pt catalysis, which would be a one-photon process.

4. Conclusion

In this work, we developed a new methodology to utilize the abundant hydrocarbons like alkanes in synthetic organic chemistry under mild conditions. A heterogeneous Pt/TiO₂ photocatalyst successfully activated the sp³C-H bonds in alkanes and THF to bring out the cross-coupling reaction. Based on the results of different experiments, a tentative mechanism was proposed for these reactions. The major route was a photocatalytic process which was a two-photon process involving radical formation of both alkane and THF. The Pt nanoparticles functioned as an electron receiver to reduce the recombination of electrons and holes. Another proposed route was a hybrid of TiO₂ photocatalysis and Pt catalysis, which was a one-photon process involving a photogenerated radical and a surface activated molecule. Thus, the Pt nanoparticles functioned as co-catalysts. These findings would allow the development of efficient reactions in terms of usage of noble metals and their catalytic activity.

5. References

- [1] H. M. L. Davies, T. Hansen and M. R. Churchill, *J. Am. Chem. Soc.*, vol. 122, p. 1587, **2000**.
- [2] P. P. Singh, S. Gudup, H. Aruri, U. Singh, S. Ambala, M. Yadav, S. D. Sawant and R. A. Vishwakarma, *Org. Bimol. Chem.*, vol. 10, p. 1587, **2012**.
- [3] D. Liu, C. Liu, H. Li and A. Lei, *Angew. Chem. Int. Ed.*, vol. 52, p. 4453, **2013**.
- [4] R. P. Pandit and Y. R. Lee, *Adv. Synth. Catal.*, vol. 356, p. 3171, **2014**.
- [5] W. T. Wei, R. J. Song and J. H. Li, *Adv. Synth. Catal.*, vol. 356, p. 1703, **2014**.
- [6] R. Parella and S. A. Babu, *J. Org. Chem.*, vol. 80, p. 2339, **2015**.

- [7] A. Tyagi, A. Yamamoto, T. Kato and H. Yoshida, *Catal. Sci. Technol.*, vol. 7, p. 2616, **2017**.
- [8] B. Ravel and M. Newville, *J. Synchrotron Radiat.*, vol. 12, p. 537, **2005**.
- [9] Jiang, E. K. London, D. J. Morris, G. J. Clarkson, M Wills, *Tetrahedron*, vol. 66, p. 9828, **2010**.
- [10] H. Yuzawa, T. Mori, H. Itoh and H. Yoshida, *J. Phys. Chem. C.*, vol. 116, p. 4126, **2012**.
- [11] E. Wada, T. Takeuchi, Y. Fujimura, A. Tyagi, T. Kato and H. Yoshida, *Catal. Sci. Technol.*, vol. 7, p. 2457, **2017**.
- [12] Y. R. Luo, *Handbook of Bond Dissociation Energies in organic compounds*, CRC Press, **2002**.
- [13] J. Zheng, T. Yu and D. G. Truhlar, *Phys. Chem. Chem. Phys.*, vol. 13, p. 19318, **2011**.
- [14] J. E. Demuth, H. Ibach and S. Lehwald, *Phys. Rev. Lett.*, vol. 40, p. 1044, **1978**.
- [15] M. A. Chesters and P. Gardner, *Spectrochim. Acta. Part A*, vol. 46, p. 1011, **1990**.
- [16] R. Raval, *Surf. Sci.*, vol. 219, p. L505, **1989**.

II-4. Photocatalytic cross-coupling between alkenes and tetrahydrofuran

Abstract

A Pt loaded TiO_2 photocatalyst successfully catalyzed the C–C cross-coupling between various alkenes and tetrahydrofuran (THF).¹ The reaction between cyclohexene and THF was systematically studied to elucidate the reaction mechanism. This reaction gave three cross-coupling products 2-cyclohexyltetrahydrofuran (**A**), 2-(cyclohexn-2-en-1-yl)tetrahydrofuran (**B**), and 2-(cyclohex-1-en-1-yl)tetrahydrofuran (**C**), each by an independent formation route. Reaction between a cyclohexene molecule and a photogenerated tetrahydrofuran radical species gave products **A** and **C**. On the other hand, the coupling of the photogenerated radicals of tetrahydrofuran and cyclohexene gave product **B**. The Pt nanoparticles on TiO_2 functioned as an electron receiver to decrease the recombination of photogenerated electrons and holes, which facilitated the cross-coupling reaction.

1. Introduction

Alkenes are an abundant and versatile class of organic molecules. Although alkenes activated with functional groups are often used in organic synthesis,²⁻⁵ few reports are there for the simple alkenes devoid of any functionality. In the previous chapters, it is described that photocatalytic cross-coupling of aromatic and saturated hydrocarbons with ethers can be promoted by metal loaded titanium oxide photocatalysts. These photocatalysts could oxidize less active molecules like ethers,^{6, 7} benzene,⁶ and cyclohexane⁷ to become radicals which underwent reactions to yield the cross-coupling products. Based on those results, we expected that these photocatalysts could activate simple alkenes as well and promote their cross-coupling reactions. Alkenes resemble in part both aromatic and saturated hydrocarbons in their electronic and structural features. Like arenes, they have π electron cloud, but, unlike them, it is localized. Further, they have $\text{sp}^3\text{C-H}$ bonds like saturated alkanes but the presence of double bond effects their reactivity, especially for the allylic carbon. Thus, it would be interesting to study their photocatalytic coupling reaction with substrates like tetrahydrofuran.

In the present work, we have employed a metal loaded TiO_2 photocatalyst to carry out the C–C cross-coupling between alkenes and tetrahydrofuran

under mild reaction conditions. The reaction between cyclohexene and tetrahydrofuran was studied in detail to elucidate the reaction mechanism.

2. Experimental Section

2.1. Preparation of catalysts

The various metal loaded TiO₂ photocatalysts (M(x)/TiO₂) were prepared by a photodeposition method mentioned in the previous chapter (Chapter II-2).

2.2. Characterization of catalysts

The prepared M(x)/TiO₂ samples were characterized by different techniques like powder-XRD, CO-pulse adsorption among others, as discussed in the previous chapters (Chapter II-2 and II-3).

2.3. Photocatalytic activity tests

2.3.1. Materials

All the chemicals were of analytical grade and used without further purification; cyclohexene (TCI Research Chemicals, >99%), tetrahydrofuran (THF) (Wako Pure Chemicals, 99%), cyclopentene (Nacalai Tesque, 98%), 1-hexene (TCI Research Chemicals, 99%), cyclohexene-*d*₁₀ (CDN Quality Stable Isotopes, 98%) and THF-*d*₈ (Euriso-Top, 99.5%). An authentic sample of one of the cross-coupling product of cyclohexene and tetrahydrofuran (**A**) was synthesized by following a reported procedure.⁸

2.3.2. Procedure for photocatalytic activity tests

The photocatalytic cross-coupling reactions between alkenes and THF were carried out in a Pyrex test tube (70 mL) under argon atmosphere as follows: at first, the M(x)/TiO₂ sample (typically, 50 or 100 mg) was irradiated with the xenon lamp through a long pass filter, allowing light of wavelength more than 350 nm, for 1 h. Then, the test tube was sealed with a silicon septum and purged with argon for 10 min, followed by the addition of alkene (1 ml) and THF (3 ml) and stirring with irradiation for the desired time. After the reaction, a part of the gaseous phase was collected in a gastight syringe and analyzed by a GC-TCD (Shimadzu GC-8A). The liquid phase was diluted with ethanol, filtered by a syringe with a PTFE filter, and analyzed by a GC-MS (Shimadzu, GCMS-QP5050A).

2.3.3. Mechanistic studies

The mechanism of the photocatalytic cross-coupling between alkenes and THF was elucidated by studying the reaction between cyclohexene and THF by using various techniques such as kinetic experiments carried out by deuterated reagents and temperature control photocatalytic reactions.

3. Results and Discussion

3.1. Characterization of catalysts

The results of various characterization techniques are discussed in previous chapters (Chapter II-2 and II-3).

3.2. Photocatalytic activity tests

3.2.1. Cross-coupling between cyclohexene and THF

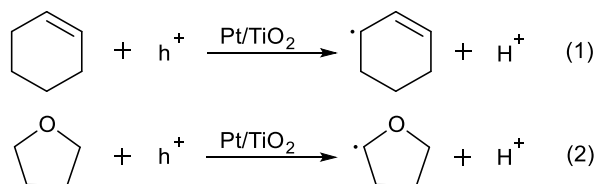
Table 1 shows the results of the photocatalytic cross-coupling reaction between cyclohexene and THF under different conditions with Pt(0.1)/TiO₂ sample. Entries 1 and 2 show the results of homocoupling of cyclohexene and THF, respectively. The reaction of cyclohexene with the Pt(0.1)/TiO₂ sample under photoirradiation in the absence of THF gave [1,1'-bi(cyclohexane)]-2,2'-diene (**1a**) and hydrogen (not shown) in the liquid and gaseous phase, respectively (Table 1, entry 1). The reaction produced lot of hydrogen, which is why its amount could not be determined accurately. The selective formation of the **1a** can be reasoned by comparing the bond dissociation energies of the C–H bonds in cyclohexene. Since the allylic position has the lowest C–H bond dissociation energy among the vinylic (457.7 kJ/mol), allylic (349.5 kJ/mol), and homoallylic (415.1 kJ/mol) C–H bonds in cyclohexene,⁹ it should be easier to generate the allylic cyclohexenyl radical, which would give the product **1a**. On the other hand, the reaction of THF with the Pt(0.1)/TiO₂ sample under photoirradiation in the absence of cyclohexane gave the following products in the liquid phase: octahydro-2,2'-bifuran (**1b**), and octahydro-2,3'-bifuran (**1c**), and 2-butyltetrahydrofuran (**1d**) (Table 1, entry 2). Hydrogen was the sole product observed in the gaseous phase (not shown). Neither of these two homocoupling reactions proceeded without the Pt/TiO₂ sample or light irradiation, implying that they were a photocatalytic reaction. So, it was proposed that the photogenerated holes on the TiO₂ photocatalyst could selectively oxidize allylic C–H bond in cyclohexene and alpha C–H bond in THF to their corresponding radicals and proton (eq. 1 and 2), which would give homocoupling products and other successive reaction products.

Table 1 Optimization of the reaction conditions for the photocatalytic cross-coupling between cyclohexene and THF with a Pt(0.1)/TiO₂ sample ^a

Entry	Reactants (ml)		Cross-coupling products (μmol) ^b			Homocoupling products (μmol) ^b		Selectivity	
	Cy	THF	A	B	C	1a ^c	1b+1c+1d ^d	S _{Cy} ^e	S _{THF} ^f
1	2.0	0.0	0.0	0.0	0.0	7.2	0.0	n.a. ^g	n.a.
2	0.0	2.0	0.0	0.0	0.0	0.0	4.0	n.a.	n.a.
3	1.0	3.0	1.7	1.5	1.4	1.1	3.9	81	54
4	0.5	3.0	2.0	1.4	1.6	0.6	12.2	89	29
5	0.2	3.0	1.3	0.9	0.8	0.2	15.8	93	16
6	3.0	0.5	0.7	0.4	0.4	6.8	0.0	18	100
7 ^h	0.5	3.0	4.4	3.8	3.1	1.3	31.6	90	26
8 ⁱ	0.5	3.0	0.0	0.0	0.0	0.0	0.0	n.a.	n.a.
9 ^j	0.5	3.0	0.0	0.0	0.0	0.0	0.0	n.a.	n.a.

^a Reaction conditions: Different amount of cyclohexene (Cy) and THF (1.0 ml of cyclohexene corresponds to 9.8 mmol, 1.0 ml of THF corresponds to 12 mmol), and 50 mg of the Pt(0.1)/TiO₂ sample were used for the reaction, the reaction time was 1 h, the wavelength of the light was ≥ 350 nm, $I = 40$ mW/cm² (at 365 ± 20 nm), and the reaction temperature was 303 K. ^b The amount of the cross-coupling products **A**, **B**, and **C** was determined from the calibration curve of **A**, which was prepared by following the literature.⁸ ^c The amount of **1a** was determined from the calibration curve of an authentic sample of 1,1'-bi(cyclohexane). ^d The amount of **1b-1d** was determined from the calibration curve of **A**. ^e Selectivity (%) for the cross-coupling products based on cyclohexene, $S_{\text{Cy}} = [100 \times (\text{total amount of A-C})]/(\text{Total amount of cyclohexene containing products})$. ^f Selectivity (%) for the cross-coupling products based on THF, $S_{\text{THF}} = [100 \times (\text{total amount of A-B})]/(\text{Total amount of THF containing products})$. ^g Not applicable. ^h 100 mg of the Pt(0.1)/TiO₂ sample was used for the reaction. ⁱ The reaction was performed without the Pt(0.1)/TiO₂ sample. ^j The reaction was performed in the dark.

This oxidation of ethers by the photogenerated holes on the TiO₂ photocatalyst has been evidenced by ESR spectroscopy, as discussed in the previous chapters, while that of cyclohexene has been evidenced in a previous work of our laboratory.¹⁰



Next, reactions were carried out with a mixture of cyclohexene and THF (Table 1, entries 3–9). The reaction between cyclohexene and THF with the

Pt(0.1)/TiO₂ sample under photoirradiation gave 3 three new peaks, hereafter referred to as peak 1 (**P1**), peak 2 (**P2**), and peak 3 (**P3**) in the increasing order of their retention time, along with the peaks for the homocoupling products from both reactants in the TIC (total ion chromatograph) of GC-MS. Based on their TIC area, **P1** was the major while **P2** and **P3** had similar areas. After comparing the experimental mass spectrum with that of an authentic sample, **P1** was assigned to 2-cyclohexyltetrahydrofuran (**A**). The remaining peaks were assigned to 2-(cyclohex-2-en-1-yl)tetrahydrofuran (**B**) and 2-(cyclohex-1-en-1-yl)tetrahydrofuran (**C**) based on the following reasons. The molecular ion peak of the remaining two peaks (**P2** and **P3**) was 2 units less than that of **P1**, indicating that the double bond of cyclohexene was retained in these compounds. Three compounds fit the specifications of GC-MS analysis for the new two peaks, as shown in figure 1, namely, 2-(cyclohex-1-en-1-yl)tetrahydrofuran (**a**), 2-(cyclohex-2-en-1-yl)tetrahydrofuran (**b**), and 2-(cyclohex-3-en-1-yl)tetrahydrofuran (**c**).

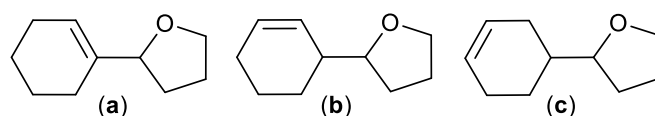
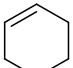
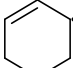
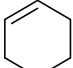


Figure 1 Possible structures of the peaks **P2** and **P3**

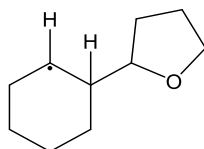
Assuming these compounds were formed by the hole-oxidation of cyclohexene to the corresponding radicals followed by coupling with the THF radicals, the stability of the cyclohexenyl radicals would be an important factor. By using the MOPAC2016 software¹¹ and PM7 method,¹² we calculated the heat of formation of the vinylic, the allylic, and the homoallylic radicals. The values are shown in Table 2. The heat of formation for each radical species was positive, among which allylic radical was the smallest (Table 2, entries 1–3). This means that the allylic cyclohexenyl radical is expected to be the most stable radical. Further, the homocoupling of cyclohexene gave [1,1'-bi(cyclohexane)]-2,2'-diene, confirming that the reaction mixture would generate the allylic-cyclohexenyl radicals. These radicals can couple with the THF radicals and give a functionalized product. Thus, the other cross-coupling product (**P2**) was assigned the structure **b** (Figure 1). This was supported by the results of the isotopic experiments, as discussed later.

Table 2 Heat of formation of cyclohexenyl radicals

Entry	Cyclohexenyl radical	Heat of formation / kJ mol ^{-1 a}
1	Vinlylic 	178.0
2	Allylic 	69.8
3	Homoallylic 	103.7

^a The heat of formation was calculated by the MOPAC2016 software⁸ using the PM7 method⁹

Due to the large heat of formation of the homoallylic and vinylic radicals, their formation would be difficult. Thus, if the reaction proceeds via radical-radical coupling, the compounds **a** and **c** should be ruled out as the probable structures of the cross-coupling product. However, another possible mechanism makes it possible to form compound **a**. Due to the large concentration of the THF radicals in the reaction system, there is high probability of its attack on the double bond of cyclohexene. This would generate a radical transition state as shown in Figure 2. Elimination of a hydrogen radical or abstraction of a proton by THF radical from the tertiary sp³ carbon of this transition state would re-generate the double bond. Thus, the remaining cross-coupling (**P3**) was assigned to **a** (Figure 1). In this way, the structure of the three cross-coupling products were assigned (Table 1, **A-C**).

**Figure 2** Proposed transition state generated by the attack of THF radical on cyclohexene

After establishing the structures of the cross-coupling products, we focused on improving their yield by varying the amount of the cyclohexene and THF. The homocoupling of THF was the major process occurring in the reactions performed with an excess of THF (Table 1, entries 3–5). This side reaction could be completely suppressed by conducting the experiment with cyclohexene in excess, although it also decreased the amount of the cross-coupling products (Table 1, entry 6). Since the mixture of 0.5 ml cyclohexene and 3 ml THF gave the largest amount of the cross-coupling products with high selectivity based on cyclohexene and appreciable selectivity based on THF, it was chosen as the optimum concentration of the two reactants (Table 1, entry 4). Increasing the amount of the Pt/TiO₂ sample increased the

amount of the cross-coupling products, albeit with a lowered selectivity based on THF (Table 1, entry 7). None of the products were obtained in the reactions done without light or Pt/TiO₂ sample, confirming that they were the products of a photocatalytic reaction (Table 1, entries 8 and 9).

Screening of M/TiO₂ photocatalysts

Table 3 shows the result of the screening of different M(x)/TiO₂ photocatalysts for the cross-coupling reaction between cyclohexene and THF under the optimized amounts of reactants (Table 3, entries 1–4). Among the various metals on the TiO₂ photocatalyst, Pt exhibited the highest activity for the formation of the cross-coupling products (Table 3, entry 1). The reaction performed with the Pd(0.1)/TiO₂ sample produced a new product peak (**P4**), assigned to 2-phenyltetrahydrofuran (**D**), which was probably a product of successive dehydrogenation of the cross-coupling products, **A**, **B** or **C** (Table 3, entry 2). The reaction performed with the pristine TiO₂ sample gave only a few products (Table 3, entry 5), suggesting that the Pt loading was necessary to obtain high product yields.

Table 3 Result of photocatalytic cross-coupling between cyclohexene and THF with various the M(0.1)/TiO₂ samples^a

Entry	Sample	Cross-coupling products (μmol)				Homocoupling products (μmol)		Yield ^b	Selectivity	
		A	B	C	D	1a	1b-1d		S _{Cy}	S _{THF}
1	Pt(0.1)/TiO ₂	4.4	3.8	3.1	0.0	1.3	31.6	0.23	89	26
2	Pd(0.1)/TiO ₂	0.8	0.2	0.3	2.5	0.0	1.5	0.07	100	71
3	Rh(0.1)/TiO ₂	2.6	2.3	1.8	0.0	0.9	13.0	0.13	88	34
4	Au(0.1)/TiO ₂	0.6	0.4	0.3	0.0	0.0	0.9	0.02	100	59
5 ^c	TiO ₂	0.5	0.3	0.3	0.0	0.2	1.3	0.02	85	46

^a 0.5 ml (4.9 mmol) cyclohexene, 3 ml (36 mmol) THF and 100 mg of the M(0.1)/TiO₂ sample were used for the reaction, other conditions were same as Table 1. ^b Total yield (%) of the cross-coupling products was calculated as 100×(amount of **A-C**)/(initial amount of cyclohexene). ^c The reaction was done with pristine TiO₂.

3.2.2. Time course

Figure 3 shows the result of the photocatalytic cross-coupling reaction between cyclohexene and THF with the Pt(0.1)/TiO₂ sample for various reaction time. The amount of all products steadily increased with time, meaning that the Pt(0.1)/TiO₂ sample exhibited long time activity. Further, the distribution of the cross-coupling products was almost constant throughout the experiments which implied that each product had an independent formation route. As the products A–C had similar structures, one might think that they are formed by a successive reaction but, the results of time course experiments denied this possibility and revealed that all were formed by an independent route. The homocoupling of cyclohexene increased steadily with time, which slightly decreased the selectivity of the functionalized products based on cyclohexene (%S_{Cy}). On the other hand, the homocoupling of THF showed an initial increase but slowed down later, which is the reason why the selectivity of the cross-coupling products based on THF was improved with time (%S-THF).

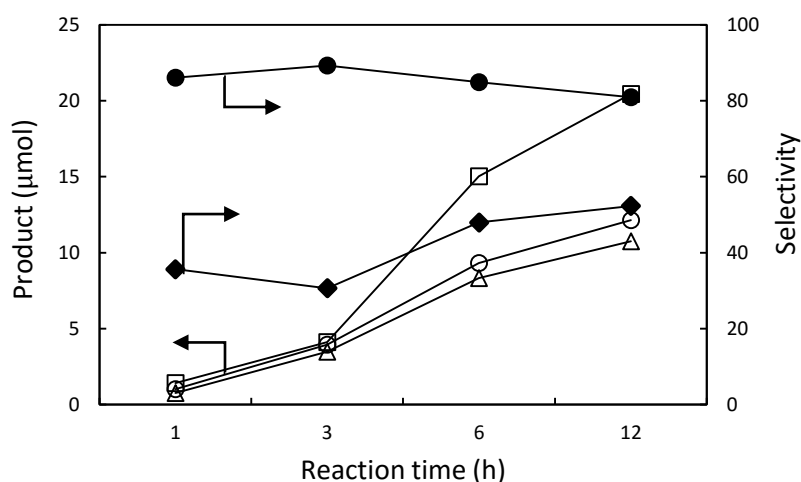


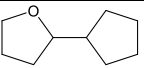
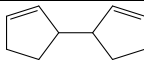
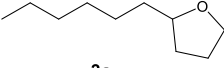
Figure 3 Time course of the photocatalytic cross-coupling between cyclohexene and THF with the Pt(0.1)/TiO₂ photocatalyst. A (square), B (circle), C (triangle), %S_{THF} (diamond), %S_{Cy} (filled circle)

3.2.3. Cross-coupling between different alkenes and THF

Not just cyclohexene, but other alkenes like cyclopentene and 1-hexene successfully underwent the photocatalytic cross-coupling with THF (Table 4). The reaction of cyclopentene and THF, with the Pt(0.1)/TiO₂ sample, gave 2-cyclopentyltetrahydrofuran (**2a**) as the only detectable cross-coupling product (Table 4, entry 1). Under the present conditions, the homocoupling of both cyclopentene and THF proceeded, although the amount of the

former's product (**2b**) was less than later (**1b** and **1c**). The cross-coupling between 1-hexene and THF also proceeded with the Pt(0.1)/TiO₂ sample to give 2-hexyltetrahydrofuran (**3a**) as the major cross-coupling product (Table 4, entry 2).

Table 4 Scope of alkenes for the photocatalytic cross-coupling with THF with the Pt(0.1)/TiO₂ sample ^a

Entry	Alkene (mmol)	Cross-coupling product (μmol) ^b	Homocoupling products (μmol) ^b	
			Alkene	THF (1b + 1c)
1	Cyclopentene (37)	 2a (0.52)	 2b (0.17)	1.11
2	1-Hexene (4)	 3a (0.49)	n.d. ^c	0.64

^a All reaction conditions were same as Table 1. ^b Amount of all products was approximately determined from the calibration curve of **A**. ^c Not detected

Under the present conditions, the homocoupling of THF also proceeded, to give **1b** and **1c**, but that of 1-hexene did not. The three alkenes exhibited different reactivity in the photocatalytic cross-coupling with THF, and from the yield of cross-coupling product, it can be assumed that cyclic alkenes were more reactive than acyclic alkenes.

3.3. Mechanistic studies

3.3.1. Kinetic experiments

The photocatalytic cross-coupling reaction between cyclohexene and THF was performed with deuterated reagents to elucidate the reaction mechanism. When compared to the reaction done without any deuterated reagent, the homocoupling of cyclohexene did not proceed in the reaction carried out with deuterated cyclohexene and THF, suggesting that the cleavage of the C–H bond of cyclohexene was the rate determining step (RDS) of the homocoupling of cyclohexene (Table 5, entries 1 and 2). As a C–D bond is slightly stronger than a C–H bond, replacement of cyclohexene with cyclohexene-*d*₁₀ will make its oxidation difficult and decrease the amount of **1a**, to give a normal kinetic isotope effect (KIE). Further, the homocoupling of THF was reduced in the reaction performed with cyclohexene and deuterated THF, indicating that the cleavage of the C–H bond of THF was the RDS of these products' formation (Table 5, entries 1 and 3). Interestingly, the homocoupling of cyclohexene increased in this

reaction, which could be explained by considering that the hole-catalyzed oxidation of cyclohexene and THF might be a competitive reaction.

Table 5 Kinetic experiments with cyclohexene and THF ^a

Entry	Deuterated reactant	Products / μmol					$k_{\text{H}}/k_{\text{D}}$ ^b				
		A	B	C	1a	1b-1d	A	B	C	1a	1b-1d
1	None	0.32	0.46	0.39	0.26	1.2	-	-	-	-	-
2	Cyclohexene- <i>d</i> ₁₀	0.37	0.15	0.15	Trace	0.9	0.8	3.0	2.6	n.a.	1.2
3	THF- <i>d</i> ₈	0.44	0.54	0.48	0.46	0.9	0.7	0.8	0.8	0.6	1.3

^a 0.2 ml (1.9 mmol) cyclohexene, 0.3 ml (3.6 mmol) THF, and 30 mg of the Pt(0.1)/TiO₂ sample were used for the reaction, other conditions were same as Table 1. ^b $k_{\text{H}}/k_{\text{D}}$ for each product was determined from its amount produced in entries 1 and 2 for entry 2, and those in entries 1 and 3 for entry 3, respectively.

The oxidation of deuterated THF would be slightly slower than that of normal THF as a C–D bond is stronger than a C–H bond. As a result, more photogenerated holes would be available for the oxidation of cyclohexene, which will ultimately increase the amount of **1a**. Thus, the cleavage of the C–H bond in cyclohexene and THF was the RDS for their homocoupling products' formation. The reaction with deuterated cyclohexene and THF increased the area of peak **P1** while reduced the area of peaks **P2** and **P3** indicating that the amount of **A** was increased while those of compounds **B** and **C** decreased (Table 5, entries 1 and 2). The value of $k_{\text{H}}/k_{\text{D}}$ calculated for peaks **P1**, **P2**, and **P3** was 0.9, 3.0, and 2.6 respectively, indicating an inverse Kinetic Isotope Effect (KIE) for **A** and a normal KIE for **B**, and **C**. Further, the reaction with cyclohexene and deuterated THF gave a larger amount of all three products (Table 5, entries 1 and 3). The value of $k_{\text{H}}/k_{\text{D}}$ calculated from this data was 0.7, 0.8, and 0.8 for **A**, **B** and **C**, respectively, indicating an inverse KIE for these three products. The observation of various KIE indicates that the cleavage of the labeled bonds in both THF and cyclohexene influence the rate-determining step for the formation of each product, as discussed below.

The inverse KIE observed for **A** during the reaction with deuterated cyclohexene can be attributed to the change in the hybridization of cyclohexene from sp² to sp³.¹³ When the double bond of cyclohexene would be attacked by THF radical, its hybridization would change from sp² (the vinylic carbon in cyclohexene) to sp³ (the complex with the THF radical as a transition state, Figure 2). This process will be accompanied by a change in

the zero-point energies, which is smaller for a C–D bond (403.2 cm⁻¹, which is difference of 586.8 cm⁻¹ for sp² to 990 cm⁻¹ for sp³) than a C–H bond (550 cm⁻¹, which is the difference of 800 cm⁻¹ for sp² to 1350 cm⁻¹ for sp³). Thus, due to small activation energy, the reaction performed with deuterated cyclohexene would be faster and hence would produce larger amount of **A** than the reaction under normal condition (Table 5, entry 2). Further, the normal KIE observed for **B** and **C** indicated that the cleavage of the C–H bond of cyclohexene would be the rate determining step for formation of compounds **B** and **C** (Table 5, entry 2). As discussed later, the formation of **B** would involve the coupling between an allylic cyclohexenyl and THF radical. **C**, on the other hand, would include the addition of THF radical on the double bond of cyclohexene followed by the elimination of a hydrogen radical from the resultant radical transition state (Figure 2). Hence, the formation of both **B** and **C** includes cleavage of a C–H bond of cyclohexene. However, for **B**, the bond is cleaved from the cyclohexene molecule, while for **C** it is cleaved from a transition state. We propose that between these two processes, the former would be more difficult as it includes the cyclohexene molecule, unlike the latter which involves the transition state. Upon the replacement of cyclohexene with cyclohexene-*d*₁₀ would make both these processes difficult as a C–D bond is stronger than a C–H bond. Further, as the former is more difficult, this replacement would decrease the formation of **B** more than **C**. Thus, the value of the k_H/k_D for **B** should be larger than **C** (Table 4, entry 2). The inverse KIE observed for the reaction carried out with cyclohexene and deuterated THF can be explained by considering the competitive oxidation of cyclohexene and THF (Table 5, entry 3), as observed for other THF containing reactions like in Chapter II-2 and II-3.

3.3.2. Temperature control experiments

In our previous work on the photocatalytic cross-coupling of arenes and alkanes with ethers, we found that the metal nanoparticles have a dual role of an electron receiver and a catalyst. To confirm this dual role in the photocatalytic cross-coupling between alkenes and ethers, temperature control reactions were performed. Table 6 shows the variation of the amount of cross-coupling products (**A–C**) with temperature during the photocatalytic reaction of cyclohexene and THF. For the reactions carried out with the Pt(0.1)/TiO₂ photocatalyst, the amount of all three products increased with temperature (Table 6, entries 1–4). The apparent activation

energies (kJ/mol) calculated from the pseudo Arrhenius plot of this data were 29.3, 21.6, and 20.3 for products corresponding to peaks **A**, **B** and **C** respectively (Table 7, entries 1–3 and Figure 4 (a)).

Table 6 Temperature control reactions between cyclohexene and THF with different photocatalysts ^a

Entry	Photocatalyst	Temperature (K)	Products (μmol)		
			A	B	C
1	Pt(0.1)/TiO ₂	300.15	2.98	1.94	1.66
2		310.15	4.27	2.19	1.76
3		314.15	5.13	2.85	2.51
4		318.15	5.76	3.19	2.58
5	TiO ₂	300.15	0.42	0.15	0.13
6		304.15	0.53	0.18	0.12
7		309.15	0.56	0.15	0.17
8		314.15	0.65	0.21	0.16

^a 0.5 ml cyclohexene, 3 ml THF, other conditions were same as Table 1

On the other hand, for the reactions performed with the pristine TiO₂ photocatalyst, the variation of the production rate with temperature was lesser than that with the Pt/TiO₂ photocatalyst (Table 6, entries 5–8). The apparent activation energies (kJ/mol) for the three products, determined from the pseudo-Arrhenius plot of this data were 23.2, 13.0, and 16.1 for products corresponding to peaks **A**, **B**, and **C** respectively (Table 7, entries 4–6 and Figure 4 (b)).

Table 7 Apparent activation energy for the photocatalytic cross-coupling reaction between cyclohexene and THF

Entry	Photocatalyst	Product	Activation energy (kJ/mol)
1	Pt(0.1)/TiO ₂	A	29.3
2		B	21.6
3		C	20.3
4	TiO ₂	A	23.2
5		B	13.0
6		C	16.1

The activation energy values for the three products were similar on the two photocatalysts. Further, these values were much smaller than those observed for the previously reported photocatalytic reactions of arenes-ethers and alkanes-ethers. Thus, the contribution of metal catalysis by the Pt nanoparticles, loaded on TiO₂, would be very small or ruled out. Hence, the role of the Pt nanoparticles was proposed to be limited to an electron

receiver on the TiO₂ photocatalyst, which would reduce the recombination between photogenerated electrons and holes and facilitate the reaction.

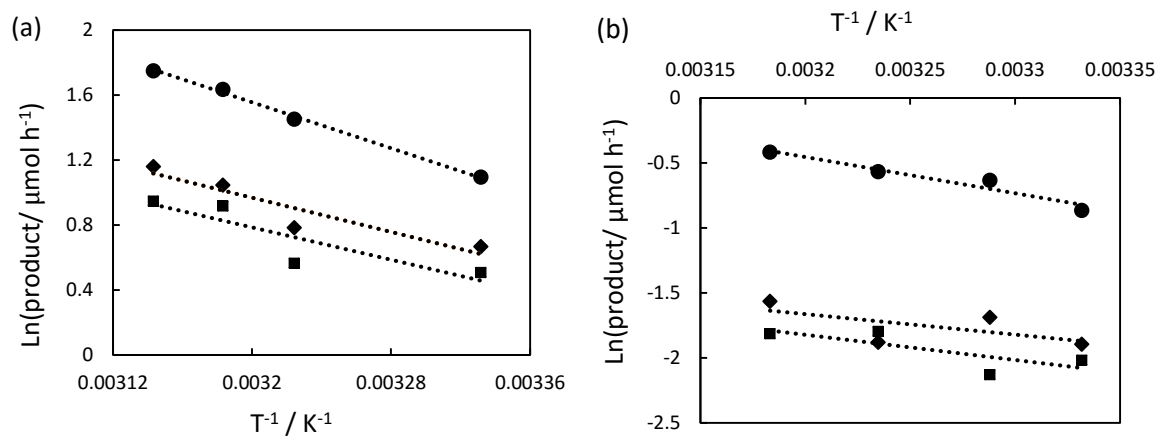


Figure 4 Pseudo Arrhenius plot for the photocatalytic cross-coupling between cyclohexene and THF with (a) Pt(0.1)/TiO₂ (b) TiO₂. A (circle), B (diamond), and C (square)

Apparently, the different electronic properties of the three hydrocarbons, arenes, alkanes, and alkenes, affect the role of the metal nanoparticles on the TiO₂ surface in their photocatalytic cross-coupling reactions with ethers. Although alkenes have some similar features both arenes and alkanes, they differ a lot in their photocatalytic reactions with ethers. The presence of localized electron cloud increases their reactivity for attack by the ether radical, unlike benzene which needs activation by Pd nanoparticles due to a delocalized electron cloud. Further, this localized electron density decreases the C–H bond dissociation energy of the adjacent allylic sp³C–H bonds which results in easier oxidation by the photogenerated holes, unlike the cyclohexane molecule where the absence of any functional group makes the sp³C–H bond unreactive. Thus, the efficiency of the photocatalytic cross-coupling reaction between alkenes and ethers might predominantly depend on the separation of the photogenerated electrons and holes on the TiO₂ photocatalyst and hence the role of the metal nanoparticles might be limited to an electron receiver.

3.3.3. Proposed reaction mechanism

The above observations are used to propose the three types of reaction mechanism for the photocatalytic cross-coupling between cyclohexene and THF by Pt/TiO₂ sample. Figure 5 (a) shows the proposed mechanism for the product A: (1) Photoexcitation of TiO₂ would generate holes and electrons,

where the holes move to surface of TiO_2 and the electrons move to Pt nanoparticles. On the TiO_2 surface, the hole oxidizes a THF molecule to make a THF radical species (2-tetrahydrofuryl radical) and a proton. This proton is reduced to hydrogen radical by the electrons present on the Pt nanoparticles. (2) The photogenerated THF radical attacks the cyclohexene molecule to make a radical complex as a transition state (**I**). Since the hybridization change of the vinylic carbon in cyclohexene molecule from sp^2 to sp^3 gave an inverse KIE for **A** in the reaction done with deuterated cyclohexene (Table 5, entry 2), this step is the RDS for the formation of **A**. (3) Finally, the radical complex **I** combines with a hydrogen radical to give the product **A**. The formation of **A** will be a one-photon process. Figure 5 (b) shows the proposed reaction mechanism for the formation of product **B**: (1) The photogenerated holes could oxidize both cyclohexene and THF molecules to generate their corresponding radical species (2-tetrahydrofuryl radical and 3-cyclohexenyl radical) and protons. This is a two-photon process. Also, as evidenced by kinetic experiments (Table 5, entry 2), the oxidation of cyclohexene is the RDS. (2) The coupling of the radicals from cyclohexene and THF gives product **B**. (3) The protons generated in the oxidation steps are reduced to hydrogen radical on Pt, followed by the formation of hydrogen. The formation of **B** would be a two photon process. Figure 5 (c) shows the proposed mechanism for the product **C**: The steps 1 and 2 for the formation of the radical species and the radical intermediate (**I**) are the same as those for **C**. (3) In this case, elimination of a hydrogen radical from the radical intermediate (**I**) takes place to re-generate the double bond and give product **C**. The cleavage of the C-H bond of the tertiary sp^3 carbon of the cyclohexene in the transition state (**I**) is the RDS in this mechanism, which gives a normal KIE in the reaction done with deuterated cyclohexene (Table 5 entry 2). (4) Coupling of the hydrogen radicals on Pt would generate hydrogen. The formation of **C** will be a one-photon process.

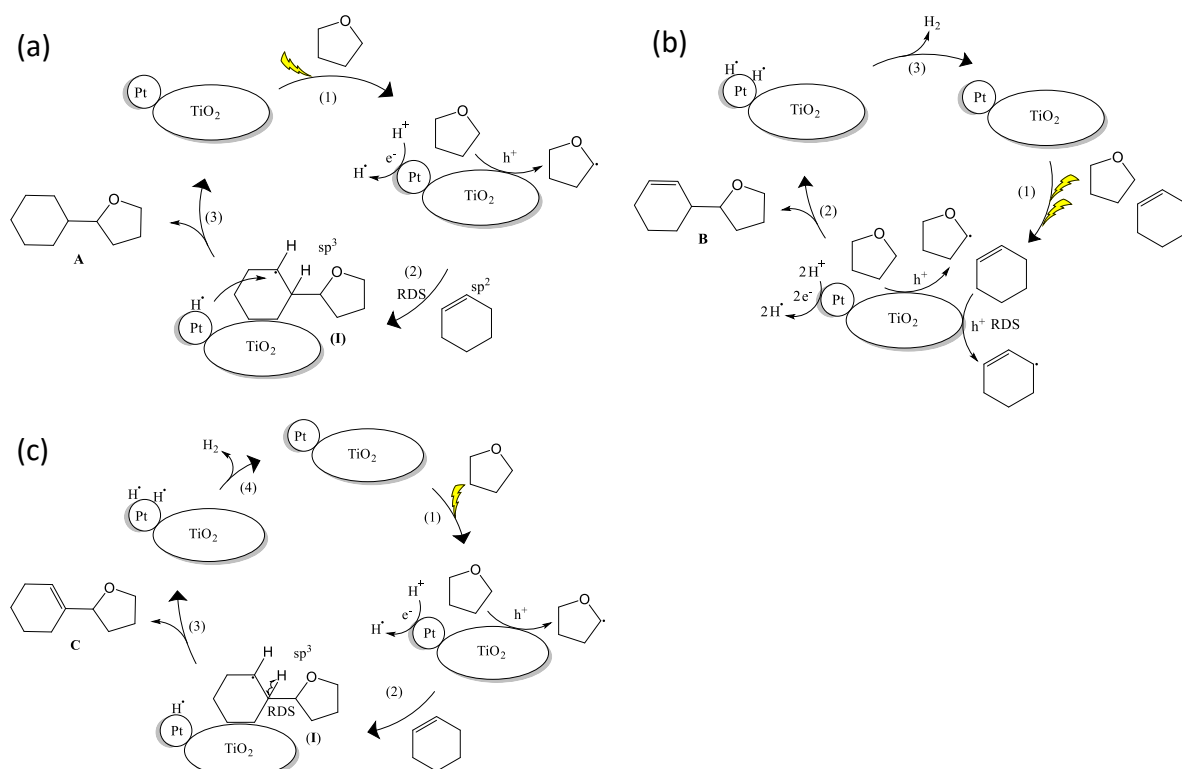


Figure 5 Three types of the reaction mechanism proposed for the formation of (a) **A**, (b) **B**, and (c) **C**

4. Conclusion

The results of the present study can be summarized as follows. A Pt/TiO₂ photocatalyst successfully catalyzed the cross-coupling reaction between alkenes and ethers. The reaction between cyclohexene and THF was examined for mechanistic investigation, which revealed that this cross-coupling reaction was a photocatalytic process involving radicals of both substrates and followed three different mechanisms for each product, namely, radical addition (**A**), radical addition-elimination (**B**), and radical-radical coupling (**C**). Also, unlike the reactions of ethers with arenes and alkanes, the contribution of the metal catalysis by Pd or Pt nanoparticles cannot be observed for the reaction between alkenes and THF. This was attributed to the different electronic properties of the alkenes from arenes and alkanes.

5. References

- [1] A. Tyagi, A. Yamamoto, M. Yamamoto, T. Yoshida and H. Yoshida, *submitted*.
- [2] R. F. Heck and J. P. Nolley, *J. Org. Chem.*, vol. 37, pp. 2320-2332, **1972**.
- [3] K. Sonogashira, Y. Tohda and N. Hagihara, *Tetrahedron Lett.*, vol. 16, pp. 4467-4470, **1975**.
- [4] N. Miyura, K. Yamada and A. Suzuki, *Tetrahedron Lett.*, vol. 36, pp. 3437-3440, **1979**.
- [5] Y. Hatanaka and T. Hiyama, *J. Org. Chem.*, vol. 53, pp. 918-920, **1988**.
- [6] A. Tyagi, T. Matsumoto, T. Kato and H. Yoshida, *Catal. Sci. Technol.*, vol. 6, p. 4577, **2016**.
- [7] A. Tyagi, A. Yamamoto, T. Kato and H. Yoshida, *Catal. Sci. Technol.*, vol. 7, p. 2616, **2017**.
- [8] X. Jiang, E. K. London, D. J. Morris, G. J. Clarkson and M. Wills, *Tetrahedron*, vol. 66, p. 9828, **2010**.
- [9] Z. Tian, A. Fattahi, L. Lis and S. R. Kass, *J. Am. Chem. Soc.*, vol. 128, p. 17087, **2006**.
- [10] E. Wada, T. Takeuchi, Y. Fujimura, A. Tyagi, T. Kato and H. Yoshida, *Catal. Sci. Technol.*, vol. 7, p. 2457, **2017**.
- [11] J. J. P. Stewart, "MOPAC2016; Stewart Computational Chemistry, Colorado Springs, CO, USA," 2016. [Online]. Available: <http://OpenMOPAC.net>.
- [12] J. J. P. Stewart, *J. Mol. Model.*, vol. 19, p. 1, **2013**.
- [13] E. V. Anslyn and D. A. Dougherty, *Modern Physical Organic Chemistry* (Chapter 8, page 428), Edwards Brothers, **2005**.

II-5. Summary

In Chapter 2, we have successfully developed a novel photocatalytic reaction system for construction of C–C bonds between various hydrocarbons and ethers by the direct activation of their C–H bonds. All reactions were carried out at mild temperatures and without the use of any additional oxidizing or reducing reagents. Appreciable product yields (> 20%) were obtained for some reactions. These values are one of the best among the cross-coupling reactions by TiO₂ photocatalyst.

Further, we succeeded elucidate the role of each catalytic component in the reaction system. The photocatalysis by TiO₂ was responsible to oxidize the various substrates into their corresponding radicals which reacted to give different products. The role of the noble metal nanoparticles in these cross-couplings was also proposed. Their primary role was that of an electron receiver to reduce the recombination of the photogenerated electrons and holes on the TiO₂ photocatalyst. However, in some reactions, the noble metal nanoparticles were found to catalyze at least one step in the photocatalytic reaction. The nature of this catalysis was proposed for the activation of the aromatic ring of an arene molecule or the activation of C–H bond of aliphatic carbon on their surface, which facilitated their reaction with the photogenerated radicals. Thus, they acted as co-catalysts in the photocatalytic reaction.

These findings strengthened our understanding of the photocatalytic organic synthesis reactions and motivated us to develop a new type of catalytic reactions consisting of a physical mixture of photocatalyst and metal catalyst, as discussed in the next chapter.

Chapter III Blended catalysts consisting of titanium oxide photocatalyst and supported metal catalyst for the carbon-carbon coupling reactions

III-1. Introduction

TiO₂ catalyzed photocatalytic organic synthesis is an emerging field. However, these reactions are often crippled by low yield due to the rapid recombination of photogenerated holes and electrons. Loading of noble metal nanoparticles on TiO₂ is one of the most frequently used techniques to overcome this problem. The photogenerated electron in the conduction band of TiO₂ can be transferred to these noble metals and so its recombination with the holes is reduced. Thus, the primary role of metal nanoparticles on TiO₂ is an electron receiver. However, these metal nanoparticles can also participate catalytically in these photocatalytic reactions which can alter the product selectivity.¹⁻¹² Such system allows the variation of the metal catalyst and photocatalyst independently depending on the reaction's requirement. However, this kind of study is hardly investigated.

In the previous chapters we had evidenced that the Pd and Pt nanoparticles loaded on TiO₂ participated catalytically in the photocatalytic cross-coupling between arenes and ethers,⁸ and alkanes and ethers,¹⁰ respectively. This revelation motivated me to develop a new class of catalysis systems, where the reactions were done with a physical mixture of TiO₂ photocatalyst and alumina supported metal catalysts (M(x)/Al₂O₃) i.e., a blended catalyst. we have also modified the monometallic M(x)/Al₂O₃ catalysts to Pd-Au bimetallic catalysts (Pd(x)Au(y)/Al₂O₃, x and y denote the loading amount of Pd and Au in weight %).

In this chapter, we have applied this new catalysis to the previously reported photocatalytic cross-coupling reactions of hydrocarbons (arenes and cyclohexane) with ethers and alkanes-ethers, and also developed a new reaction of photocatalytic Ullmann coupling of aryl halides. The blended catalytic system developed in this work is one of first example of photocatalytic C–C cross-coupling reactions.

References

- [1] B. Ohtani, K. Iwai, S. Nishimoto and S. Sato, *J. Phys. Chem. B.*, vol. 17, p. 3349, **1997**.
- [2] J. Lee and W. Choi, *Environ. Sci. Technol.*, vol. 38, p. 4026, **2004**.
- [3] J. M. Herrmann, *Top. Catal.*, vol. 39, p. 3, **2006**.
- [4] H. Gekko, K. Hashimoto and H. Kominami, *Phys. Chem. Chem. Phys.*, vol. 14, p. 7965, **2012**.
- [5] H. Yoshida, Y. Fujimura, H. Yuzawa, J. Kumagai and T. Yoshida, *Chem. Commun.*, vol. 49, p. 3793, **2013**.
- [6] Y. Shiraishi, H. Sakamoto, K. Fujiwara, S. Ichikawa and T. Hirai, *ACS Catal.*, vol. 4, p. 2418, **2014**.
- [7] Z. Zhang, V. Merk, A. Hermanns, W. E. S. Unger and J. Kneipp, *ACS Catal.*, vol. 7, p. 7803, **2017**.
- [8] A. Tyagi, T. Matsumoto, T. Kato and H. Yoshida, *Catal. Sci. Technol.*, vol. 6, p. 4577, **2016**.
- [9] E. Wada, T. Takeuchi, Y. Fujimura, A. Tyagi, T. Kato and H. Yoshida, *Catal. Sci. Technol.*, vol. 7, p. 2457, **2017**.
- [10] A. Tyagi, A. Yamamoto, T. Kato and H. Yoshida, *Catal. Sci. Technol.*, vol. 7, p. 2616, **2017**.
- [11] E. Wada, A. Tyagi, A. Yamamoto and H. Yoshida, *Photochem. Photobio. Sci.*, accepted, vol. 16, p. 1744, **2017**.
- [12] A. Tyagi, A. Yamamoto, M. Yamamoto, T. Yoshida and H. Yoshida, *submitted*.
- [13] A. Tyagi, A. Yamamoto, and H. Yoshida, *to be submitted*.

III-2. Photocatalytic cross-coupling between arenes and tetrahydrofuran

Abstract

A physical mixture of TiO₂ photocatalyst and alumina supported Pd catalyst (Pd(x)/Al₂O₃) exhibited higher activity than the TiO₂ photocatalyst alone for the photocatalytic cross-coupling between arenes and tetrahydrofuran (THF). The reaction did not proceed without TiO₂ photocatalyst, thus eliminating the possibility of plasmonic catalysts by the metals. Introduction of slight amount of Au to the Pd(x)/Al₂O₃ catalysts further improved their catalytic activity. The physical mixture of the TiO₂ photocatalyst and the Pd(2.0)Au(1.0)/Al₂O₃ catalyst gave a higher yield of the cross-coupling product than the Pd(3.0)/TiO₂ photocatalyst for the photocatalytic reaction benzaldehyde and THF.

1. Introduction

In our previous study on the photocatalytic cross-coupling between arenes and ethers with the Pd/TiO₂ photocatalysts, the Pd nanoparticles were evidenced to have a dual role of an electron receiver and metal catalyst. Encouraged by that result, we focused on the enhancement of the product yield and selectivity by modifying the metal's properties. Generally, the metal catalysis is deeply affected by the physical properties of metal nanoparticles like dispersion, particle size, and electronic state. In this work we have tried to modify these properties of the Pd nanoparticles by preparing the Pd-Au bimetallic catalysts and study its effect on the photocatalytic cross-coupling between arenes and THF. In order to realize it, at first, we examined a blended catalyst, which is a physical mixture of the TiO₂ photocatalyst and a supported metal catalyst. The separation of the metal catalyst part from the TiO₂ photocatalyst enabled us to design the supported metal catalysts independently since the modification of the metal catalysts on the TiO₂ surface often leads the strong metal support interaction (so-called SMSI). The bimetallic catalysts were characterized by various techniques and a correlation between the electronic state of Pd and its catalytic activity was proposed.

2. Experimental Section

2.1. Preparation of catalysts

The Pd(x)/TiO₂ photocatalysts were prepared by a photodeposition method as mentioned in Chapter II-2. Alumina supported Pd catalysts (Pd(x)/Al₂O₃) were prepared by an impregnation method as follows. 4 g of Al₂O₃ sample, obtained from Catalysis Society of Japan as JRC-ALO-7 (γ phase, specific surface area 204 m²/g) was dispersed in 100 mL ion-exchanged water. Then, after 10 min of stirring, desired amount of aqueous solution of PdCl₂ (Kishida, 99%) was added. The suspension was stirred at room temperature for 1 h, and later at 373 K to evaporate it to dryness. The solid so obtained was dried overnight at 323 K and powdered to obtain Pd(x)/Al₂O₃ catalysts, where x denotes its loading amount in weight%.

The supported Pd-Au bimetallic catalysts were prepared by a previously reported procedure with some modifications as discussed below.¹ 2 g of the support (Al₂O₃ (JRC-ALO-7) or SiO₂ (JRC-SIO-9, 334 m² g⁻¹) and desired volume of aqueous solutions of PdCl₂ and HAuCl₄.4H₂O were dispersed in 60 ml ion-exchanged water. The suspension was vigorously stirred at room temperature for 15 min. The pH of the suspension was adjusted to 10 by using an aqueous solution of NaOH (1 M). The resultant slurry was stirred for 24 h at room temperature. Then, the contents were filtered and dried overnight in an electric oven (323 K). Finally, the powder was reduced at 423 K under pure H₂ for 30 min to get Pd(x)Au(y)/support samples, where x and y refer to the loading amount of the two metals in weight%. The total loading amount of the metals on the support was fixed to 3 wt.%. For comparison, supported Pd(3.0) and Au(3.0) samples were also prepared by a similar procedure.

2.2. Characterization of catalysts

The Pd(x)/Al₂O₃ catalysts were characterized by different techniques. A CO pulse adsorption experiment was used to determine the particle size and metal dispersion. CO pulse adsorption tests were carried out on a homemade experimental set-up and CO analysis was done by a GC coupled with TCD (Shimadzu, GC-8A). The procedure involved reduction of the Pd(x)/Al₂O₃ samples, as pre-treatment, under hydrogen (11%) and argon mixture at 673 K for 15 min followed by cooling to room temperature in argon (100%). X-ray absorption fine structure (XAFS) was used to study the electronic state of Pd on Al₂O₃. The Pd-L_{III} edge spectra were recorded at beam line 6N1 at the Aichi Synchrotron Radiation Center of Knowledge Hub Aichi (Toyota,

Japan) in a fluorescence X-ray yield mode with a silicon drift detector (Vortex Electronics) using a Ge(111) monochromator. The spectra were analyzed by Athena software.² The various Pd(*x*)Au(*y*)/Al₂O₃ bimetallic catalysts were characterized by different techniques like UV-DRS, TEM, XRD and XAFS. UV-DRS measurements were carried out on JASCO V-570. XRD measurements of the Pd(*x*)Au(*y*)/SiO₂ and Pd(*x*)Au(*y*)/Al₂O₃ samples were carried out on a XRD-6000 Shimadzu. TEM measurements were carried out on a JEM-2200FS Field Electron Microscope. Pd-K edge and Au-L_{III} edge XAFS measurements were carried out at the BL01B1 beam line of the synchrotron facility at SPring8 in the RIKEN Harima institute (Hyogo, Japan) (proposal no. 2017A1477,2017A1511). Spectra were analyzed by Athena software.

2.3. Photocatalytic activity tests

2.3.1. Materials

All chemicals were of analytical grade and used without further purification, the details of which are shown in Chapter II-2.

2.3.2. Procedure for activity tests

All photocatalytic activity tests were carried out in a procedure similar to that in Chapter II-2.

3. Results and Discussion

3.1. Catalyst characterization

3.1.1. Pd(*x*)/Al₂O₃ samples

CO pulse adsorption

CO pulse adsorption analysis was employed to determine the dispersion and the size of Pd on Al₂O₃ in the Pd(*x*)/Al₂O₃ samples (Table 1). The particle size and dispersion of Pd in the two samples were similar (Table 1, entries 1 and 2).

Table 1 Metal dispersion and particle size in the Pd(*x*)/Al₂O₃ samples

Entry	Sample	Metal dispersion	Particle size (nm)
1	Pd(0.1)/Al ₂ O ₃	34.5	3.2
2	Pd(1.0)/Al ₂ O ₃	48.8	2.3

XAFS

Figure 1 shows the normalized Pd-L_{III} edge XANES spectra of the Pd foil (Figure 1 a), the fresh Pd(1.0)/Al₂O₃ sample (Figure 1 b), and the Pd(1.0)/Al₂O₃ sample reduced by hydrogen at 673 K (Figure 1 c). The XANES features in the fresh Pd(1.0)/Al₂O₃ sample were clearly different from the Pd foil. On the other hand, the reduced Pd(1.0)/Al₂O₃ sample had similar XANES features as Pd foil. These results indicate that the Pd nanoparticles on the Al₂O₃ in the fresh samples were in the oxidized state to some extent but could be reduced by hydrogen treatment.

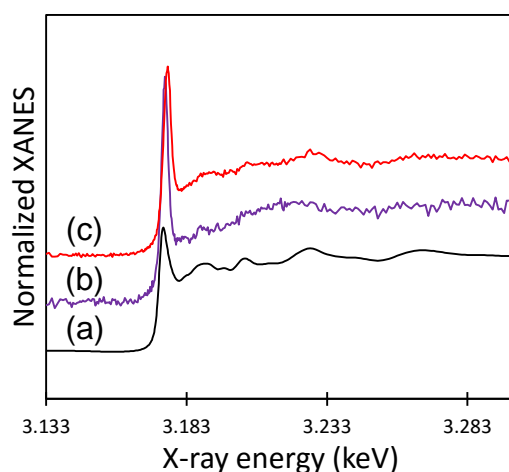


Figure 1 Normalized Pd-L_{III} XANES spectra of (a) a Pd foil, (b) the fresh Pd(1.0)/Al₂O₃ sample, and (c) the Pd(1.0)/Al₂O₃ sample reduced by H₂ at 673 K.

3.1.2. Pd(x)Au(y)/Al₂O₃ samples

TEM

Figure 2 show the TEM images and particle distribution histograms of the Pd(3.0)/Al₂O₃ (Figure 2 a1–3) Au(3.0)/Al₂O₃ (Figure 2 b1–3) and Pd(2.0)Au(1.0)/Al₂O₃ (Figure 2 c1–3) samples. Well dispersed nanoparticles were obtained in all three samples with an average particle size of 3 to 4 nm. The small particle size in the Pd(2.0)Au(1.0)/Al₂O₃ samples hindered the EDX mapping because of which their structure could not be confirmed. However, an arbitrarily chosen nanoparticle from this sample had a uniform image and fringe spacing (Figure 3), indicating its crystallinity. Thus, it can be proposed that like the pure Pd and Au samples, the Pd(2.0)Au(1.0)/Al₂O₃ samples were also crystalline.

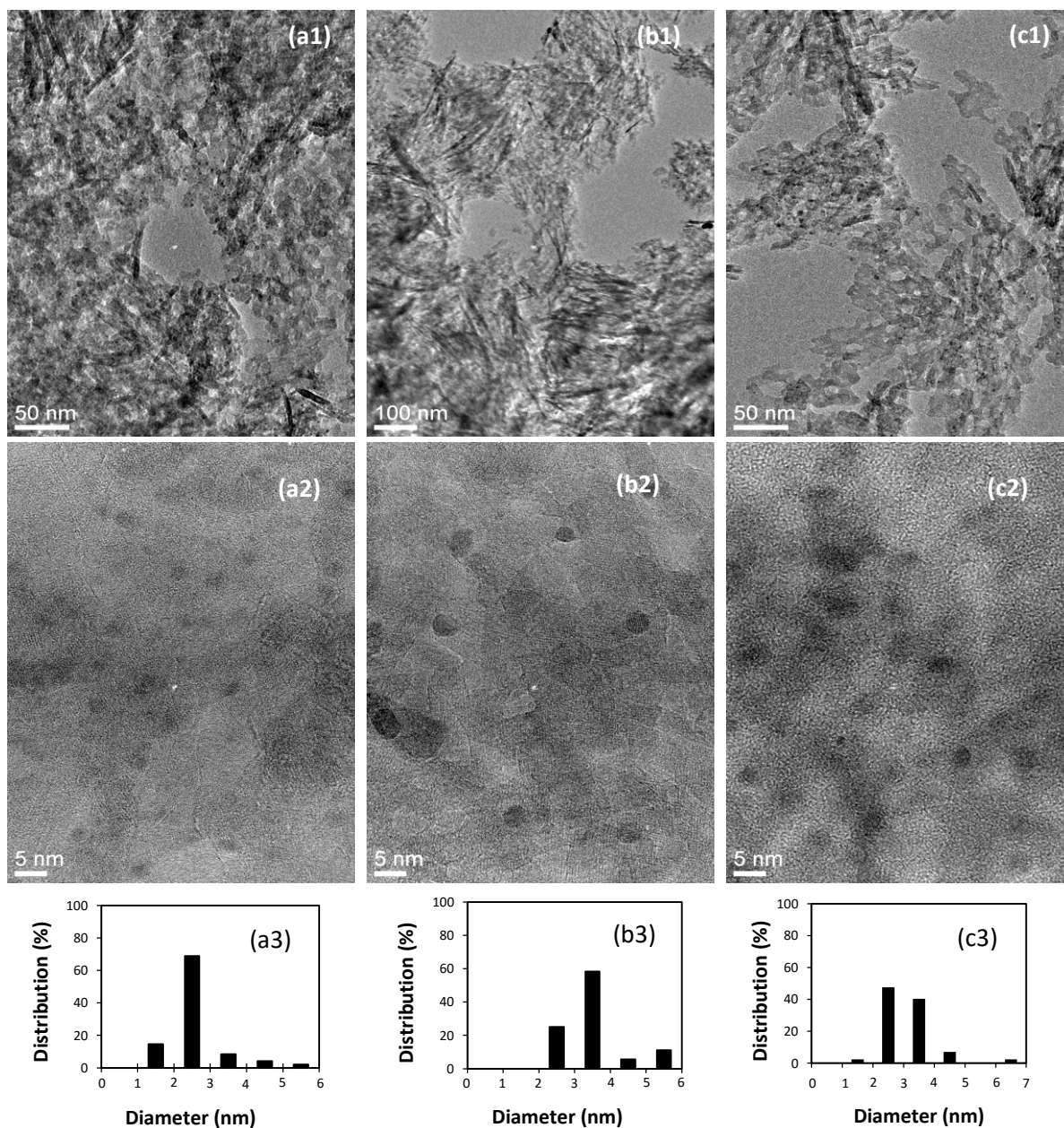


Figure 2 TEM images of Pd(3.0)/Al₂O₃ (a1-2), Au(3.0)/Al₂O₃ (b1-2), and Pd(2.0)Au(1.0)/Al₂O₃ (c1-2) and particle distribution histograms for Pd(3.0)/ Al₂O₃ (a3), Au(3.0)/ Al₂O₃ (b3), and Pd(2.0)Au(1.0)/Al₂O₃ (c3) samples

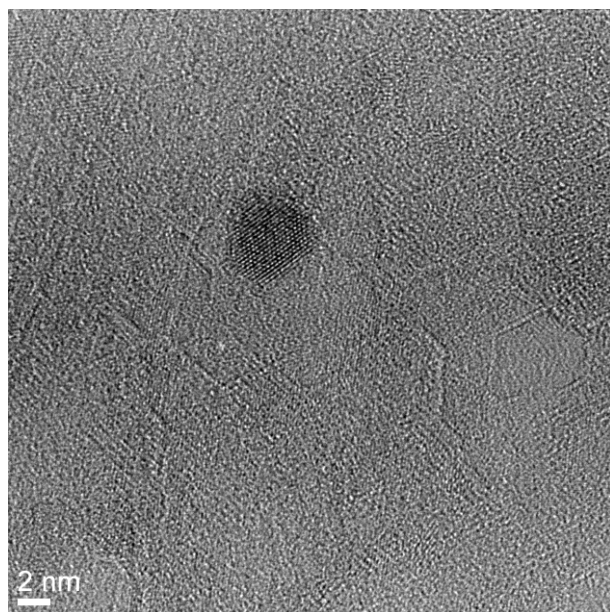


Figure 3 TEM image of a single nanoparticle in the Pd(2.0)Au(1.0)/Al₂O₃ sample

XRD

Figure 4 shows the powder XRD patterns of bare Al₂O₃ support (Figure 4a) and Pd(*x*)Au(*y*)/Al₂O₃ samples (Figure 4 b–e). According to the literature, the Pd (111), (200), and (220) diffractions should be at $2\theta = 40.1^\circ$, 46.5° , and 68.1° respectively (ICSD coll. Code 41517) while the Au (111), (220), and (311) diffractions should be at $2\theta = 38.19^\circ$, 64.58° , and 77.1° respectively (ICSD coll. Code 52249). These signals were not observed in the XRD patterns of the prepared monometallic Pd(3.0)/Al₂O₃ sample and the Pd(*x*)Au(*y*)/Al₂O₃ samples, which could be due to the formation of small nanoparticles as evidenced by TEM (Figure 2). Another possibility is the interference of the broad diffraction peaks from Al₂O₃ around $2\theta = 38^\circ$, 46° , and 65° which overlapped with the diffractions from Pd and Au. To avoid the interference by the Al₂O₃ support, we prepared SiO₂ supported samples and characterized them by XRD. As discussed later, like the Al₂O₃ supported samples, the Pd(2.0)Au(1.0)/SiO₂ sample exhibited higher catalytic activity than the Pd(3.0)/SiO₂ and Au(3.0)/SiO₂ samples. Hence, characterization of the SiO₂ supported samples should be applicable for the Al₂O₃ supported samples.

Figure 5 shows the powder XRD pattern of the SiO₂ support (Figure 5a), the Pd(3.0)/SiO₂ (Figure 5b), Pd(2.0)Au(1.0)/SiO₂ (Figure 5c), and Au(3.0)/SiO₂

samples (Figure 5d). The Pd(111), Pd(200), and Pd(220) peak was clearly visible at $2\theta = 40.1^\circ$, 46.5° , and 68.1° (ICSD coll. Code 41517) in the Pd(3.0)/SiO₂ sample. These peaks also appeared in the Pd(2.0)Au(1.0)/SiO₂ sample which indicated the presence of Pd metal in this sample. The diffraction pattern from Au was not visible in either Au(3.0)/SiO₂ or Pd(2.0)Au(1.0)/SiO₂ sample which suggests that the Au species might be small and well dispersed in these samples. These results also suggests that the bimetallic Pd(2.0)Au(1.0)/SiO₂ sample might not be an alloy, as in that case the diffraction peak of Pd in the 30–50° region would be shifted from the monometallic Pd(3.0)/SiO₂ sample.³ As such shift was not observed, the formation of an alloy structure can be ruled out in these samples.

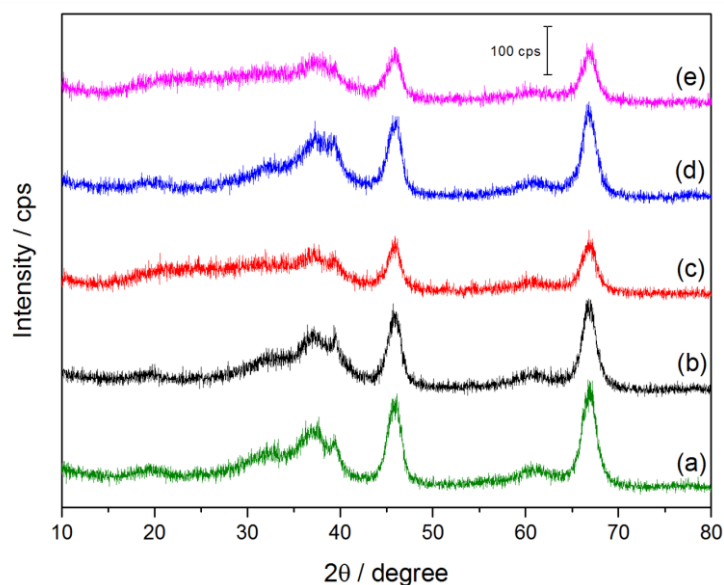


Figure 4 XRD pattern of (a) Al₂O₃, (b) Pd(3.0)/Al₂O₃, (c) Pd(2.5)Au(0.5)/Al₂O₃, (d) Pd(1.5)Au(1.5)/Al₂O₃, and (e) Pd(0.5)Au(2.5)/Al₂O₃

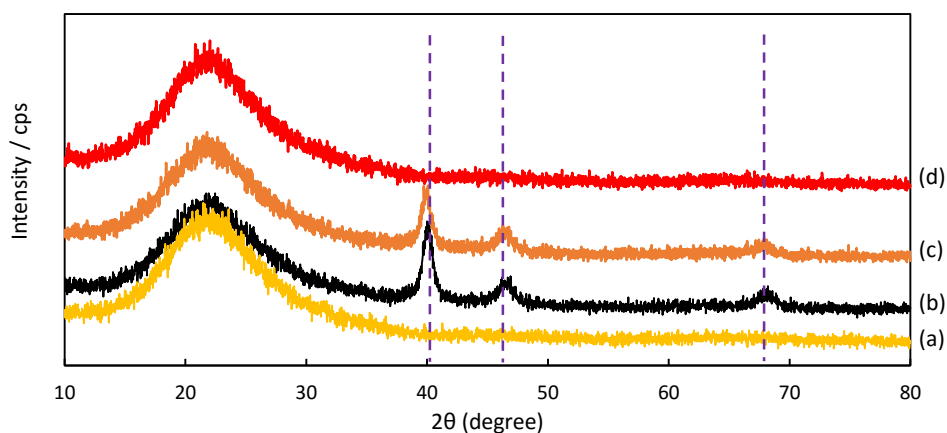


Figure 5 XRD patterns of (a) SiO₂, (b) Pd(3.0)/SiO₂, (c) Pd(2.0)Au(1.0)/SiO₂, and (d) Au(3.0)/SiO₂

UV-DRS

Figure 6 shows the UV-DRS spectra of the monometallic Pd(3.0)/Al₂O₃ sample (Figure 6a), different Pd(x)Au(y)/Al₂O₃ samples (Figure 6 b–e), and the monometallic Au(3.0)/Al₂O₃ sample (Figure 6f). The Pd(3.0)/Al₂O₃ sample did not show any plasmonic peak (Figure 6a). Increasing the Au content in the Pd(x)Au(y)/Al₂O₃ samples changed the spectra (Figure 6 b–e) and the Au plasmon peak around 525 nm was clearly visible in the Pd(0.5)Au(2.5)/Al₂O₃ (Figure 6e) and Au(3.0)/Al₂O₃ samples (Figure 6f). These results indicate that the state of Pd nanoparticles was affected by the introduction of Au in the Pd(x)Au(y)/Al₂O₃ samples. Further, as the spectra of the bimetallic Pd(x)Au(y)/Al₂O₃ samples could not be simulated by the monometallic Pd(3.0)/Al₂O₃ and Au(3.0)/Al₂O₃ samples, it can be proposed that the Pd(x)Au(y)/Al₂O₃ samples do not have independent Pd and Au nanoparticles, but those in close contact with each other.

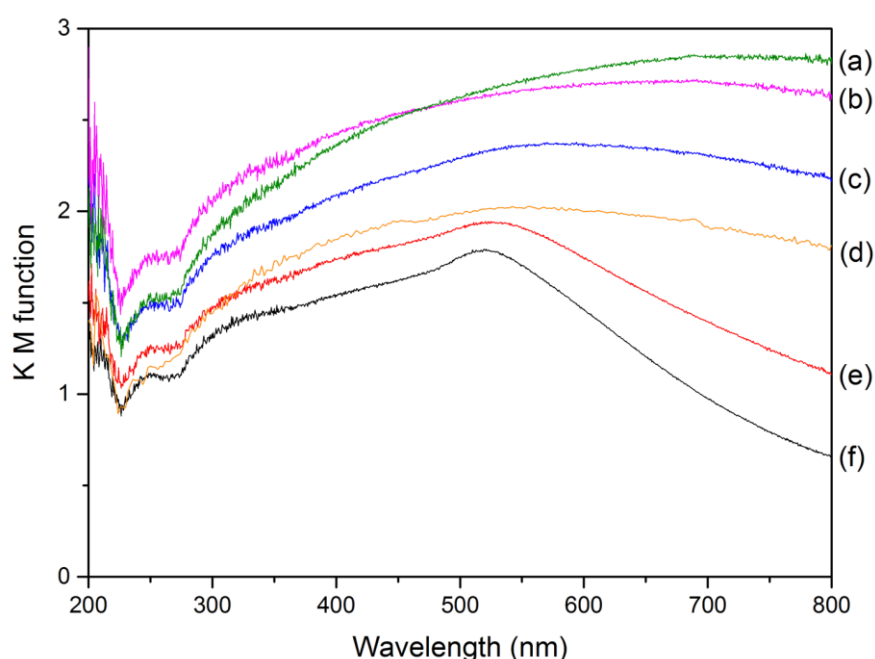


Figure 6 UV-DRS spectra of (a) Pd(3.0)/Al₂O₃, (b) Pd(2.5)Au(0.5)/Al₂O₃, (c) Pd(2.0)Au(1.0)/Al₂O₃, (d) Pd(1.5)Au(1.5)/Al₂O₃, (e) Pd(0.5)Au(2.5)/Al₂O₃, (f) Au(3.0)/Al₂O₃

XAFS

Figure 7 shows the normalized Pd-K edge XANES in the reference Pd foil (Figure 7a), monometallic Pd(3.0)/Al₂O₃ sample (Figure 7b) and the various Pd(x)Au(y)/Al₂O₃ samples. The spectral features in the prepared samples

were clearly different from those of the foil, which would mainly originate from the property of nanoparticles. The samples containing a large amount of Au exhibited slightly different shape from others (Figure 7f), suggesting the Pd atoms are affected by the Au atoms and have local structure or electronic state different from those in the Pd metal. Also, a clear shift in the absorption edge towards the lower energy was observed in the order: the reference Pd foil (Figure 8a), the monometallic Pd(3.0)/Al₂O₃ sample (Figure 8b), the bimetallic Pd(2.5)Au(0.5)/Al₂O₃, and Pd(2.0)Au(1.0)/ Al₂O₃ samples (Figure 8c and d). The shift from Pd foil to monometallic Pd(3.0)/ Al₂O₃ sample is commonly observed in supported metal nanoparticles, and can be attributed to the acidic property of the Al₂O₃ support. It is the further shift from the monometallic Pd to the bimetallic Pd-Au samples which is intriguing, as it indicates that the Pd species became electron deficient upon the introduction of Au.⁴ This would arise if the Pd atoms and Au atoms in nanoparticles are in intimate contact in the form of a core-shell structure, and a transfer of electron density occurs from Pd atoms to Au atoms, i.e., Pd(shell)^{δ+}-Au(core)^{δ-}.

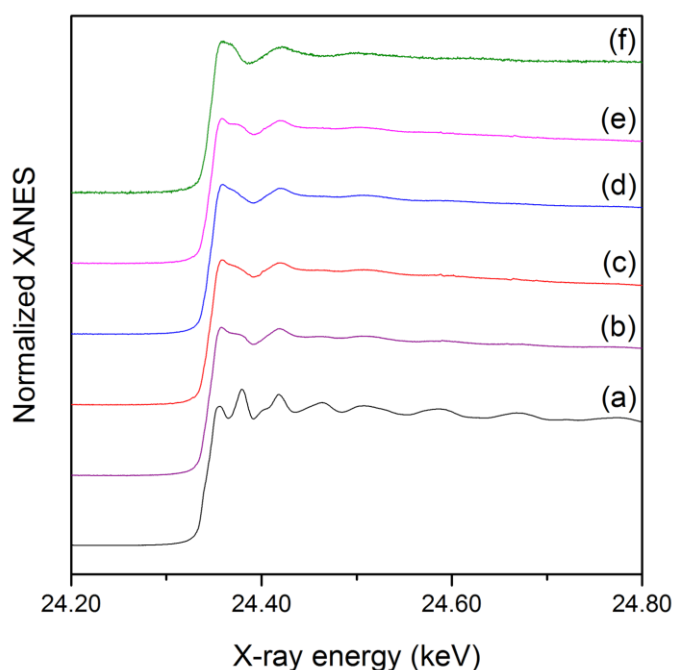


Figure 7 Pd K-edge XANES in (a) Pd foil, (b) Pd(3.0)/Al₂O₃, (c) Pd(2.5)Au(0.5)/Al₂O₃, (d) Pd(2.0)Au(1.0)/Al₂O₃, (e) Pd(1.5)Au(1.5)/Al₂O₃, (f) Pd(0.5)Au(2.5)/Al₂O₃

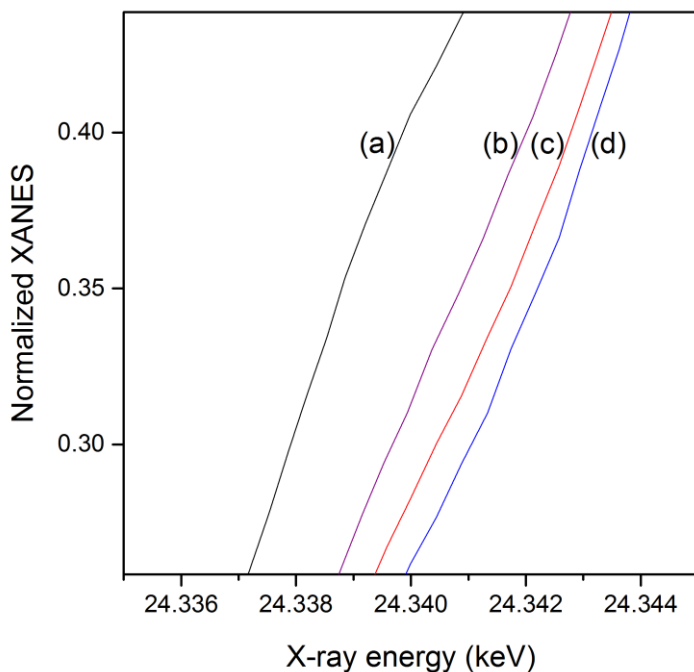


Figure 8 Expanded Pd K-edge XANES of (a) a Pd foil reference foil, (b) the monometallic Pd(3.0)/Al₂O₃ sample, and the bimetallic (c) Pd(2.5)Au(0.5)/Al₂O₃ and (d) Pd(2.0)Au(1.0)/Al₂O₃ samples

Figure 9 shows the normalized XANES of Au L_{III}-edge. The XANES features of the prepared Al₂O₃ supported samples, especially at the higher energy region, were similar to that of Au foil, indicating that the Au species in these samples were almost metallic. However, the Au absorption edge was clearly shifted in the prepared supported samples at 11919.7 eV (Figures 9b–e) from the Au foil at 11920.2 eV (Figure 9a), suggesting that the Au atoms became electron sufficient on the support. Moreover, although a clear absorption peak could be observed around 11.923 keV in the Au foil and the monometallic Au(3.0)/Al₂O₃ sample, which corresponds to the transition from the filled core 2p_{3/2} level to the vacant d orbitals,⁵ it was gradually lost in the bimetallic Pd(x)Au(y)/Al₂O₃ samples, indicating the filling of the d orbitals in Au, which would arise due to the transfer of electron density from Pd to Au nanoparticles, i.e., Pd(shell)^{δ+}–Au(core)^{δ-}.

Thus, the XANES results revealed that the Pd-Au nanoparticles had intimate contact in the bimetallic Pd(x)Au(y)/Al₂O₃ samples which affected their local structure and facilitated electron transfer between Pd and Au. Further, as the Pd species was found to be slightly oxidized and Au metallic, it is proposed

that the bimetallic Pd(x)Au(y)/Al₂O₃ samples would have a core-shell structure consisting of Pd shell and Au core which is shown in Figure 10.

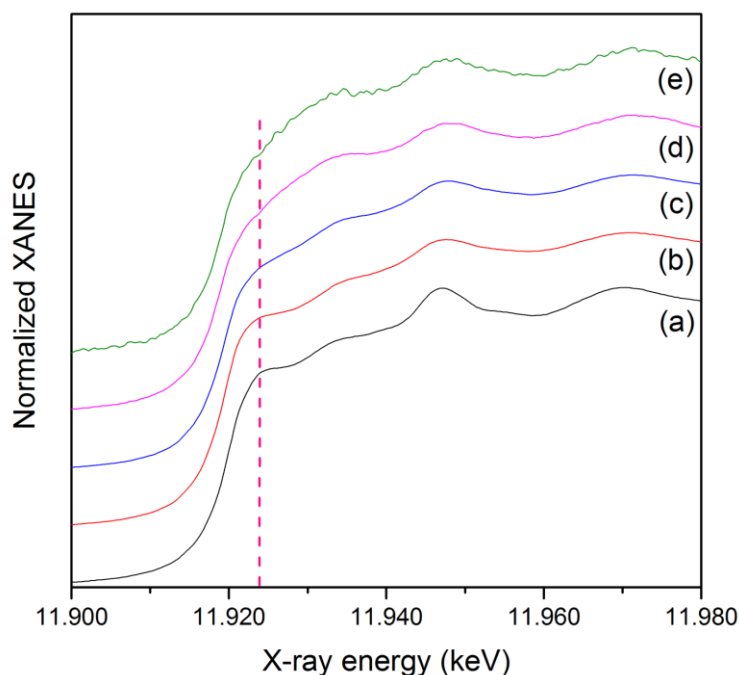


Figure 9 Au L_{III}-edge XANES in (a) Au foil, (b) Au(3.0)/Al₂O₃ (c) Pd(0.5)Au(2.5)/Al₂O₃, (d) Pd(1.5)Au(1.5)/Al₂O₃, and (e) Pd(2.0)Au(1.0)/Al₂O₃

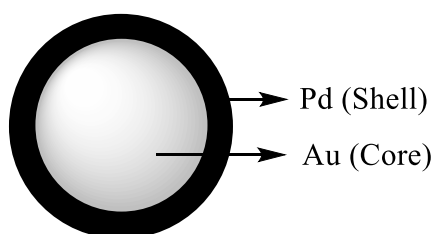
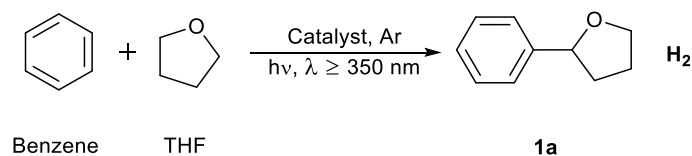


Figure 10 Proposed structure for the bimetallic Pd(x)Au(y)/Al₂O₃ samples

3.2. Photocatalytic activity tests

3.2.1. Cross-coupling between benzene and THF



Scheme 1 Photocatalytic cross-coupling between benzene and THF

In this study, the photocatalytic cross-coupling reaction between benzene and THF gave 2-phenyltetrahydrofuran (**1a**) as the only cross-coupling

product (Scheme 1). Table 2 shows the results of the photocatalytic reaction between tetrahydrofuran and benzene carried out with the physically mixed catalysts. As **1a** was the major product of this reaction, only its amount is discussed in Table 2. The reaction carried out with pristine TiO₂ did not yield **1a** (Table 2, entry 1). The reaction carried out with a physical mixture of the TiO₂ photocatalyst and the fresh Pd(0.1)/Al₂O₃ catalyst did not produce **1a** (Table 2, entry 2). However, the reaction carried out with a physical mixture of the TiO₂ photocatalyst and a reduced Pd(0.1)/Al₂O₃ sample yielded **1a** (Table 2, entry 3). However, **1a** was not formed in the reaction carried out without TiO₂ (Table 2, entry 4). These results show that the cross-coupling between benzene and THF requires both the TiO₂ photocatalysis and Pd metal catalysis. The XANES analysis had revealed that the Pd species in the fresh sample was slightly oxidized but reduction by H₂ changed the electronic state of the Pd species and it was reduced (metallic).

Table 2 Cross-coupling between benzene and THF with different catalysts ^a

Entry	Catalyst	Amount of 1a (μmol)
1	TiO ₂	0.0
2 ^b	TiO ₂ + Pd(0.1)/Al ₂ O ₃	0.0
3 ^{b, c}	TiO ₂ + red- Pd(0.1)/Al ₂ O ₃	0.9
4 ^d	red-Pd(0.1)/Al ₂ O ₃	0.0

^a Reaction conditions: 2 ml (22.4 mmol) benzene, 2 ml (24 mmol) THF, 50 mg of TiO₂ was used, reaction time was 1 h, λ of irradiated light was ≥ 350 nm, I = 40 mW/cm², the amount of **1a** was approximately determined from the calibration curve of 1-ethoxyethylbenzene. ^b 50 mg of each catalyst. ^c The Pd(0.1)/Al₂O₃ sample was reduced under H₂ (100%, flow rate: 15 ml/min) for 30 min at 673 K. ^d Reaction was done with 50 mg of the reduced Pd(0.1)/Al₂O₃ sample under irradiation.

So, it can be proposed that the reduced Pd nanoparticles are important to catalyze the photocatalytic cross-coupling reaction between benzene and THF (Table 2, entries 2 and 3). The initial screening of the physically mixed catalysts revealed that the electronic state of the Pd species was crucial for the photocatalytic cross-coupling reaction between benzene and THF. To further understand the relationship between the electronic state of Pd and its catalytic activity, we screened the Pd(x)Au(y)/Al₂O₃ catalysts for the photocatalytic cross-coupling reaction. Table 3 shows the results of the reactions carried out with different catalysts. The reaction carried out with pristine TiO₂ did not produce **1a** but the Pd(3.0)/TiO₂ photocatalyst produced **1a** (Table 3, entries 1 and 2). Next, reactions were carried out with a physical mixture of the TiO₂ photocatalyst and various Pd(x)Au(y)/Al₂O₃ catalysts i.e. blended catalysts. The product yield varied with the Pd content

in the Pd(*x*)Au(*y*)/Al₂O₃ catalysts (Table 3, entries 3–7) and the highest yield was obtained for a physical mixture of the TiO₂ photocatalyst and the Pd(2.0)Au(1.0)/Al₂O₃ catalyst (Table 3, entry 4). The reaction performed with the TiO₂ photocatalyst and the pure Au(3.0)/Al₂O₃ catalyst did not give **1a** (Table 3, entry 8).

Table 3 Cross-coupling between benzene and THF with various Pd(*x*)Au(*y*)/Al₂O₃ catalysts ^a

Entry	Catalyst	1a (μmol)	Selectivity ^b	Yield ^c
1	TiO ₂	0.0	-	-
2	Pd(3.0)/TiO ₂	17.0	> 99	0.07
3	TiO ₂ + Pd(3.0)/Al ₂ O ₃	22.8	> 99	0.10
4	TiO ₂ + Pd(2.5)Au(0.5)/Al ₂ O ₃	29.2	> 99	0.12
5	TiO ₂ + Pd(2.0)Au(1.0)/Al ₂ O ₃	25.2	> 99	0.11
6	TiO ₂ + Pd(1.5)Au(1.5)/Al ₂ O ₃	11.3	> 99	0.05
7	TiO ₂ + Pd(0.5)Au(2.5)/Al ₂ O ₃	4.2	> 99	0.02
8	TiO ₂ + Au(3.0)/Al ₂ O ₃	0.0	-	-
9 ^d	Pd(2.0)Au(1.0)/Al ₂ O ₃	0.0	-	-
10	TiO ₂ + Pd(3.0)/SiO ₂	0.7	> 99	0.003
11	TiO ₂ + Pd(2.0)Au(1.0)/SiO ₂	1.1	> 99	0.004
12	TiO ₂ + Au(3.0)/SiO ₂	0.5	> 99	0.002

^a Reaction conditions were same as Table 2. ^b Selectivity (%) to **1a** was calculated as 100 × (amount of **1a**) / (amount of benzene containing products). ^c Yield (%) of **1a** was calculated as 100 × (amount of **1a**) / (initial amount of benzene). ^d Reaction was done with 50 mg of Pd(2.0)Au(1.0)/Al₂O₃ catalyst under photoirradiation.

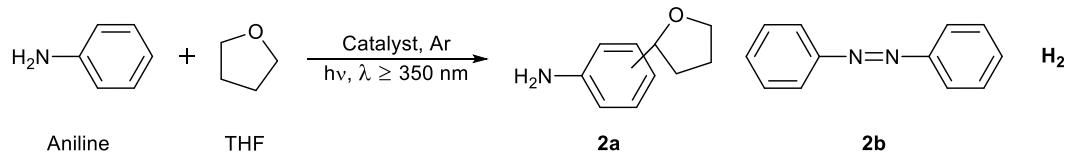
These results indicate that Pd was the active component in these bimetallic Pd(*x*)Au(*y*)/Al₂O₃ catalysts and the Au nanoparticles might affect the electron density of the Pd species, which would influence its catalytic activity. We confirmed that the Pd(*x*)Au(*y*)/Al₂O₃ catalysts alone cannot yield **1a** (Table 3, entry 9). Thus, the two catalytic components, the TiO₂ photocatalyst and the Pd-Au bimetallic catalysts, work in synergy to yield cross-coupling product. We also screened SiO₂ supported metal catalysts for this cross-coupling reaction. Although the product yield was larger than the pristine TiO₂, it was much smaller than alumina supported catalysts (Table 3, entries 1, 10–12). However, even in these catalysts, the Pd-Au bimetallic catalyst (Table 3, entry 11) exhibited higher activity than pure Pd (Table 3, entry 10) and pure Au catalysts (Table 3, entry 12). The structure of the Pd(2.0)Au(1.0) bimetallic catalysts on Al₂O₃ and SiO₂ might not be same which could be a reason for their different catalytic activities (Table 3, entries 5 and 11).

3.2.2. Cross-coupling between substituted benzenes and THF

After screening the bimetallic Pd(x)Au(y)/Al₂O₃ catalysts for the photocatalytic cross-coupling between benzene and THF, we changed benzene to substituted benzene and examined their activity for the cross-coupling with THF. At first we examined benzene substituted with electron donating groups like NH₂ and CH₃.

The reaction between aniline and THF, carried out with Pd(3.0)/TiO₂ photocatalyst under light irradiation, gave a mixture of two cross-coupling products namely, 2-(tetrahydrofuran-2-yl)aniline and 4-(tetrahydrofuran-2-yl)aniline (shown collectively as **2a**) and the homocoupling products from aniline, di(phenyl)diazine (**2b**). Table 4 shows the amount of the cross-coupling products (**2a**) and the homocoupling product of aniline (**2b**) produced in the reaction between aniline and THF done by using different catalysts. A small amount of the cross-coupling products were produced in the reaction carried out with the pristine TiO₂ photocatalyst (Table 4, entry 1). The amount of **2a** did not vary much even after loading Pd on the TiO₂ photocatalyst, although that of **2b** increased (Table 4, entry 2). Cross-coupling products were also produced in the reaction carried out with a physical mixture of the TiO₂ photocatalyst and the Pd(3.0)/Al₂O₃ catalyst, but the yield was lower than the reaction carried out with photocatalyst alone (Table 4, entry 3). It indicated that these Pd nanoparticles on Al₂O₃ had small catalytic activity in this reaction. Compared to the Pd(3.0)/Al₂O₃ catalyst, the yield of both cross-coupling and homocoupling products of aniline increased with the introduction of Au to the Pd(3.0)/Al₂O₃ catalyst (Table 4, entries 4–6). The reaction done with a physical mixture of the TiO₂ photocatalyst and the Pd(2.0)Au(1.0)/Al₂O₃ catalyst gave the highest yield of the cross-coupling products with maximum selectivity due to low yield of aniline homocoupling product (Table 4, entry 5). As this composition of Pd and Au gave the best results, further reactions were performed with this catalyst. Table 5 shows the results of the photocatalytic cross-coupling reaction between toluene and THF carried out with different catalysts. This reaction gave a mixture of two cross-coupling products namely 2-(o-tolyl)tetrahydrofuran and 2-(p-tolyl)tetrahydrofuran (shown collectively as **3a**), oxidation products from toluene like benzaldehyde (**3b**) and benzyl alcohol (**3c**).

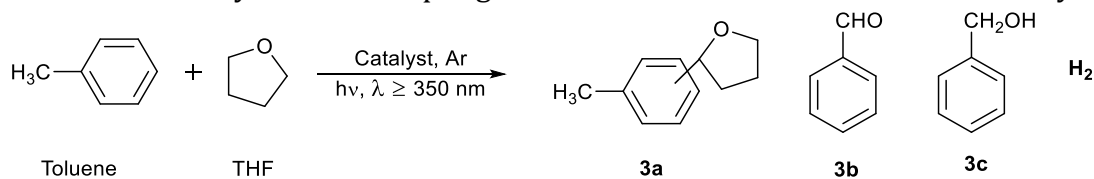
Table 4 Photocatalytic cross-coupling between Aniline and THF with different catalysts ^a



Entry	Catalyst	2a (μmol) ^b	2b (μmol) ^b	Selectivity ^c	Yield ^d
1	TiO ₂	4.2	14.9	21.9	0.019
2	Pd(3.0)/TiO ₂	5.2	22.1	19.0	0.024
3	TiO ₂ + Pd(3.0)/Al ₂ O ₃	3.4	20.2	14.4	0.015
4	TiO ₂ + Pd(2.5)Au(0.5)/Al ₂ O ₃	3.6	38.8	8.4	0.016
5	TiO ₂ + Pd(2.0)Au(1.0)/Al ₂ O ₃	5.2	17.6	22.8	0.023
6	TiO ₂ + Pd(1.5)Au(1.5)/Al ₂ O ₃	5.2	30.1	14.7	0.023
7	TiO ₂ + Au(3.0)/Al ₂ O ₃	3.7	34.2	9.7	0.016

^a 2 ml aniline (21.9 mmol), 2 ml THF (24 mmol), other conditions and calculations were same as Table 3. ^b The amount of all products was approximately determined from the calibration curve of 1-ethoxyethylbenzene. ^c Selectivity (%) to cross-coupling products was calculated as $100 \times (\text{amount of } \mathbf{2a}) / (\text{amount of } \mathbf{2a} \text{ and } \mathbf{2b})$. ^d Yield (%) of the cross-coupling products was calculated as $100 \times (\text{amount of } \mathbf{2a}) / (\text{initial amount of aniline})$

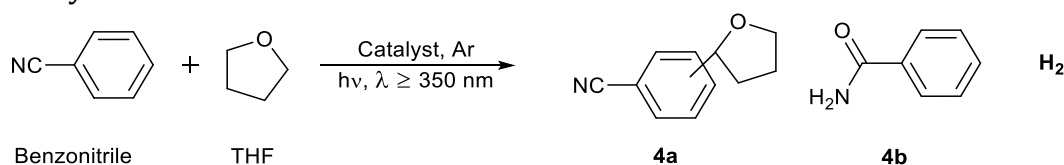
Although the oxidation products from toluene like benzaldehyde (**3b**) and benzyl alcohol (**3c**) were also obtained, the oxygen would originate from adsorbed water or surface hydroxyl groups on the catalysts. The reaction carried out with the pristine TiO₂ photocatalyst did not yield any cross-coupling product, only oxidation products were obtained (Table 5, entry 1). The Pd loaded TiO₂ photocatalyst yielded cross-coupling products along with the two oxidation products (Table 5, entry 2). Introduction of Al₂O₃ supported catalysts significantly suppressed the oxidation of toluene (Table 5, entries 3–5). Introduction of the Pd(3.0)/Al₂O₃ catalyst to the reaction mixture containing the pristine TiO₂ photocatalyst yielded small amount of cross-coupling products indicating the catalytic ability of Pd nanoparticles in this photocatalytic reaction (Table 5, entry 3). The reaction carried out with the physically mixed TiO₂ photocatalyst and the Pd(2.0)Au(1.0)/Al₂O₃ catalyst gave cross-coupling products with the highest selectivity (Table 5, entry 4). No products were with the physical mixture of the TiO₂ photocatalyst and the Au(3.0)/Al₂O₃ sample (Table 5, entry 5). After examining benzene substituted with electron donating groups, we employed benzene with electron withdrawing groups like CN and CHO for the cross-coupling reaction with THF.

Table 5 Photocatalytic cross-coupling between Toluene and THF different catalysts ^a

Entry	Catalyst	3a (μmol) ^b	3b + 3c (μmol) ^b	Selectivity ^c	Yield ^d
1	TiO ₂	0.0	9.9	-	-
2	Pd(3.0)/TiO ₂	10.3	5.9	63.5	0.05
3	TiO ₂ + Pd(3.0)/Al ₂ O ₃	2.8	2.8	50.0	0.01
4	TiO ₂ + Pd(2.0)Au(1.0)/Al ₂ O ₃	5.2	0.6	89.7	0.02
5	TiO ₂ + Au(3.0)/Al ₂ O ₃	0.0	0.0	0.0	-

^a 2 ml toluene (19.01 mmol), 2 ml THF (24 mmol), other conditions were same as Table 3. ^b The amount of all products was approximately determined from the calibration curve of 1-ethoxyethylbenzene. ^c Selectivity to the cross-coupling products was calculated as $100 \times (\text{amount of } \mathbf{3a}) / (\text{amount of } \mathbf{3a}, \mathbf{3b} \text{ and } \mathbf{3c})$. ^d Yield of the cross-coupling products was calculated as $100 \times (\text{amount of } \mathbf{3a}) / (\text{amount of toluene})$.

Table 6 shows the results of the cross-coupling reaction between benzonitrile and THF carried out with different catalysts. This reaction gave a mixture of three cross-coupling products namely, 2-(tetrahydrofuran-2-yl)benzonitrile, 3-(tetrahydrofuran-2-yl)benzonitrile, and 4-(tetrahydrofuran-2-yl)benzonitrile (shown collectively as **4a**), and a benzonitrile derived product, benzamide (**4b**). Low yield of cross-coupling products was obtained in the reaction done with the bare TiO₂ photocatalyst

Table 6 Photocatalytic cross-coupling between benzonitrile and THF with different catalysts ^a

Entry	Catalyst	4a (μmol) ^b	4b (μmol) ^b	Selectivity ^c	Yield ^d
1	TiO ₂	6.1	0.9	87	0.03
2	Pd(3.0)/TiO ₂	19.3	4.8	80	0.09
3	TiO ₂ + Pd(3.0)/Al ₂ O ₃	10.9	5.1	68	0.05
4	TiO ₂ + Pd(2.0)Au(1.0)/Al ₂ O ₃	52.1	39.7	57	0.26
5	TiO ₂ + Au(3.0)/Al ₂ O ₃	12.4	3.6	78	0.06

^a 2 ml benzonitrile (19.4 mmol), 2 ml THF (24 mmol), other conditions were same as Table 3. ^b the amount of all products was approximately determined from the calibration curve of 4-(tetrahydrofuran-2-yl)benzonitrile, synthesized as per literature.⁴ ^c Selectivity(%) to cross-coupling products was calculated as $100 \times (\text{amount of } \mathbf{4a}) / (\text{amount of } \mathbf{4a} \text{ and } \mathbf{4b})$. ^d Yield(%) of cross-coupling products was calculated as $100 \times (\text{amount of } \mathbf{4a}) / (\text{initial amount of benzonitrile})$

and it improved with loading Pd on the TiO₂ photocatalyst (Table 6, entries 1 and 2). Introduction of the Pd(3.0)/Al₂O₃ catalyst to the reaction mixture containing the TiO₂ photocatalyst increased the cross-coupling yield (Table 6, entry 3). These results indicated that the Pd nanoparticles could participate catalytically in the photocatalytic cross-coupling reaction. The highest yield of cross-coupling products was obtained in the reaction carried out with the physically mixed catalytic mixture of the TiO₂ photocatalyst and Pd(2.0)Au(1.0)/Al₂O₃ catalyst (Table 6, entries 4). In fact, this value was larger than that obtained from the reaction carried out with Pd(3.0)/TiO₂ photocatalyst alone (Table 6, entries 2 and 5). Unlike the previous reaction, the Au/Al₂O₃ catalysts also showed some catalytic activity for the cross-coupling reaction (Table 6, entry 5). Next, we performed the photocatalytic cross-coupling between benzaldehyde and THF with different catalysts (Table 7). The reaction gave three cross-coupling products namely, 2-(tetrahydrofuran-2-yl)benzaldehyde, 3-(tetrahydrofuran-2-yl)benzaldehyde, and 4-(tetrahydrofuran-2-yl)benzaldehyde (shown collectively as **5a**) along with benzoic acid (**5b**), and benzyl alcohol (**5c**) from benzaldehyde. Similar to the previous reactions, the yield of cross-coupling products increased upon the introduction of the Pd species on the TiO₂ surface (Table 7, entry 2) or on Al₂O₃ surface (Table 7, entry 3). Further, the reaction done with mixture of the TiO₂ photocatalyst and the Pd(2.0)Au(1.0)/Al₂O₃ catalyst gave the largest product yield among the tested catalysts (Table 5, entries 4).

Table 7 Photocatalytic cross-coupling between benzaldehyde and THF with different catalysts ^a

Entry	Catalyst	5a (μmol) ^b	5b (μmol) ^b	5c (μmol) ^b	%S ^c	%Y ^d
1	TiO ₂	151.8	292.5	55.6	37	0.76
2	Pd(3.0)/TiO ₂	246.6	400.2	29.6	36	1.24
3	TiO ₂ + Pd(3.0)/Al ₂ O ₃	211.2	333.3	46.1	43	1.06
4	TiO ₂ + Pd(2.0)Au(1.0)/Al ₂ O ₃	344.8	359.8	49.7	46	1.73
5	TiO ₂ + Au(3.0)/Al ₂ O ₃	166.6	283.3	74.3	38	0.87

^a 2 ml benzaldehyde (19.9 mmol), 2 ml THF (24 mmol), other conditions were same as Table 3. ^b The amount of all products was approximately determined from the calibration curve of 4-(tetrahydrofuran-2-yl)benzotrile; %S: selectivity to the cross-coupling products, calculated as 100 × (amount of **5a**) / (amount of **5a**, **5b**, and **5c**). ^d %Y: yield of the cross-coupling products, calculated as 100 × (amount of **5a**) / (initial amount of benzaldehyde).

Similar to the benzonitrile–THF reaction, the Au/Al₂O₃ catalyst also showed some catalytic activity for the cross-coupling reaction (Table 7, entry 5). These results prove that the photocatalytic cross-coupling reactions between arenes and THF are indeed a hybrid of TiO₂ photocatalysis and metal catalysis. The metal catalysis can work even if the metal was not loaded on TiO₂ but on a photo-inactive support like Al₂O₃. Also, the electronic state of the Pd species was important in these reactions. The mechanism of these reactions was proposed to involve the Pd catalysis for the activation of the aromatic ring (Chapter II-2). The Pd nanoparticles might withdraw the electron density from the aromatic ring and facilitate the attack of the photogenerated ether radical. The results of the cross-coupling reaction between substituted benzene and THF support this proposal as the product yield varied with the nature of substituent i.e. if it was electron donating or withdrawing. Table 8 shows the comparison of the total amount of the cross-coupling products obtained in the reaction of benzene and THF, toluene and THF, and benzonitrile and THF by the blended TiO₂ photocatalyst and Pd(2.0)Au(1.0)/Al₂O₃ catalyst. Since these systems exhibited high selectivity for the cross-coupling products, it was reasonable to compare the amount of cross-coupling products unlike aniline and THF, and benzaldehyde and THF systems where a large amount of side products were obtained from arenes. From the values mentioned in Table 8, it can be proposed that the yield of cross-coupling products increased with the electron deficiency of the aromatic ring (Table 8, entries 1–3). The higher activity of the bimetallic Pd(2.0)Au(1.0)/Al₂O₃ catalyst over the monometallic catalysts (Pd/Al₂O₃ and Au/Al₂O₃) and the photocatalyst (Pd/TiO₂) should be related to the change in the electronic properties of the Pd metal atoms. TEM results showed that the metal dispersion and particle size in these three catalysts was similar. Further, XAFS measurements revealed that the two metals influenced the electronic structure of each other, which was suggested by XANES. Thus, the change in the electronic properties of these bimetallic catalysts and not the physical factors like particle size or dispersion should be responsible for their high catalytic activity.

It has been widely accepted that in the Pd-Au bimetallic catalysts, a transfer of electron density from Pd to Au occurs, which generates an electron rich Au species and electron deficient Pd species. This type of Pd should be able to activate the benzene ring more easily than monometallic Pd species on the

Al₂O₃ support or the Pd species on the TiO₂ photocatalyst, so that this catalyst exhibited the highest activity for the cross-coupling reaction between arenes and THF. However, this is just a proposal and more studies are needed to understand these results.

Table 7 Comparison of the yield of cross-coupling products obtained in the reaction between different arenes and THF by a physical mixture of TiO₂ and Pd(2.0)Au(1.0)/Al₂O₃

Entry	Arene	Total amount of cross-coupling products (μmol)
1	Toluene	5.2
2	Benzene	25.2
3	Benzonitrile	56.3

4. Conclusion

In this work we successfully developed a new methodology to carry out the photocatalytic cross-coupling between arenes and ethers by using a physical mixture of TiO₂ photocatalyst and bimetallic Pd(*x*)Au(*y*)/Al₂O₃ catalysts. The best activity and selectivity was obtained for the reaction carried out with the TiO₂ photocatalyst and the bimetallic Pd(2.0)Au(1.0)/Al₂O₃ catalyst. This new methodology will allow us to control the product selectivity by varying the two catalysts independently.

5. References

- [1] K. Taniguchi, X. Jin, K. Yamaguchi and N. Mizuno, *Chem. Commun.*, vol. 51, p. 14969, **2015**.
- [2] B. Ravel and M. Newville, *J. Synchrotron Radiat.*, vol. 12, p. 537, **2005**.
- [3] F. Gao and D. W. Goodman, *Chem. Soc. Rev.*, vol. 41, p. 8009, **2012**.
- [4] A. F. Lee, C. J. Baddeley, C. Hardcare, R. M. Ormerod, and R. M. Lambert, *J. Phys. Chem.*, vol. 99, p. 6096, **1995**.
- [5] H. Miura, K. Endo, R. Ogawa, and T. Shishido, *ACS Catal.*, vol. 7, p. 1543 **2017**.

III-3. Photocatalytic cross-coupling between cyclohexane and tetrahydrofuran

Abstract

A physical mixture of TiO₂ photocatalyst and alumina supported metal catalyst (M(x)/Al₂O₃, M: Pd and Pt) exhibited higher activity than the TiO₂ photocatalyst alone for the photocatalytic cross-coupling between cyclohexane and tetrahydrofuran (THF). The cross-coupling product couldn't be obtained without TiO₂ photocatalyst, thus eliminating the possibility of plasmonic catalysts by the metals. Thus, the reaction was proposed to be a hybrid of TiO₂ photocatalysis and metal catalysis.

1. Introduction

In our previous study on the photocatalytic cross-coupling reaction between alkanes and THF, we proved that the reaction was a hybrid of TiO₂ photocatalysis and Pt metal catalysis. The metal catalysis was proposed to be responsible for the thermal activation of the alkanes and THF which could react more easily with a photogenerated radical than those before the activation. This type of molecular activation is reported to proceed efficiently on various supported nanoparticles in some processes like dry reforming of methane,¹ methane activation,² CO₂ hydrogenation,³ and so on. So, we examined various supported metal catalysts for the photocatalytic cross-coupling between cyclohexane and THF and investigated the relationship between the electronic state of the metal and the catalytic activity.

2. Experimental Section

2.1. Catalyst preparation

Pt(0.1)/TiO₂ photocatalysts were prepared by a photodeposition method as mentioned in Chapter II-2. Pt(0.1)/Al₂O₃ catalysts were prepared by an impregnation method (Chapter III-2) by using H₂PtCl₆·6H₂O (Wako Pure Chemicals, 99%) as Pt precursor. The preparation of the Pd(x)Au(y)/Al₂O₃ bimetallic catalysts is discussed in Chapter III-2.

2.2. Characterization of catalysts

The characterization details and results of Pt(0.1)/TiO₂ photocatalyst and Pd(x)Au(y)/Al₂O₃ bimetallic catalysts were mentioned in Chapter II-2 and

Chapter III-2 respectively. Pt dispersion and particle size in the supported Pt samples was determined by CO pulse adsorption method. The electronic state of Pt nanoparticles in the Pt(0.1)/Al₂O₃ samples was studied by XAFS. The spectra were recorded at BL9C of Photon Factory at the Institute of Materials Structure Science, High Energy Accelerator Research Organization (KEK-PF, Tsukuba Japan). The reference samples, Pt foil and PtO₂, were measured in a transmission mode, whereas the Pt(0.1)/Al₂O₃ sample was measured in fluorescence mode. Spectra were analyzed by Athena software.⁴

2.3. Photocatalytic activity tests

The materials and procedure for the photocatalytic activity tests was same as Chapter II-2.

3. Results and Discussion

3.1. Catalyst characterization

CO pulse adsorption

Table 1 shows the result for the CO pulse adsorption tests for the supported Pt samples. Small, well dispersed Pt nanoparticles were obtained on both supports (Table 1, entries 1 and 2). The Pt dispersion was larger and the particle size was smaller on the Al₂O₃ support than those on the TiO₂ support.

Table 1 Pt dispersion and particle size in the supported Pt samples

Entry	Sample	Metal dispersion	Particle size (nm)
1	Pt(0.1)/TiO ₂	42.6	2.7
2	Pt(0.1)/Al ₂ O ₃	56.7	1.9

XAFS

XAFS revealed the electronic state of the Pt nanoparticles in the Pt(0.1)/Al₂O₃ sample. Figure 1 shows normalized Pt-L_{III} edge XANES of the reference Pt foil and PtO₂ samples (Figure 1, a and c), and the Pt(0.1)/Al₂O₃ sample recovered after the activity test (Figure 1, b). The Pt(0.1)/Al₂O₃ sample showed slightly larger white line intensity than Pt foil and a similar feature in the post edge region around 11.6 eV to PtO₂ sample. These results suggest that the Pt nanoparticles on the Al₂O₃ support were in a slightly oxidized state.

3.2. Photocatalytic activity tests

Table 2 shows the results of the cross-coupling reaction between cyclohexane and THF carried out with various catalysts. The reaction done with an excess of cyclohexane and small amount of THF gave

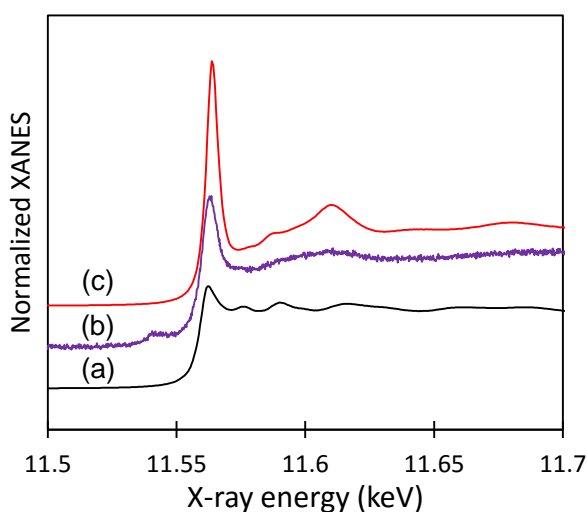


Figure 1. Normalized Pt-L_{III} edge XANES spectra of (a) a Pt foil, (b) the Pt(0.1)/Al₂O₃ sample recovered after the reaction test, and (c) the PtO₂ powder.

2-cyclohexyltetrahydrofuran (**1a**) as the cross-coupling product along with 1,1'-bicyclohexane (**1b**), as the homocoupling product of cyclohexane. A low yield of **1a** was obtained in the reaction carried out with the pristine TiO₂ photocatalyst and the major product was **1b** (Table 2, entry 1). Loading of Pt on the TiO₂ photocatalyst led to a tenfold increase in the yield of both **1a** and **1b** (Table 2, entry 2). In the previous work, we had proposed that apart from being an electron receiver, the Pt nanoparticles also had a catalytic role in this cross-coupling reaction (Chapter II-2). The nature of this catalysis was proposed to be the thermal activation of C–H bonds in alkanes and THF which facilitates their reaction with a photogenerated radical species. We believe that this kind of metal catalysis can also proceed on the supported metal catalysts. To confirm this proposal, reaction was carried out with a physical mixture of the TiO₂ photocatalyst and the Al₂O₃ supported metal catalysts, M(0.1)/Al₂O₃, (M: Pt, Pd, and Rh) (Table 2, entries 3–6). Among the three M(0.1)/Al₂O₃ catalysts, small increase in the yield of **1a** was observed for the case with the Pt(0.1)/Al₂O₃ catalyst while the introduction of the Rh(0.1)/Al₂O₃ sample was not helpful. The Pd(0.1)/Al₂O₃ catalyst gave the largest yield of **1a**. It should be noticed that the product yield in all these cases were smaller than those obtained for Pt(0.1)TiO₂ photocatalyst indicating that the major route for this reaction would be a photocatalytic pathway where the separation of photogenerated electron-hole pair would be crucial and promoted by the Pt nanoparticles deposited on the TiO₂ surface. Interestingly, the introduction of the M(0.1)/Al₂O₃ catalysts to the

reaction mixture improved the yield of **1b** as well (Table 2, entries 3–5). This is reasonable because a thermally activated molecule can undergo reaction with a same or different radical species, generated photocatalytically, to give cross-coupling or homocoupling product, respectively. Neither product was produced in the reaction performed with the Pd(0.1)/Al₂O₃ catalyst alone under photoirradiation (Table 2, entry 6). This result revealed that the proposed metal catalysis cannot function alone and requires the TiO₂ photocatalysis.

Table 2 Photocatalytic cross-coupling between THF and cyclohexane with different catalysts ^a

Entry	Catalyst	Products (μmol) ^b		Selectivity ^c	Yield ^d
		1a	1b		
1	TiO ₂	0.2	0.5	28.6	0.16
2	Pt(0.1)/TiO ₂	2.1	2.5	45.6	1.70
3	TiO ₂ + Pt(0.1)/Al ₂ O ₃	0.3	0.9	25.0	0.24
4	TiO ₂ + Pd(0.1)/Al ₂ O ₃	0.7	1.5	31.8	0.56
5	TiO ₂ + Rh(0.1)/Al ₂ O ₃	0.1	0.2	33.3	0.08
6 ^e	Pd(0.1)/Al ₂ O ₃	0.0	0.0	-	-

^a Reaction conditions: 3 ml (27.7 mmol) cyclohexane, 10 μl (123 μmol) THF, 50 mg of each catalyst was used; reaction time was 1 h; λ ≥ 350 nm; I = 40 mW/cm². ^b The amount of both products was determined from the calibration curve of their authentic samples. ^c Selectivity to **1a** calculated as 100 × (amount of **1a**) / (amount of **1a** and **1b**). ^d Yield of **1a** calculated as 100 × (amount of **1a**) / (initial amount of THF). ^e Reaction was performed with 50 mg of the Pd(0.1)/Al₂O₃ sample under photoirradiation.

As the introduction of the Pd(0.1)/Al₂O₃ catalyst gave the largest product yield, we decided to modify these catalysts for this reaction. In the presence of the TiO₂ photocatalyst, the increase of the loading amount of Pd on the Al₂O₃ support from 0.1 to 3.0 wt.% slightly increased the yield of **1a** and decreased the yield of **1b** and thus improved the selectivity to **1a** significantly (Table 2, entry 4 and Table 3, entry 1). The difference in the selectivity could be related to the different state of the Pd nanoparticles in these two catalysts, which might be due to a different preparation method. The Pd(0.1)/Al₂O₃ sample was prepared by an impregnation method followed by calcination in air before using for a reaction. On the other hand, the Pd(3.0)/Al₂O₃ sample, which belonged to the Pd(x)Au(y)/Al₂O₃ series, was prepared by a wetness-impregnation method which involved the reduction of catalysts under pure H₂ atmosphere before using for the

reaction test. A detailed explanation of how this difference in metal state affects the product selectivity is difficult at this point and requires further investigation. Introduction of Au to Pd species did not change their activity much and the yield of both products increased only slightly when compared to pure Pd catalyst (Table 3, entries 2–4). The Au(3.0)/Al₂O₃ catalyst was inactive for this reaction (Table 3, entry 5). The introduction of Au/Al₂O₃ much decreased the intrinsic activity of TiO₂ photocatalyst, probably due to the shading of light by it which would obstruct the photo absorption by TiO₂ photocatalyst without the acceleration of the reaction. It should be noted that in other cases of the physical mixture, the products were actually obtained even though they shade the light. This fact means that the reaction was promoted by the supported metal catalysts. These results confirmed that the metal catalysis contributes to the photocatalytic cross-coupling between cyclohexane and THF. However, unlike the reaction between arene and THF, the product yield did not increase much upon the usage of these catalysts. This difference could be explained by the different activation mechanisms involved in these two systems. The present reaction involves direct activation of sp³C–H bonds which is a difficult and energy intensive process due to the high stability of these bonds. The thermal energy gained during the photoirradiation of this mixture, might not be sufficient and hence, much higher temperatures might be needed to see enhanced activity of this mixture.

Table 3 Photocatalytic cross-coupling between THF and cyclohexane with a physical mixture of TiO₂ photocatalyst and Pd(x)Au(y)/Al₂O₃ catalysts ^a

Entry	Catalyst	Products (μmol)		Selectivity	Yield
		1a	1b		
1	TiO ₂ + Pd(3.0)/ Al ₂ O ₃	1.2	1.2	50.0	0.97
2	TiO ₂ + Pd(2.0)Au(1.0)/ Al ₂ O ₃	0.8	0.7	53.6	0.65
3	TiO ₂ + Pd(1.5)Au(1.5)/ Al ₂ O ₃	1.5	1.5	50.0	1.21
4	TiO ₂ + Pd(0.5)Au(2.5)/ Al ₂ O ₃	1.1	0.9	55.0	0.89
5	TiO ₂ + Au(3.0)/ Al ₂ O ₃	0.0	0.0	-	-

^a All reaction conditions were same as Table 2.

On the other hand, the reaction between arenes and THF would involve the activation of the aromatic ring, probably by the interaction between the metal and the π electron density of aromatic ring. This might be a relatively

easier process than C–H bond activation and could be accelerated in the temperatures achieved during photoirradiation and by varying the electronic state of metal.

4. Conclusion

In this work, we evidenced the involvement of metal catalysis in the photocatalytic cross-coupling between cyclohexane and THF. The nature of this catalysis would be the thermal activation of the C–H bonds in both substrates and facilitate their reaction with a photogenerated radical. Further, this proposed catalysis could proceed even if the metals were not supported on TiO₂ but on a photo-inactive support like Al₂O₃. As the product yield did not change drastically with the metal or its electronic state, it can be proposed that this catalysis was difficult to proceed at room temperature and the major product formation route would be TiO₂ photocatalysis. These findings are very interesting and we believe that they would help in understating the role of metal nanoparticles in the photocatalytic reaction and allow the development of more efficient catalysts.

5. References

- [1] D. Pakhare and J. Spivey, *Chem. Soc. Rev.*, vol. 43, p. 7813, **2014**.
- [2] J. J. Spivey and G. Hutchings, *Chem. Soc. Rev.*, vol. 43, p. 792, **2014**.
- [3] W. Wang, S. Wang, X. Ma and J. Gong, *Chem. Soc. Rev.*, vol. 40, p. 3703, **2011**.
- [4] B. Ravel and M. Newville, *J. Synchrotron Radiat.*, vol. 12, p. 537, **2005**.

III-4. Photocatalytic Ullmann coupling of aryl halides

Abstract

The present work discusses a novel method for the Ullmann coupling of aryl halides to give biaryls by using photocatalysis. Various aromatic and heteroaromatic aryl halides successfully underwent Ullmann coupling to give their corresponding biaryls. A physical mixture of TiO₂ photocatalyst and Al₂O₃ supported Pd-Au bimetallic catalysts exhibited higher activity and selectivity for the biphenyl production from iodobenzene than the photocatalyst alone did. A detailed study was conducted to understand the reaction mechanism and elucidate the role of both catalytic components in the blended catalysts.

1. Introduction

Biaryl moiety is found in several important compounds. For example, natural products like Biphenomycin B (antibiotic),¹ biologically active part of agrochemicals like Boscalid² and other pharmaceuticals³, all contain biaryls (Figure 1). Further, polyaromatic molecules found immediate use as dyes, organic conductor or semiconductors, and ligands for organometallic catalysts and much more. Thus, it is important to develop efficient strategies to carry out this important reaction. Over the years, various methods have been developed to make aryl-aryl bonds like Ullmann coupling,⁴ Gomberg-Bachmann reaction,⁵ Scholl reaction,⁶ Suzuki-Miyaura coupling,⁷ and many more. However, due to its simplicity and scope, Ullmann coupling remains a popular method to synthesize biaryls.^{8,9}

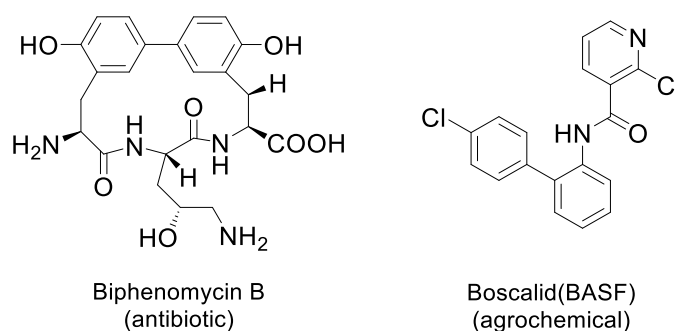
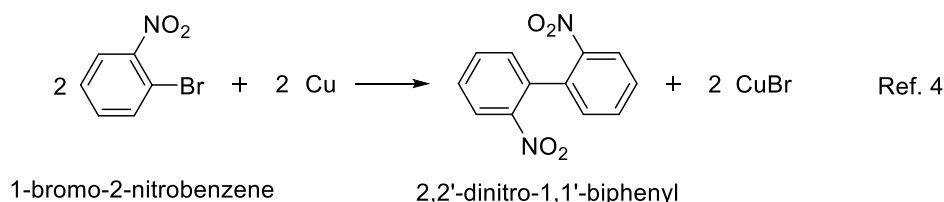


Figure 1 Some examples of compounds containing biaryls moiety

This reaction in the original report of this reaction required a Cu catalyst (Scheme 1).⁴ The reaction was carried out at 100–360°C temperature range with or without a solvent. Although the use of a cheap and non-toxic metal like Cu was attractive, its stoichiometric amount and other harsh conditions

were employed. Thus, significant efforts have been made in terms of catalyst amount and other conditions to carry out the reaction under mild reaction conditions.¹⁰ In our ongoing efforts to develop novel photocatalytic organic synthesis reactions, we have investigated an application of the TiO₂ photocatalysis for the Ullmann coupling of aryl halides under mild reaction conditions. The photocatalytic degradation of aryl halides like chlorobenzene has been widely studied¹¹⁻¹⁵ but its extension to synthesize useful compounds like biaryls is still uncommon,^{16,17} especially with a TiO₂ photocatalyst. In this study, we have developed a novel method for the photocatalytic Ullmann coupling of aryl halides by using a physical mixture of a TiO₂ photocatalyst and an alumina supported Pd-Au bimetallic catalyst. The coupling of iodobenzene to give biphenyl was thoroughly investigated and a tentative reaction mechanism was proposed.



Scheme 1 Ullmann coupling of aryl halides by a Cu catalyst

2. Experimental Section

2.1. Preparation of catalysts

The M(x)/TiO₂ photocatalysts were prepared by a photodeposition method as reported in the previous chapter (Chapter II-2). Pd(x)Au(y)/Al₂O₃ catalysts were prepared by a wetness-impregnation method, as mentioned in the previous chapter (Chapter III-1).

We also prepared TiO₂ supported Pd-Au bimetallic catalysts, Pd(2.0)Au(1.0)/TiO₂ by a photodeposition method as follows. 2 g of TiO₂ photocatalyst was suspended in 175 ml of distilled water and stirred with photoirradiation for 30 min. Then, 50 ml CH₃OH and desired volume of aqueous solutions of HAuCl₄·4H₂O and PdCl₂ were added and the suspension was stirred in dark for 15 min followed by photoirradiation for 1 h with photoirradiation. After photoirradiation, the suspension was filtered, washed with distilled water and dried overnight in an electric oven.

2.2. Characterization of catalysts

The $M(x)/TiO_2$ photocatalysts and $Pd(x)Au(y)/Al_2O_3$ catalysts were characterized by various techniques as discussed in previous chapters (Chapter II-2 and Chapter III-1).

2.2. Photocatalytic activity tests

2.2.1. Materials

All chemicals were of analytical grade and used without further purification; iodobenzene (Nacalai Tesque), 3-iodotoluene (TCI Research Chemicals), 4-iodotoluene (TCI Research Chemicals), bromobenzene (TCI Research Chemicals), chlorobenzene (Wako Pure Chemicals), 5-bromopyrimidine (TCI Research Chemicals), 2-chloropyridine (Wako Pure Chemicals), 2-bromopyridine (TCI Research Chemicals), methanol (Nacali Tesque), acetonitrile (Nacalai Tesque), di-methylformamide (DMF, Nacalai Tesque), and isopropyl alcohol (Nacalai Tesque).

2.2.2. Procedure for the activity tests

The photocatalytic Ullmann coupling of different aryl halides was carried out in a Pyrex test tube (70 ml). The desired catalyst sample (the $M(x)/TiO_2$ sample or the mixture of the TiO_2 sample with the Pd/Al_2O_3 or $Pd(x)Au(y)/Al_2O_3$ sample) were pre-treated by irradiation with a xenon lamp ($\lambda \geq 350$ nm) for 30 min. Then, 2 ml of a solvent and aryl halide was added and the test tube was sealed with a silicon septum and purged with argon gas for 10 min. The contents were then stirred with irradiation for the desired time. After the reaction, the liquid phase was filtered by using a syringe equipped with a PTFE filter and then analysed by GC-MS (Shimadzu GC-8A) using decane as an internal standard.

3. Results and Discussion

3.1. Photocatalytic Ullmann coupling of Iodobenzene

3.1.1. Screening of catalysts

The initial reaction tests were performed with iodobenzene as the aryl halide and acetonitrile as a solvent (Table 1). The reaction done with the $Pd(0.1)/TiO_2$ photocatalyst gave biphenyl (**BP**), benzene (**B**), succinonitrile (**SN**), and benzyl cyanide (**BzCN**) as products (Table 1, entry 1). Biphenyl and benzene were probably formed from iodobenzene. Succinonitrile was the homocoupling product of acetonitrile, formed by its oxidation, while benzyl cyanide was probably formed by the reaction between iodobenzene and

acetonitrile. Biphenyl was not observed in the reaction done with the pristine TiO₂ photocatalyst (JRC TIO-8, ST01) (Table 1, entry 2). Interestingly, when compared to Pd(0.1)/TiO₂, the amount of benzene decreased in the reaction done with a physical mixture of TiO₂ and Pd(0.1)/Al₂O₃, which increased the selectivity to biphenyl (%S) (Table 1, entries 1 and 3). These results indicate that loading of Pd on the TiO₂ photocatalyst was necessary to get high yield of benzene, i.e. to activate iodobenzene. Further, as the amount of biphenyl formed in the case of Pd/TiO₂ and physical mixture was similar, it can be proposed that Pd, irrespective of its support, was required for the formation of biphenyl (Table 1, entries 1 and 3).

Then, the reactions were carried out with a physical mixture of the TiO₂ photocatalyst (JRC TIO-8, ST01) and different Pd(x)Au(y)/Al₂O₃ bimetallic samples. The yield (μmol) and %S of biphenyl obtained in these reactions was much larger than that in the reaction with the Pd(0.1)/TiO₂ sample and the physical mixture of the TiO₂ photocatalyst and the Pd(0.1)/Al₂O₃ catalyst (Table 1, entries 1, 3, and 4-7). Among the different combinations, the mixture with the Pd(2.0)Au(1.0)/Al₂O₃ catalyst gave the largest amount of biphenyl with high selectivity such as 93 % (Table 1, entry 5). The obtained values were higher than the mixture of TiO₂ with the Pd(3.0)/Al₂O₃ or Au(3.0)/Al₂O₃ samples indicating the promotional effect of the bimetallic Pd-Au species (Table 1, entries 5, 8, and 9). Loading of the Pd or Au metal particles on the TiO₂ photocatalyst of the mixture was beneficial for the increase of the product yields, but not helpful for the selective formation of biphenyl (Table 1, entries 10 and 11). The reaction done with a physical mixture of the Pd(0.1)/TiO₂ photocatalyst and the Pd(2.0)Au(1.0)/Al₂O₃ catalyst yielded biphenyl with just 53% selectivity. The reaction carried out without the TiO₂ photocatalyst under photoirradiation did not yield any product, ruling out the possibility of plasmonic catalysis of the Pd(2.0)Au(1.0)/Al₂O₃ catalysts in the present reaction conditions (Table 1, entry 12). Since the Pd(2.0)Au(1.0) bimetallic composition showed the maximum activity for the selective formation of biphenyl, further experiments were performed with its mixture with TiO₂. The effect of the properties of the TiO₂ sample on the photocatalytic reaction was also studied (Table 2) where the crystal phase and the surface area of the TiO₂ photocatalyst were varied.

Table 1 Ullmann coupling of iodobenzene in acetonitrile with different catalysts ^a

Entry	Catalyst	Products (μmol) ^b				%S ^c
		BP	B	SN	BzCN	
1	Pd(0.1)/TiO ₂	0.03	0.09	0.65	0.07	25
2	TiO ₂	0.00	0.05	0.37	0.0	n.a. ^d
3 ^e	Pd(0.1)/Al ₂ O ₃ + TiO ₂	0.02	0.04	0.52	0.0	33
4 ^e	Pd(2.5)Au(0.5)/Al ₂ O ₃ + TiO ₂	0.49	0.05	0.53	0.16	91
5 ^e	Pd(2.0)Au(1.0)/Al ₂ O ₃ + TiO ₂	0.98	0.07	1.11	0.17	93
6 ^e	Pd(1.5)Au(1.5)/Al ₂ O ₃ + TiO ₂	0.51	0.04	1.04	0.16	93
7 ^e	Pd(0.5)Au(2.5)/Al ₂ O ₃ + TiO ₂	0.13	0.05	0.63	0.05	72
8 ^e	Pd(3.0)/Al ₂ O ₃ + TiO ₂	0.58	0.08	1.19	0.07	88
9 ^e	Au(3.0)/Al ₂ O ₃ + TiO ₂	0.07	0.02	0.39	0.0	77
10 ^e	Pd(2.0)Au(1.0)/Al ₂ O ₃ + Pd(0.1)/TiO ₂	1.27	0.74	1.16	0.41	63
11 ^e	Pd(2.0)Au(1.0)/Al ₂ O ₃ + Au(0.1)/TiO ₂	1.04	0.91	0.95	0.53	53
12 ^f	Pd(2.0)Au(1.0)/Al ₂ O ₃	0.0	0.0	0.0	0.0	0.0

^a Reaction conditions: 10 μl (89.7 μmol) iodobenzene, 2 ml acetonitrile, 25 mg of each catalyst was used, the reaction time was 30 min, $\lambda \geq 350$ nm, $I = 40$ mW/cm². ^b Amount of all products was determined from the calibration curve of their authentic sample. ^c %S: Selectivity to biphenyl (**BP**) (%) = (100 X (amount of **BP** (μmol)) / (amount of **BP** and **B** (μmol))). ^d not applicable. ^e 25 mg of photocatalyst and 25 mg of M(x)/Al₂O₃ catalyst was used. ^f The reaction was carried out without TiO₂ photocatalyst under photoirradiation.

For the anatase TiO₂, the amount of the biphenyl increased with increasing the surface area (Table 2, entries 1–3). For the TiO₂ samples with similar surface area, the amount of biphenyl was the maximum for the mixture of Rutile and Anatase followed by anatase and rutile (Table 2 entries 3–5). Based on these results, further reactions were performed with the mixture of JRC-TIO-4 and the Pd(2.0)Au(1.0)/Al₂O₃ catalyst.

Table 2 Ullmann coupling of iodobenzene in acetonitrile with a mixture of different TiO₂ photocatalyst and Pd(2.0)Au(1.0)/Al₂O₃ catalyst ^a

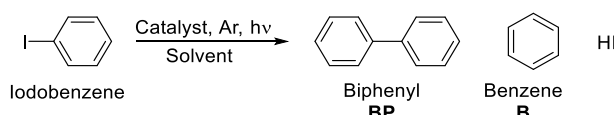
Entry	Catalyst	Phase	Specific surface area (m ² /g)	Product (μmol)				%S
				BP	B	SN	BzCN	
1	JRC-TIO-8	Anatase	335	0.98	0.07	1.11	0.17	93
2	JRC-TIO-10	Anatase	128	0.77	0.09	0.24	0.09	89
3 ^c	JRC-TIO-1	Anatase	75	0.31	0.22	0.00	0.17	58
4 ^c	JRC-TIO-6	Rutile	50	0.24	0.03	0.05	0.03	88
5 ^c	JRC-TIO-4	Anatase + Rutile	50	1.21	0.18	0.23	0.27	87

^a All reaction conditions were same as Table 1

3.1.2. Screening of solvents

The effect of solvent on the yield of biphenyl was also studied (Table 3). Among the different solvents screened, the alcoholic solvents like methanol and isopropyl alcohol gave larger yield of biphenyl than other solvents, although the selectivity was low due to a large production of benzene (Table 3, entries 3 and 4). As discussed later in the reaction mechanism, the formation of benzene would involve the abstraction of H⁺ from the solvent. Thus, the amount of benzene formed in a solvent will depend on its oxidation reactivity to the oxidative hole of the photocatalyst.

Table 3 Ullmann coupling of iodobenzene in different solvents with a mixture of the TiO₂ photocatalyst (TIO-4) and the Pd(2.0)Au(1.0)/Al₂O₃ catalyst ^a



Entry	Solvent	Product (μmol)		Selectivity ^b	Yield ^c
		BP	B		
1	Acetonitrile	1.21	0.18	87	2.69
2	Dimethylformamide	3.27	1.99	62	7.29
3	Methanol	7.88	11.13	41	17.5
4	Isopropyl alcohol	4.69	6.35	42	10.4
5	Triethylamine	1.80	11.06	14	4.0

^a 2 ml solvent, other conditions were same as Table 1. ^b Selectivity to **BP** was calculated as 100 × (amount of BP)/(amount of **BP** and **B**). ^c Yield of BP was calculated as 100 × (amount of **BP**)/(maximum theoretical yield of **BP**, i.e. 44.85 μmol for 89.7 μmol iodobenzene)

Thus, the alcoholic solvents also gave the highest yield of benzene among all solvents. Since methanol gave the highest yield of biphenyl, further experiments were performed with methanol as a solvent and efforts were made to improve the selectivity.

3.1.3. Effect of NaOH addition

In a previous report, the photocatalytic dechlorination of chlorobenzene was found to be accelerated by the addition of sodium hydroxide (NaOH) or simply Na⁺ due to the removal of the Cl⁻ by Na⁺.^{12,18} Surprisingly, biphenyl was not detected in those conditions in the literature. On the other hand, in our reaction system, dehalogenation of iodobenzene gave both benzene and biphenyl. So, it was interesting to study the effect of NaOH addition to the Ullmann coupling of iodobenzene in CH₃OH. The results are shown in Table 4. The amount of biphenyl increased with the addition of NaOH and reached

the maximum at the addition of 100 μl of NaOH with 65% yield with 80.1% selectivity to biphenyl. Further addition of NaOH increased benzene production which decreased both %Y and %S to biphenyl. The reasons for the improved yield and selectivity of biphenyl upon NaOH addition could be similar to the previous reports. The Na^+ ions might be responsible to remove iodide anion which would help the formation of phenyl radical and facilitate its further reactions. Also, the OH^- ions might consume H^+ and suppress benzene formation which would improve the %S to biphenyl. However, the enhanced production of benzene at high concentration of NaOH ($>100 \mu\text{l}$) cannot be explained at this point.

Table 4 Effect of addition of NaOH to the Ullmann coupling of iodobenzene with a physical mixture of the TiO_2 (TIO-4) photocatalyst and the $\text{Pd}(2.0)\text{Au}(1.0)/\text{Al}_2\text{O}_3$ catalyst ^a

Entry	Volume of NaOH added (μl)	Product (μmol)		Selectivity	Yield
		BP	B		
1	0	7.9	11.1	41.4	17.6
2	10	11.6	11.2	50.8	25.8
3	50	24.9	8.4	74.8	55.5
4	100	29.3	7.3	80.1	65.3
5	500	22.9	27.1	45.7	51.1
6	1000	23.5	25.1	48.4	52.4

^a 2 ml methanol, other reaction conditions were same as Table 1. For selectivity and yield calculations see Table 3.

3.1.4. Variation of Pd-Au bimetallic catalysts

Under the optimized reaction conditions, we performed some control experiments to clarify the relationship between the two catalytic components of the physical mixture. Table 5 shows the results of the experiments performed with different amount of catalysts. When compared to the mixture containing equal amount of both catalysts, increasing the amount of photocatalyst did not affect the biphenyl yield but increased the yield of benzene (Table 5, entry 2). This is reasonable because the photogenerated electrons and holes should be responsible for the generation of phenyl radical from iodobenzene which would give benzene. On the other hand, increasing the amount of metal catalyst slightly suppressed the biphenyl production but significantly increased benzene production, indicating that the metal catalysts also played some role in benzene production (Table 5, entry 3). The amount of BP was quite close in the three experiments so it is difficult to find a direct correlation between

the amount of the catalysts and products' yield because other factors might also get influenced by this change for example, the solid to liquid ratio, shading effect by photo-inactive Al₂O₃ support and so on. As the mixture of equal amount of the two catalysts gave the highest selectivity to biphenyl, further reactions were performed with this weight composition.

Table 5 Ullmann coupling of iodobenzene with different amount of catalysts in physical mixture ^a

Entry	Catalysts' amount (mg)		Product (μmol)		Selectivity	Yield
	TiO ₂	Pd(2.0)Au(1.0)/Al ₂ O ₃	BP	B		
1	25	25	29.3	7.3	67.7	65.3
2	50	25	29.9	14.9	66.8	66.6
3	25	50	23.5	13.0	64.2	52.4

^a 2 ml methanol, 100 μl NaOH, other conditions were same as Table 1. For selectivity and yield calculations see Table 3.

We also examined the effect of loading Pd-Au bimetallic catalysts on the TiO₂ photocatalyst. Table 6 shows the results of the photocatalytic Ullmann coupling of Iodobenzene with the Pd(2.0)Au(1.0)/TiO₂ samples. The reaction yielded much lower amount of biphenyl than the physical mixture of the TiO₂ photocatalyst and the Al₂O₃ supported Pd-Au bimetallic catalysts, but the yield of benzene was similar in the two catalysts (Table 6, entries 1 and 2). Thus, it is noted that the TiO₂ supported catalysts produced biphenyl with less selectivity. Several reasons might be possible for this difference, for example, the structure of the two Pd-Au bimetallic catalysts was different on the two supports, or their dispersion, particle size etc. might be different. More studies are required to elucidate the exact the exact reason.

Table 6 Ullmann coupling of iodobenzene with different Pd-Au bimetallic catalysts ^a

Entry	Catalyst	Product (μmol)		Selectivity	Yield
		BP	B		
1 ^b	TiO ₂ + Pd(2.0)Au(1.0)/Al ₂ O ₃	24.1	11.5	67.9	53.7
2 ^c	Pd(2.0)Au(1.0)/TiO ₂	9.9	16.2	37.8	22.1

^a For reaction conditions and caption, see Table 5. ^b 25 mg of both catalysts; ^c 25 mg of catalyst

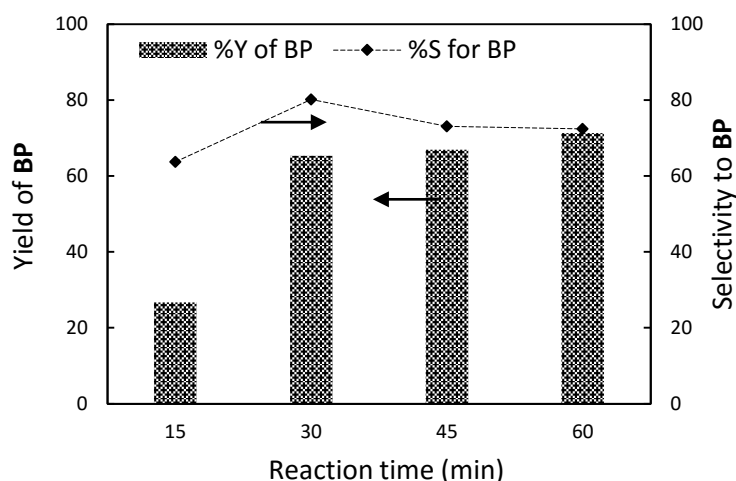
3.1.5. Time course

Table 7 shows the time course of the photocatalytic Ullmann coupling of Iodobenzene. The %Y of biphenyl significantly increased by increasing the reaction time from 15 to 30 min. However, further elongation of the reaction time did not increase the yield biphenyl, only benzene formation was enhanced. Thus, 30 min was chosen as the optimum reaction time to get selective production of biphenyl. Figure 4 shows these results in graphically.

Table 7 Time course for the photocatalytic Ullmann coupling of iodobenzene ^a

Entry	Reaction time (min)	Product (μmol)		Selectivity	Yield
		BP	B		
1	15	11.9	6.8	63.7	26.7
2	30	29.3	7.3	80.1	65.3
3	45	30.0	11.1	73.1	66.9
4	60	31.9	12.2	72.4	71.3

^a For reaction conditions and captions, see Table 5.

**Figure 4** Time course of the photocatalytic Ullmann coupling of iodobenzene

3.1.6. Material balance

To confirm the reaction stoichiometry, reactions were carried out in (trifluoromethyl)benzene as solvent. Table 8 shows the results of the Ullmann coupling of alcoholic mixture of iodobenzene in methanol with (trifluoromethyl)benzene as solvent using a mixture of the TiO_2 photocatalyst and the $\text{Pd}(2.0)\text{Au}(1.0)/\text{Al}_2\text{O}_3$ catalyst.

Table 8 Photocatalytic Ullmann coupling of iodobenzene in (trifluoromethyl)benzene^a

Entry	Volume of CH_3OH (μl)	Product (μmol)		Amount of Iodobenzene remaining after the reaction (μmol)	Material balance ^b
		BP	B		
1	2	3.7	5.7	51.2	1.03
2	5	3.8	3.6	40.9	1.05
3	20	2.5	4.2	40.3	1.06

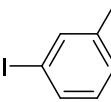
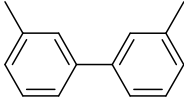
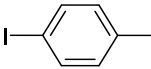
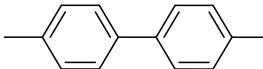
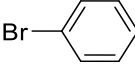
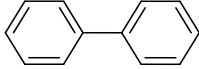
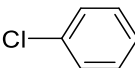
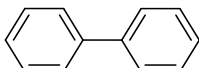
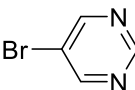
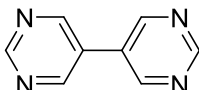
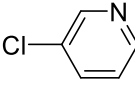
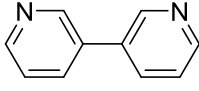
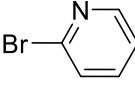
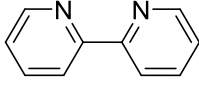
^a Reaction conditions were same as Table 5. ^b Material balance = [sum of the amount of **B**, **BP**, iodobenzene after the reaction (μmol)] / [initial amount of iodobenzene (μmol)]

The reaction was performed with different volume of methanol (Table 8, entries 1–3). The material balance was unity in these cases, indicating that benzene and biphenyl were the only products obtained from iodobenzene.

3.2. Ullmann coupling of other aryl halide

Table 9 shows the results of the photocatalytic Ullmann coupling of various aryl halides. Different aromatic and heteroaromatic halides successfully underwent coupling to give the corresponding biaryls and arene (Table 9, entries 1–7). Thus, the developed methodology for Ullmann coupling had good substrate scope.

Table 9 Photocatalytic Ullmann coupling of different aryl halides with a mixture of the TiO₂ photocatalyst and the Pd(2.0)Au(1.0)/Al₂O₃ catalyst ^a

Entry	Aryl halide	Product	Product (μmol) ^b	S(%) ^c
1 ^d		 1	28.3	66.2
2 ^d		 2	3.28	59.7
3		 3	17.6	24.8
4		 3	7.6	11.3
5 ^e		 4	31.8	49.6
6 ^f		 5	11.0	21.8
7		 6	40.2	50.4

^a Reaction time was 1 h, other conditions were same as Table 5. ^b Product amount was determined from the calibration curve of an authentic sample, unless otherwise mentioned. ^c Selectivity to biaryl, S(%) = 100 X [(amount of biaryls (μmol))/(amount of biaryl + arene (μmol))]. ^d Reaction time was 30 min, 1.7 mg of aryl halide was used, amount of biaryl was determined from the calibration curve of **1**. ^e 21.2 mg of aryl halide was used, amount of biaryls was determined from the calibration curve of **6**. ^f Amount of biaryl was determined from the calibration curve of **6**.

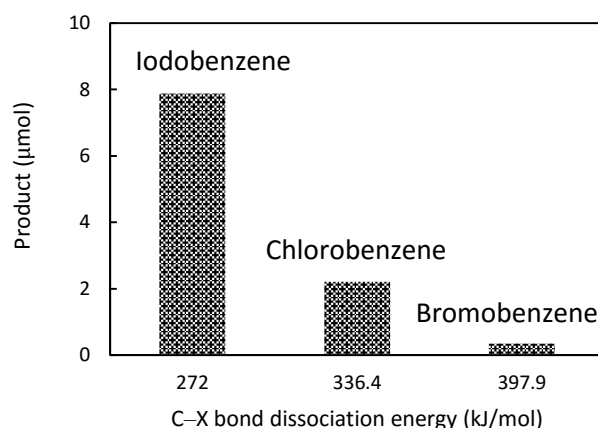


Figure 5 Variation in the biphenyl yield with C-X bond dissociation energy

For mono-substituted aromatics, like benzene and pyridine, the yield of biaryl increased with decrease in the C-X bond dissociation energy. For example, %Y biphenyl decreased as Iodobenzene > Bromobenzene > Chlorobenzene (Figure 5) and for bipyridine as 2-bromopyridine > 2-chloropyridine (Table 9, entries 6 and 7). This is reasonable because a weaker bond can be broken easily which would improve the biaryl yield.

3.3. Mechanistic Studies

3.3.1. Electron trapping

The photocatalytic Ullmann coupling and benzene formation are believed to proceed by the photogenerated electrons as discussed below. To confirm this proposal, effect of the addition of an electron scavenger to the reaction system was studied. Carbon tetrachloride (CCl_4) was chosen as the electron scavenger. Table 10 shows the results of the reaction performed with different volume of carbon tetrachloride. The amount of biphenyl decreased with the addition of carbon tetrachloride (Table 10, entries 1-4 and Figure 6). These results evidenced that the formation of biphenyl involves the photoexcited electrons on the TiO_2 photocatalyst. However, the benzene production was slightly increased upon the addition of carbon tetrachloride (Table 10, entries 1-4). Although benzene production would also involve photogenerated electrons on the TiO_2 photocatalyst, the present results show that its formation followed a different route so that other factors were crucial for benzene formation. As the electrons are consumed by carbon tetrachloride, the recombination between holes and electrons might

decrease. This would promote methanol oxidation. Thus, the oxidation of solvent might have a positive effect on the benzene production.

Table 10 Effect of carbon tetrachloride addition to the Photocatalytic Ullmann coupling of iodobenzene with a physical mixture of the TiO₂ photocatalyst and the Pd(2.0)Au(1.0)/Al₂O₃ catalyst ^a

Entry	Volume of CCl ₄ (μl)	Product (μmol)		Selectivity	Yield
		BP	B		
1	0	31.9	12.2	72.4	71.1
2	20	33.0	21.7	60.4	73.5
3	100	28.7	22.1	56.4	63.9
4	1000	15.3	18.7	45.0	34.1

^a Reaction conditions were same as Table 5.

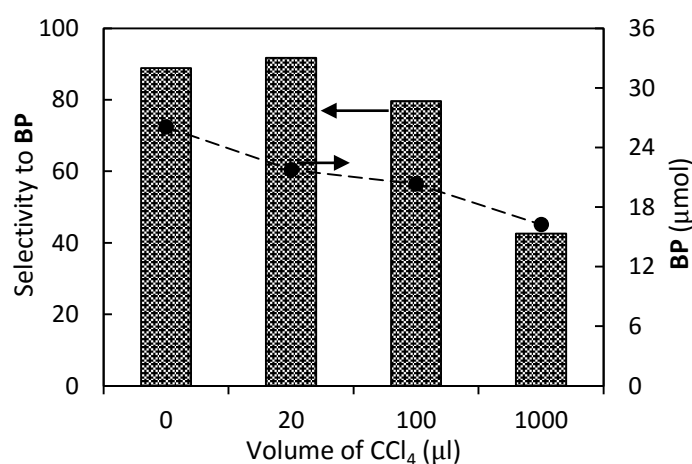


Figure 6 Effect of CCl₄ addition to the photocatalytic Ullmann coupling of iodobenzene

3.3.2. Reaction with deuterated solvent

As mentioned in the last section, the solvent was believed to be important for benzene formation. To confirm this proposal, reactions were performed with deuterated methanol (CD₃OD). Table 11 shows the results of the Ullmann coupling of iodobenzene carried out in deuterated methanol. The yield of benzene was drastically decreased in the reaction carried out with deuterated methanol (Table 11, entry 2).

Table 11 Comparison of the results of photocatalytic Ullmann coupling of iodobenzene in methanol and deuterated methanol ^a

Entry	Solvent	Product (μmol)	
		BP	B
1	CH ₃ OH	3.9	16.2
2	CD ₃ OD	4.7	6.3

^a Reaction conditions were same as Table 5

These results confirmed that for benzene production, solvent oxidation was an important step. Interestingly, the amount of biphenyl was slightly increased in this reaction (Table 11, entry 2). This result suggests that these two processes were a competitive reaction. This will be discussed later.

3.3.3. Temperature control reactions

The Pd-Au bimetallic catalysts seemed to play an important role in this photocatalytic Ullmann coupling reaction. As, they are not loaded on the TiO₂ photocatalyst, they cannot act as an electron receiver. This suggests that the metals might have a catalytic role in these reactions. To confirm this proposal, the effect of temperature on the photocatalytic Ullmann coupling of iodobenzene was studied. Table 12 shows the results of these experiments. For the reactions, performed with the physical mixture of the TiO₂ photocatalyst and the Pd(2.0)Au(1.0)/Al₂O₃ catalyst, the yield of biphenyl steadily increased with temperature (Table 12, entries 1–3). However, the amount of benzene did not vary much with temperature. A pseudo Arrhenius plot of this data is shown in figure 7. The apparent activation energy was calculated as 16.2 kJ/mol for biphenyl and 8.7 kJ/mol for benzene (Figure 7 a). None of the products were formed in the reaction carried out at high temperature in dark, indicating that the reaction was photocatalyzed (Table 12, entry 4). Similar experiments were performed with the pristine TiO₂ photocatalyst (Table 12, entries 5–7). This reaction yielded only benzene. The yield of benzene did not change with temperature and the apparent activation energy for benzene formation was 1.5 kJ/mol. From these results, we propose that the metal nanoparticles could utilize the thermal energy and catalyze biphenyl production. The nature of this catalysis is proposed to be the activation of the C–X bond in aryl halides. Metals like Pd are known to activate the aryl halides molecules by oxidative addition¹⁹ or injection of electron into the halogen atom.^{16,20} However, as the Ullmann coupling did not proceed with the Pd(2.0)Au(1.0)/Al₂O₃ catalysts alone or with the physical mixture in dark, it can be postulated that these bimetallic catalysts cannot activate the aryl halide to generate the aryl radical and halide anion alone and require the TiO₂ photocatalysis. Thus, it is suggested that the metal nanoparticles can activate a surface adsorbed aryl halide molecule and facilitate its reaction with a photogenerated aryl radical.

Table 12 Effect of temperature on the photocatalytic Ullmann coupling of Iodobenzene with different catalysts ^a

Entry	Temperature (K)	Catalyst	Product (μmol)	
			BP	B
1	304.2	TiO ₂ + Pd(2.0)Au(1.0)/Al ₂ O ₃	7.7	12.2
2	309.2		8.7	13.3
3	313.2		9.3	13.4
4 ^b	313.2	TiO ₂ + Pd(2.0)Au(1.0)/Al ₂ O ₃	0.0	0.0
5	305.2	TiO ₂	0.0	22.5
6	309.2		0.0	22.0
7	314.2		0.0	22.9

^a Reaction time was 1 h, other conditions were same as Table 5. ^b the reaction was performed in dark

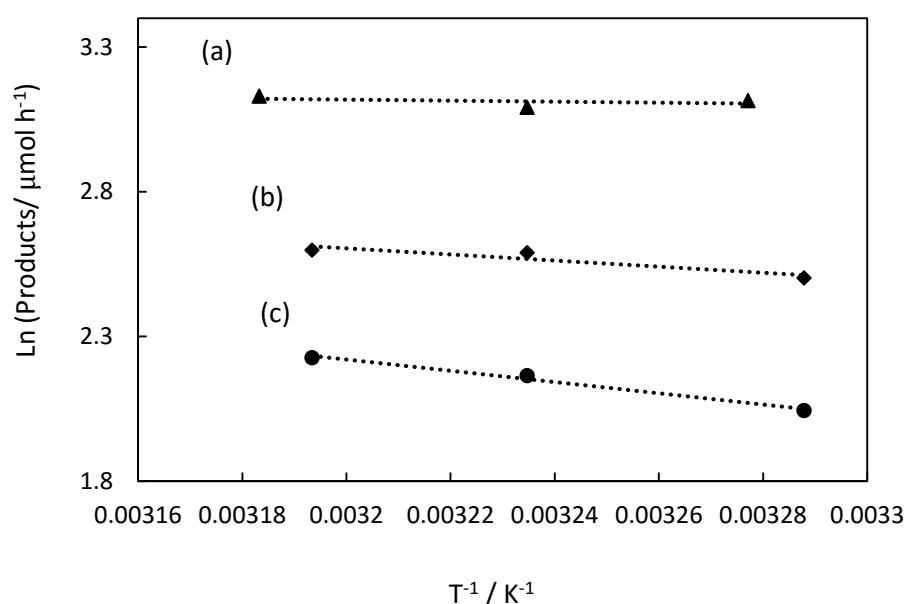


Figure 7 Pseudo Arrhenius plot for photocatalytic Ullmann coupling of iodobenzene (a) benzene formation with the TiO₂ photocatalyst, and (b) benzene (c) biphenyl production with a mixture of the TiO₂ photocatalyst and the Pd(2.0)Au(1.0)/Al₂O₃ catalysts.

3.4. Proposed reaction mechanism

The above results have been summarized to propose the following reaction mechanism for the photocatalytic Ullmann coupling of Iodobenzene (Figure 8). (1) Photoexcitation of TiO₂ would generate electrons and holes in the conduction and valance bands, respectively. (2) The holes would oxidize solvent (here CH₃OH) to generate its radical and a proton. (3) The electrons would reduce iodobenzene to give phenyl radical and iodide anion. (4) The phenyl radical can abstract proton from the solvent molecule to yield

benzene. This step might be the rate determining step for benzene formation, as suggested by the reactions with deuterated methanol (Table 11). (5) A direct coupling of these phenyl radicals would yield biphenyl. Thus, one of the routes for the biphenyl formation might be a radical coupling mechanism. The results of the temperature control experiments indicated that the apparent activation energy for the biphenyl production was about 15 kJ/mol. A radical coupling reaction might be an easy process and would not require thermal energy. Thus, there might be another possible route for biphenyl formation where the Pd-Au bimetallic catalysts might have catalytic role. As the recombination rate of the photogenerated electrons and holes on a pristine TiO₂ photocatalyst is high, the conversion of iodobenzene molecule might not be large which would result in high concentration of iodobenzene molecule. These molecules might be adsorbed on the surface of the Pd-Au bimetallic catalysts. (5') These adsorbed molecules might be activated due to the interaction with metals as mentioned before and can react with a photogenerated phenyl radical, hence produce the biphenyl through a radical addition-elimination process. Thus, the reaction would be a hybrid of the TiO₂ photocatalysis and metal catalysis.

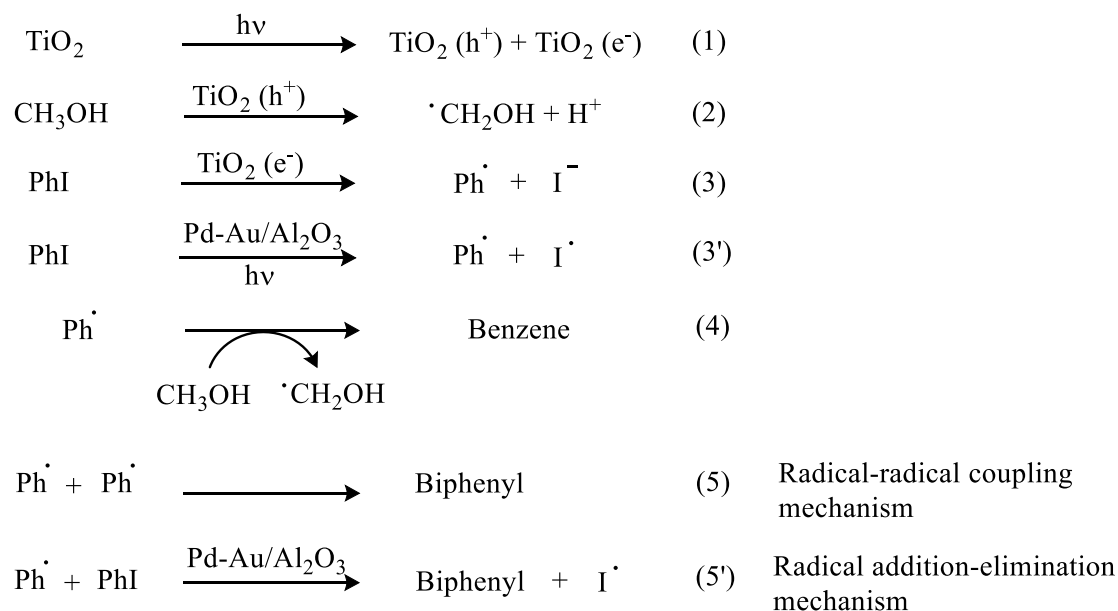


Figure 8 Proposed reaction mechanism for the photocatalytic Ullmann coupling of iodobenzene by a physical mixture of TiO₂ photocatalyst and Pd(2.0)Au(1.0)/Al₂O₃ catalyst under UV light irradiation

4. Conclusion

In this work, we have developed a novel strategy to carry out the Ullmann coupling of various aryl halides to give biaryls. A physical mixture of the TiO₂ photocatalyst and the Pd-Au bimetallic catalyst was more active and selective for biphenyl production from iodobenzene. Detailed investigations of the coupling of iodobenzene indicated that the biphenyl production was a hybrid of TiO₂ photocatalysis and Pd-Au metal catalysis. These results are clear evidence that the metal nanoparticles loaded on TiO₂ have dual role and it is possible to vary the two components independently to control the product selectivity and improve its yield in a reaction. This blended catalyst will provide a wide possibility to design efficient catalytic systems.

5. References

- [1] U. Schmidt, V. Leitenberger, H. Griesser, J. Schmidt and R. Meyer, *Synthesis*, p. 1248, **1992**.
- [2] M. E. Matheron and M. Porchas, *Plant Dis.*, vol. 88, p. 665, **2004**.
- [3] A. H. Douglas, G. T. Bourne and M. L. Smythe, *Chem. Rev.*, vol. 103, p. 893, **2003**.
- [4] F. Ullmann and J. Bielecki, *Chem. Ber.*, vol. 34, p. 2174, **1901**.
- [5] M. Gomberg, W. E. Bachmann, *J. Am. Chem. Soc.*, vol. 46, p. 2339, **1924**.
- [6] P. Kovacic, M. B. Jones, *Chem. Rev.*, vol. 87, p. 357, **1987**.
- [7] N. Miyaura, K. Yamada and A. Suzuki, *Tetrahedron Letters*, vol. 36, pp. 3437, **1979**.
- [8] P. E. Fanta, *Synthesis*, vol. 1, p. 9, **1974**.
- [9] J. Hassan, M. Sevignon, C. Gozzi, E. Schulz and M. Lemarie, *Chem. Rev.*, vol. 102, p. 1359, **2002**.
- [10] I. Cepanec, *Synthesis of Biaryls*, Elsevier, **2004**.
- [11] C. Sun, D. Zhao, C. Chen, W. Ma and J. Zhao, *Environ. Sci. Technol.*, vol. 43, p. 157, **2009**.

- [12] K. Fuku, K. Hashimoto and H. Kominami, *Catal. Sci. Technol.*, vol. 1, p. 586, **2011**.
- [13] Y. Shiraishi, Y. Takeda, Y. Sugano, S. Ichikawa, S. Tanaka and T. Hirai, *Chem. Commun.*, vol. 47, p. 7863, **2011**.
- [14] J. T. Petroff II, A. H. Nguyen, A. J. Porter, F. D. Morales, M. P. Kennedy, D. Weinstein, H. E. Nazer and R. D. McCulla, *J. Photo. Chem. Photobiol. A: Chemistry*, vol. 335, p. 149, **2017**.
- [15] H. Sakamoto, J. Imai, Y. Shiraishi, S. Tanaka, S. Ichikawa and T. Hirai, *ACS Catalysis*, vol. 7, p. 5194, **2017**.
- [16] Q. Xiao, S. Sarina, A. Bo, J. Jia, H. Liu, D. P. Arnold, Y. Huang, H. Wu and H. Zhu, *ACS Catalysis*, vol. 4, p. 1725, **2014**.
- [17] W. Yoo, T. Tsukamoto and S. Kobayashi, *Org. Lett.*, vol. 17, p. 3640, **2015**.
- [18] K. Fuku, K. Hashimoto and H. Kominami, *Chem. Commun.*, vol. 46, p. 5118, **2010**.
- [19] L. Xue and Z. Lin, *Chem. Soc. Rev.*, vol. 39, p. 1692, **2010**.
- [20] F. Wang, C. Li, H. Chen, R. Jiang, L. D. Sun, Q. Li, J. Wang, J. C. Yu and C. H. Yan, *J. Am. Chem. Soc.*, vol. 135, p. 5588, **2013**.

III-5. Summary

In this chapter, we successfully developed a novel blended catalyst consisting of a TiO₂ photocatalyst and a Al₂O₃ supported Pd-Au bimetallic catalyst for the various C–C coupling reactions like cross-coupling between an arene and THF, cyclohexane and THF, and homocoupling of aryl halides. For the reactions involving aromatic substrates like arenes or aryl halides, the Pd-Au bimetallic catalysts exhibited higher activity than monometallic Pd or Au catalysts. However, for aliphatic substrates like cyclohexane, the activity of the bimetallic catalysts was similar to monometallic Pd but much higher than monometallic Au catalysts. This change was attributed to the different activation mechanism of aromatic and aliphatic substrates. For aromatic substrates, the interaction between the aromatic electron density and Pd was the proposed activation mechanism, while for aliphatic substrates, the direct C–H bond activation of alkanes was important.

These findings have allowed the development of highly efficient and selective organic synthesis reactions by TiO₂ photocatalyst. Further, the novel blended catalysts developed in this work have several advantages like, the independent variation of the two catalytic components, the photocatalyst and metal catalyst, as per the reaction's requirement, control over the physical and electronic properties of either type of catalyst, and so on.

Chapter IV General Conclusion

Based on the summaries of each chapter, the following conclusions are made:

1. In this work, several new photocatalytic organic synthesis reactions were developed by using an abundant, safe, and in-expensive TiO_2 photocatalyst. Metal loaded TiO_2 (M/TiO_2) photocatalysts were found to successfully activate the C–H bonds in various ethers and hydrocarbons like arenes, alkanes, and alkenes and catalyze the successive C–C bond formation between the two fragments with hydrogen evolution. The reactions were quite selective and yielded only one cross-coupling product in most of the cases. All reactions were carried out at room temperature without any additional metal co-catalysts, oxidizing or reducing agents. The noble metal nanoparticles loaded on TiO_2 photocatalyst were found to have a dual role in these reactions namely, an electron receiver and catalyst. The electron receiving ability of these metals reduced the recombination between the photogenerated electrons and holes, which enhanced their activity compared to the pristine TiO_2 photocatalyst. Further, metals like Pd were found to have an additional catalytic role in some reactions, especially those between aromatic substrates and ethers. The exact nature of this catalysis is unknown and might require more studies, but was tentatively proposed to be the activation of aromatic moiety by the interaction with the aromatic electron density. The electronic state of metal was crucial for this kind of catalysis. It was found that metallic Pd was more active than oxidized Pd. However, for the reactions involving non-aromatic substrates like cyclohexane and cyclohexene, the role of metal was mainly an electron receiver to ensure the efficient separation of the photogenerated electrons and holes although the catalytic property was also confirmed to contribute in part. Hence, metals like Pt, with high work function, exhibited the highest activity in these cross-coupling reactions.
2. Further studies of the mechanism of the cross-coupling reactions between arenes and ethers reaction revealed that the proposed metal catalysis could also work even if the metals were loaded on an inert photo-inactive support like Al_2O_3 . This revelation was used for the development of a novel

catalytic system consisting of a mixture of TiO₂ photocatalyst and Al₂O₃ supported metal catalysts. This catalytic system allowed an independent variation of the photocatalyst and metal catalyst depending on the reaction's requirement. We developed the catalysts consisting of Al₂O₃ supported Pd-Au bimetallic catalysts and TiO₂ photocatalyst for the cross-coupling between arenes and tetrahydrofuran. The blended catalysts with an optimum Pd-Au composition exhibited much higher activity than the M/TiO₂ photocatalyst alone.

3. Finally, we explored the scope of this blended catalyst and developed a new methodology for the Ullmann coupling of aryl halides under mild reaction conditions. The two catalyst components worked in synergy to yield biaryls with high selectivity when compared to the either catalyst alone. As per the best of our knowledge, this is the first report of such reaction by a TiO₂ photocatalyst.

Outlook and perspective

In this thesis, we have demonstrated that TiO₂ photocatalysis is a promising technology to carry out selective organic synthesis under mild reaction conditions. TiO₂ photocatalysis has been widely investigated for degradation of organic pollutants, water splitting and many other reactions, but its application for organic synthesis has not received much attention as it is generally considered to be inefficient and unselective. However, our results revealed that a clear understanding of the substrate properties, the reaction mechanism, and role of each catalytic component can allow the development of efficient and selective reactions. Although the product yields are low, these types of systems are worth exploring as they can be carried out under much milder reaction conditions than the existing methods. Further, the novel methodology of physical mixtures that we have developed allows the independent modification of the catalyst components which could further improve the efficiency and selectivity of reactions.

We believe that these findings would motivate other researchers to investigate this exciting field of photocatalytic organic synthesis and this methodology can be applied industrially.

List of publications

Chapter 2

1. **Akanksha Tyagi**, Tomoya Matsumoto, Tatsuhisa Kato, and Hisao Yoshida
“Direct C–H bond activation of ethers and successive C–C bond formation with benzene by a bifunctional palladium–titania photocatalyst”
Catal. Sci. Technol., vol. 6, p. 4577, **2016**.
2. **Akanksha Tyagi**, Akira Yamamoto, Tatsuhisa Kato, and Hisao Yoshida
“Bifunctional property of Pt nanoparticle deposited on titanium oxide for the photocatalytic sp^3C – sp^3C cross-coupling reactions between tetrahydrofuran and alkanes”
Catal. Sci. Technol., vol. 7, p. 2616, **2017**.
3. **Akanksha Tyagi**, Akira Yamamoto, Muneaki Yamamoto, Tomoko Yoshida, and Hisao Yoshida
“Direct cross-coupling between alkenes and tetrahydrofuran with platinum-loaded titanium oxide photocatalyst”
Submitted.

Chapter 3

1. **Akanksha Tyagi**, Akira Yamamoto, and H. Yoshida
“Novel blended catalysts consisting of TiO_2 photocatalyst and supported Pd-Au bimetallic catalyst for direct dehydrogenative cross-coupling between arenes and tetrahydrofuran”
To be submitted.
2. **Akanksha Tyagi**, Akira Yamamoto, and H. Yoshida
“Novel room temperature photocatalytic Ullmann coupling of aryl halides by a physical mixture of TiO_2 photocatalyst and alumina supported Pd-Au bimetallic catalysts”
To be submitted.

Other publications as a co-author

1. Emiko Wada, Tomoaki Takeuchi, Yuki Fujimura, **Akanksha Tyagi**, Tatsuhisa Kato, and Hisao Yoshida
“Direct cyanomethylation of aliphatic and aromatic hydrocarbons with acetonitrile over metal loaded titanium oxide photocatalyst”
Catal. Sci. Technol., vol. 7, p. 2457, **2017**.

2. Emiko Wada, **Akanksha Tyagi**, Akira Yamamoto, and Hisao Yoshida
“Dehydrogenative lactonization of diols with platinum-loaded titanium
oxide photocatalyst”
Photochem. Photobio. Sci., vol. 16, p. 1744, **2017**.

Achievements

Presentations (International conferences)

1. **(Poster)** ○Akanksha Tyagi, Akira Yamamoto, Hisao Yoshida, “Efficient room temperature photocatalytic Ullmann coupling of aryl halides”, OKCAT2017, 2017.10.27–28, Osaka (Japan), no. PS-1.
2. **(Poster)** ○Akanksha Tyagi, Akira Yamamoto, Hisao Yoshida, “Pt/TiO₂ hybrid catalysts for the sp³C–sp³C cross-coupling reaction between cyclohexane and tetrahydrofuran”, EUROPACAT2017, 2017.08.27–31, Florence (Italy), no. P3. 104.
3. **(Poster)** ○Akanksha Tyagi, Akira Yamamoto, Hisao Yoshida, “Fixation of carbon dioxide by amines with titanium oxide photocatalysts”, The 16th International Congress on Catalysis (ICC 16), 2016.07.03–08, Beijing (China), no. PF210.
4. **(Poster)** ○Akanksha Tyagi, Akira Yamamoto, Hisao Yoshida, “CO₂ functionalization by amines over titania photocatalysts”, International Symposium on Nanostructured Photocatalysts and Catalysts (NPC2016), Post Symposium of 26th IUPAC Photochemistry, 2016.04.09–10, Osaka (Japan), no. P09.
5. **(Oral)** ○Akanksha Tyagi, Akira Yamamoto, Hisao Yoshida, “Carbon dioxide fixation by titanium oxide photocatalysts”, 26th IUPAC International Symposium on Photochemistry, and 12th Korean-Japan Symposium on Frontier Photoscience (KJFP-2016), 2016.04.03–08, Osaka (Japan), no. 5CS01.
6. **(Poster)** ○Akanksha Tyagi, Tomoya Matsumoto, Akira Yamamoto, Hisao Yoshida, “Direct alpha arylation of various ether with palladium loaded titanium oxide photocatalyst”, The international Chemical Congress of Pacific Basin Societies 2015 (Pacifichem2015), 2015.12.15–20, Honolulu (USA), no. 928.
7. **(Invited Oral)** ○Akanksha Tyagi, Tomoya Matsumoto, Hisao Yoshida, “Direct and selective alpha functionalization of ethers over metal loaded TiO₂ photocatalysts”, Photocatalysis 1, 2015.09.03–04, Tokyo (Japan).
8. **(Oral)** ○Akanksha Tyagi, Tomoya Matsumoto, Hisao Yoshida, “Direct alpha arylation of ethers over metal loaded TiO₂ photocatalysts”, GSC-7 and 4th JACI/GSC Symposium, 2015.07.05–08, Tokyo (Japan).

Presentations (Domestic conferences in Japan)

1. **(Oral)** ○**Akanksha Tyagi**, Akira Yamamoto, Hisao Yoshida, “Room temperature Ullmann coupling of aryl halides by metal loaded TiO₂ photocatalysts”, 第 36 回 固体・表面光化学討論会, 2017.11.21–22, Shiga, no. 104.
2. **(Oral)** ○**Akanksha Tyagi**, Akira Yamamoto, Hisao Yoshida, “Photocatalytic Ullmann coupling by a physical mixture of TiO₂ photocatalyst and alumina supported metal catalyst”, 第 15 回触媒化学ワークショップ, 2017.07.31–08.02, Toyama, no. B 3.
3. **(Oral)** ○**Akanksha Tyagi**, Akira Yamamoto, Tatsuhisa Kato, Hisao Yoshida, “Photocatalytic cross-coupling of ethers over metal loaded titanium oxide hybrid catalysts”, 第 119 回触媒討論会, 2017.03.21–22, Tokyo, no. 1B03 (B1).
4. **(Oral)** ○**Akanksha Tyagi**, Akira Yamamoto, Hisao Yoshida, “Role of supported metal nanoparticles in photocatalytic coupling of THF with cyclohexane”, 第 35 回固体表面光化学討論会, 2016.11.21–22, Muroran, no. M07.
5. **(Poster)** ○**Akanksha Tyagi**, Akira Yamamoto, Hisao Yoshida, “Bifunctional role of metals on TiO₂ in photocatalytic cross-coupling between THF and cyclohexane”, 第 6 回 CSJ 化学フェスタ 2016, 2016.11.14–16, Tokyo, no. P4-107.
6. **(Oral)** ○**Akanksha Tyagi**, Akira Yamamoto, Hisao Yoshida, “Role of metal nanoparticles in the photocatalytic cross-coupling between tetrahydrofuran and cyclohexane”, 第 14 回触媒化学ワークショップ, 2016.08.01–03, Kanagawa, no. B 6.
7. **(Oral)** ○**Akanksha Tyagi**, Tomoya Matsumoto, Tatsuhisa Kato, Hisao Yoshida, “Direct activation of sp³C-H bonds in ethers for successive C-C bond formation with by metal loaded titanium oxide photocatalysts”, 日本化学会 第 96 春季年会, 2016.3.24–27, Kyoto, no. 3B1-08.
8. **(Poster)** ○**Akanksha Tyagi**, Akira Yamamoto, Hisao Yoshida, “Formylation of amines by carbon dioxide with metal loaded titania photocatalyst”, 第 117 回触媒討論会, 2016.3.21–22, Osaka, no. 1P22.

9. **(Poster)** ○Akanksha Tyagi, Tomoya Matsumoto, Akira Yamamoto, Hisao Yoshida, “Direct photocatalytic activation of sp^3C-H bonds in ethers for C-C bond formation”, 第 8 回触媒表面化学研究発表会, 2015.10.30, Osaka, no. P12.
10. **(Oral)** ○Akanksha Tyagi, Akira Yamamoto, Hisao Yoshida, 第 13 回触媒化学ワークショップ, 2015.8.2-4, Tokushima, no. B 16.
11. **(Poster)** ○Akanksha Tyagi, Tomoya Matsumoto, Hisao Yoshida, “Benzene functionalization using ethers over metal loaded TiO_2 photocatalysts”, 回日本化学会 第 95 春季年会, 2015.03.26-29, Chiba, no. PA150.

Awards

1. **Outstanding research** award, OKCAT2017, 2017.10.27-28, Osaka (Japan).
2. **Student Excellence Lecture** award by Catalysis Society of Japan at 第 119 回触媒討論会, 2017.03.21-22, Tokyo (Japan).
3. **CSJ poster presentation** award for excellent research by Chemical Society of Japan at 第 6 回 CSJ 化学フェスタ 2016, 2016.11.14-16, Tokyo (Japan).
4. **Outstanding research** award, 8th Symposium for Catalyst Surface Chemistry (第 8 回触媒表面化学研究発表会), 2015.10.30, Osaka (Japan).